Organocatalysis in Continuous Flow

Sebastiaan A. van den Berg

Thesis committee

Promotor

Prof. Dr H. Zuilhof

Professor of Organic Chemistry

Wageningen University

Co-promotor

Dr T. Wennekes

Assistant professor, Laboratory of Organic Chemistry

Wageningen University

Other members

Prof. Dr J. van der Gucht, Wageningen University

Prof. Dr F. P. J. T. Rutjes, Radboud University Nijmegen

Dr T. Noël, Eindhoven University of Technology

Dr C. Wiles, Chemtrix B.V., Geleen

Organocatalysis in Continuous Flow

Sebastiaan A. van den Berg

Thesis

submitted in fulfilment of the requirements for the degree of doctor

at Wageningen University

by the authority of the Rector Magnificus

Prof. Dr A.P.J. Mol,

in the presence of the

Thesis Committee appointed by the Academic Board

to be defended in public

on Friday, April 1st 2016

at 1.30 p.m. in the Aula.

"Be not afraid of growing slowly,

be afraid only of standing still."

Contents

Organocatalysis in Continuous Flow

Chapter 1

Introduction

Flow chemistry

Chemistry, in its most basic form, studies the composition, structure, and change of matter. As far back as the Greek and the Egyptians, people have tried to understand the building blocks that make up matter around us. People also tried to change one kind of material into another, because the aimed for material had desirable properties. An early example would be soap. By adding water to ashes, the water would extract potassium carbonate from the ashes and become basic. Using this caustic solution, the low-value material fat can be turned into the high-value material soap.

If we look back a few hundred years, we find another example. So-called "alchemists" tried to turn one material into another, more valuable material: they tried to turn lead into gold. Although this process is not possible by chemical means it underlines the basic goal of chemistry: changing the properties of materials to make them more useful and valuable. While the alchemists were unsuccessful in transmuting lead into gold, they did discover many other interesting processes and laid the foundation for modern-day chemistry.

Fast-forward to the twenty-first century. Chemistry has given us important materials such as medicines, fertilizers, polymers, and petrochemicals. These are made from smaller building blocks via processes that have been discovered over many years of research. The batch-wise way we make these molecules also changed very little from the time of the alchemists. Round-bottom flasks, reflux condensors, and other glassware remained surprisingly similar to those used two hundred years ago. On the one hand this points to the effectiveness of these instruments. On the other hand it reveals a lack of progress in this area and the use of these round-bottom flasks and other glassware indeed has drawbacks.

This thesis is concerned with the application of the next generation of chemical glassware: miniaturized continuous flow reactors, which show great potential in reaction optimization, efficiency, and safety. Specifically, this work tries to

implement (solid-supported) catalysis in these miniaturized reactors to enable faster and greener chemistry. This introduction will therefore elaborate on continuous flow, microreactors, and solid-supported catalysis.

Continuous Flow

Modern chemists, at the forefront of scientific discovery, work on a relatively small scale in the lab, often milligrams to grams. Reasons for working on this small scale are the costs and safety issues associated with large amounts of chemicals. The name of the game in the research lab is often "get the molecule", which focuses on discovery of new molecules with desirable properties. In industry, it is not only about discovering new molecules, but also producing these molecules as efficiently as possible on a much larger scale, often between tons and kilotons per year. The batch-wise production process for a given molecule discovered on a small scale often cannot simply be scaled up a thousand fold for industrial purposes. Why is that?

Let us take a simple example. We have a small round-bottom flask that can hold 100 mL of liquid. A fast reaction was identified to produce a certain molecule. In the process to get this prized molecule we have to cool the round-bottom flask because the fast reaction generates a lot of heat. Without cooling a thermal runaway would cause an explosion. The volume of the flask is 0.0001 m^3, while the surface area is 0.01 m^2 giving it a surface-to-volume ratio of 100. On a lab scale an ice bath is sufficient to cool this 100 mL round-bottom flask.

Now let us assume we scale up this process a thousand fold, to a 100 L round-bottom reactor. The surface area of this "flask" is now roughly 1 m^2. The surface-to-volume ratio has decreased to 10. This means that there is less surface area per volume available to dissipate heat. On this 100 L scale the reaction is now harder to cool and keep under control. Because of these cooling issues thermal runaway also becomes a much bigger problem as the resulting explosion would now involve a thousand times more material.
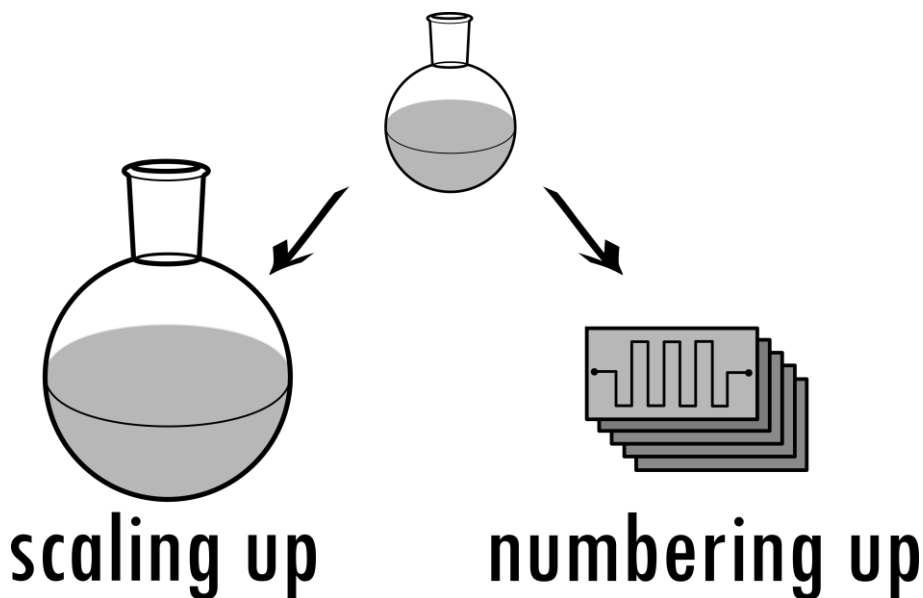
Figure 1. Scale up of a laboratory process can be done by increasing the reactor volume often leading to issues with heat transfer and mixing. Scale up can also be performed by translating the process to a flow process that is readily scaled up in a larger flow system or by running the reaction in parallel.

Localized hot spots may form in the 100 L reactor due to reduced mixing and heat transfer capacities. These hot spots could lead to unwanted by-products and a lower yield, which makes the process more costly and less environmentally friendly.

From a safety standpoint the reaction would be ideally carried out in one thousand 100 mL round-bottom flasks or even one million 0.1 mL flasks as an "explosion" would only involve minute quantities of material. As one can imagine this would require high infrastructure investments and would be very labor-intensive and cumbersome. Working up a million or even just a thousand batch-wise reactions is simply not feasible.

Now imagine a 0.1 mL round-bottom flask with a tap on the bottom and a tube attached to the top. The surface-to-volume ratio will be higher due to its smaller volume. Therefore, the heat transfer is better allowing the reactor to be kept at a specific temperature. As soon as the tap is opened the product stream comes out

with almost only target material because the reaction is quick. The reaction flask is continuously refilled with reagents and only a small amount of material is reacting at a given time. Even if thermal runaway occurs the explosion will only involve 0.1 mL of material. Nevertheless, the small reactor continually produces product. Given enough time it will produce the same amount of material as the 100 L reactor, albeit a lot safer and with less downtime.

In the above example the reaction is continuously carried out in a flowing medium. This concept is called *continuous flow chemistry*. In continuous flow chemistry streams of dissolved reagents are combined and mixed. The reagents react and are carried away in the solvent stream. This continuous flow concept can be combined with the small reactor described above to create so-called "microreactors".

At its most basic level a microreactor is a small platform with channels, inlets, and outlets. The reaction can be performed in a small chip in which microchannels (several hundreds of micrometers in diameter) have been created, but other types of reactors exist as well, e.g. tubular reactors or falling-film reactors. The underlying concept remains the same: the chemistry is performed in a continuously flowing fashion. The internal volume of the microreactor chip can be anywhere from tens of nanoliters[1] to several milliliters. The microreactor chip can be made of materials such as PDMS (a polymer), stainless steel, silicon, and glass.[2] PDMS has a low solvent compatibility (not suited for organic solvents) and glass cannot handle reactions in which fluorine or fluoride is formed. Nevertheless, glass and metal are most commonly found in synthetic applications.[3] For extreme applications of flow chemistry silicon carbide can be used, which is more resistant to corrosion than stainless steel. Silicon carbide reactors were used for the harsh conditions of the Wolff-Kishner reaction in which a carbonyl is reduced using potassium hydroxide and aqueous hydrazine at 200 °C and 14 bar.[4] Each reactor material therefore has its own distinct advantages and disadvantages, depending on the reaction that is being performed.

One of the earliest examples of microreactor technology was presented in 1997. Jensen and co-workers at MIT designed, fabricated, and operated a silicon-based microreactor capable of performing gas-phase partial oxidation reactions. These reactions are extremely exothermic and have the potential to literally explode. Nevertheless, the authors could operate the microdevice safely and monitor the output using mass spectrometry.[5]
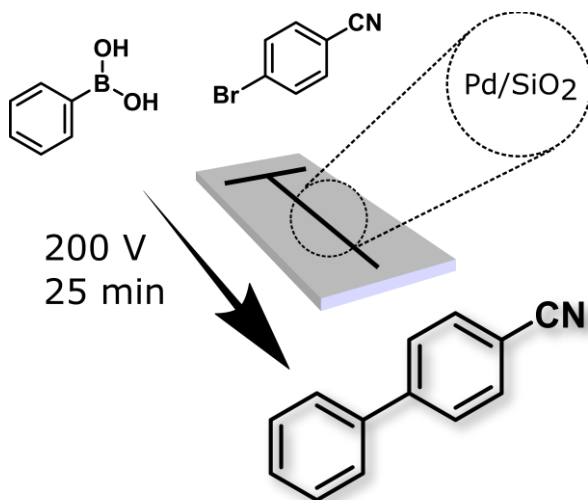
Figure 2: Flow synthesis of 4-cyanobiphenyl using a solid-supported palladium catalyst.

A few years later in 2000, Haswell and colleagues reported the use of a glass microreactor for a Suzuki coupling reaction to yield 4-cyanobiphenyl (see Figure 2).[6] The use of aqueous tetrahydrofuran enabled them to use electro-osmotic flow (EOF) to mobilize the liquid inside the channels. Furthermore, the palladium catalyst was supported inside the channels on silica. They were able to show that the flow reaction outperformed the batch reaction almost seven-fold (67±7% conversion in flow *vs.* 10% conversion in batch), hinting at the greater efficiency that can potentially be obtained in flow. However, electro-osmotic flow requires a polar modifier and is not always suitable for organic reactions.

Another example of electro-osmotic flow in continuous reactions was presented by Wiles et al., who used silyl enol ethers to perform an aldol reaction, generating ß-hydroxyketones. The flow reaction reached complete conversion faster than the corresponding reaction in batch (20 min *vs.* 24 h).[7]
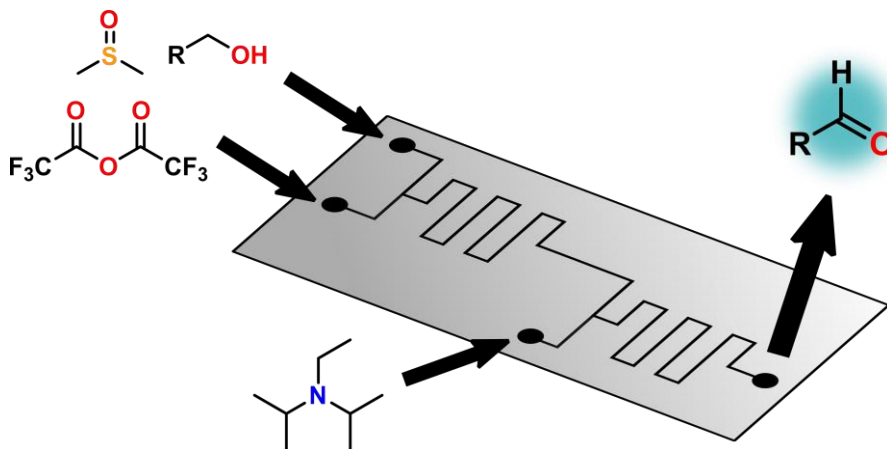

Figure 3: Swern-Moffat oxidation of alcohols in continuous flow, allowing the reaction to proceed roughly 150 °C above the normal batch reaction temperature.

One of the advantages of the microchannels is their large surface-to-volume ratio. This gives rise to excellent heat transfer capabilities, in turn reducing hot spot formation and allowing extremely exothermic reactions to be conducted safely, sometimes even well above the reaction temperature used in batch. A great example is the Swern oxidation conducted in microreactors (see Figure 3). In batch, the exothermic character of this reaction is controlled by cooling the reaction to –78 °C, avoiding potential by-product formation as well. This reaction was performed in continuous flow by Nieuwland et al. Mixing of reagents in their microreactor was complete within 32 ms and the reaction could be conducted at 70 °C, roughly 150 °C higher than the conventional batch procedure.[1] The flow inside the microchannels is typically laminar, which means mixing is governed by diffusion. For most reactions, mixing by T-mixers is sufficient. Extremely fast and homogeneous mixing can be achieved by specially designed microstructured mixers.[8, 9] The increased heat transfer capacity of microreactors may also allow higher concentrations to be used,

decreasing solvent use.[10] The heat transfer capability means that the reaction can be kept at the same temperature by externally cooling or heating the microreactor. If the reactor can be pressurized, then solvents can be heated above their atmospheric boiling points. Glass microreactors are often able to withstand 25 bar of pressure, allowing e.g. the use of dichloromethane at 175 °C. This opens up new and unconventional process windows, potentially accelerating reactions and decreasing by-product formation even further.

The use of electro-osmotic flow became less prevalent over the course of the following years, losing terrain to syringe pumps, HPLC pumps, and pressure-driven systems. The field of continuous flow chemistry expanded and series of reactions were coupled, yielding complete assembly lines for molecules. Notable examples come from the labs of Ley and Baxendale. The multistep synthesis of (±)-oxomaritidine, an alkaloid, heavily relies on solid-supported reagents, scavengers and microreactors. In seven continuous steps the target compound was synthesized in 40% yield.[11] Another example is the three-step synthesis of ibuprofen by McQuade and co-workers. The synthesis was re-designed in such a way that excess reagents and by-products do not interfere with subsequent reaction steps. The sequence starts from simple building blocks and uses three consecutive flow reactors with a total residence time of just ten minutes. The synthetic protocol yields 0.54 g ibuprofen/h, with an overall yield of 68% (51% after recrystallization).[12] Finally, the flow synthesis of imatinib, an anti-cancer drug, was performed by Ley and co-workers. Again, the synthesis deviated from the typical batch protocols to avoid insoluble materials. Using a very pragmatic approach the reactions were implemented in an automated (not fully continuous flow) sequence yielding the final compound after chromatographic purification in 32% overall yield (>95% purity).[13]

Jensen and co-workers showed in 2011 how the integration of chemical synthesis, analysis, and computerized control leads to rapid identification of reaction parameters. The Diels-Alder reaction between isoprene and maleic anhydride was performed in a Corning glass microreactor. The output was directly introduced into an inline HPLC system and the analysis fed into an algorithm running on a personal

computer. The algorithm then decided the next set of experiments to be carried out. This meant that the reaction could be rapidly optimized and subsequently scaled up 500-fold.[14] Several other hyphenated microreactor systems have been produced where reactions can be monitored using UV/VIS, IR, NMR, HPLC, and GC methods. For further examples of automated reaction optimization in continuous flow, see the review of McMullen and Jensen.[2]

Perhaps one of the greatest advantages of microreactors for industry is their scalability. Processes are developed using a lab-scale reactor as it consumes relatively small amounts of (precious) reagents, allowing rapid optimization at minimal cost. One way to achieve large-scale production is to simply take several microreactors and use them in parallel, a process called "numbering up".[3] Taking the process from a lab-scale microreactor to a larger-scale mesoreactor hardly changes the surface-to-volume ratio, which means that the process parameters do not need to change significantly. Take for example the Swern oxidation performed by Nieuwland et al. The reaction optimization was performed in a 140 nL microreactor and "scaled up" to a 500 nL microreactor. While this may seem unimpressive, the larger microreactor was still able to achieve a throughput of 12 g/day with yields exceeding 96%.[1] Even more impressive is the direct 200-fold scale up of the $KMnO_4$-mediated Nef oxidation of nitroalkanes to carbonyls by Sedelmeier and co-workers.[15] This is possible due to similar characteristics of the smaller and larger reactors, allowing direct use of reaction conditions found in the smaller reactor for the larger scale reactor.

Microreactors have their drawbacks. Although developments in reactor design are progressing rapidly, most microreactors cannot handle solids. Work is ongoing to produce "slurry" reactors. The use of ultrasound sometimes helps to disperse any precipitate and form a well-behaved suspension.[15] However, typically the entire reaction must be performed in solution and the reagents and products must not precipitate. If this happens the risk of clogging the microchannels is great and may cause failure of the (expensive) microreactor chip.

Later in this chapter we will revisit why this is a serious challenge in applying microreactor technology. Let us first look at another pillar of this thesis.

Application of catalysis in flow

A catalyst, according to the IUPAC, is "a substance that increases the rate of a reaction without modifying the overall standard Gibbs energy change in the reaction"; the process is then called catalysis.

Catalysts can be quite simple such as aqueous acid or base, or they can be complex, such as the proteins that help speed up reactions in our bodies. Catalysts do not influence the final thermodynamic equilibrium of a reaction: they merely modify the activation energy barriers, allowing reactions to proceed faster. Catalysts fall into three broad categories: transition metals, peptides, and the recently rediscovered organocatalysts.[16] One of the first documented uses of organocatalysis in organic chemistry was the Hajos–Parrish–Eder–Sauer–Wiechert reaction, where L-proline is used as a chiral catalyst (see Figure 4).[17] Quinine was used by Hiemstra and Wynberg for asymmetric thio-Michael additions.[18] Quinine acts as a chiral base and can catalyze a wide variety of organic transformations.
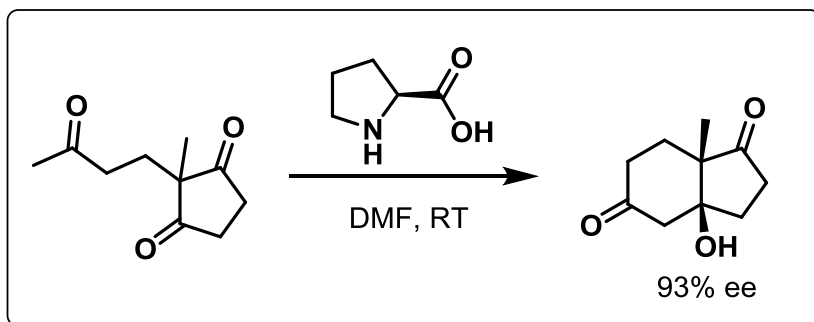

Figure 4. The Hajos–Parrish–Eder–Sauer–Wiechert reaction yields optically active bicyclic ketol starting from achiral starting material. L-Proline catalyzes this reaction and introduces the required chirality.

After these examples the interest in organocatalysis waned for a long time in favor of transition-metal catalysis. Transition-metal catalysis often involves toxic and/or

expensive metals and typically requires much more stringent conditions such as exclusion of oxygen. In the early 2000s, organocatalysis was re-discovered by List and co-workers who showed that the simple amino acid L-proline could catalyze aldol reactions.[16] Subsequently, proline was shown to be able to stereoselectively catalyze a wide variety of reactions, such as Mannich, aldol, Michael, and Knoevenagel reactions.[17] Drawbacks of proline catalysis are the high catalyst loading (typically, 10–20 mol%)[19] and low temperatures with concomitant long reaction times needed for reactions (reaction times of seven days are no exception). Improved proline-derived catalysts broadened the solvent scope and allowed lowering of the catalyst loading.[19, 20] One notable example is from the group of Wennemers, who found a tripeptide by elegant high-throughput screening. This tripeptide was able to catalyze the 1,4-addition of aldehydes to nitroolefins at low catalyst loading (1 mol%).[21]

The use of organocatalysis did not remain confined to the field of synthetic organic chemistry. In polymer chemistry, certain types of polymers can be produced using guanidine and amidine bases,[22] N-heterocyclic carbenes[23] and phosphines[24]. These organocatalysts give no asymmetric induction, but allow control over the polymerization rate and thus the resulting polymeric materials. Later in this thesis the polymerization of L-lactide is investigated in flow using an organocatalyst.

Solid-supported catalysis

Catalysis can be performed homogeneously (all reagents and reactants in the same phase) or heterogeneously. The use of homogeneous catalysis in flow is inherently wasteful, as the residence times are often short and the catalyst is therefore only used briefly before being quenched and collected. Furthermore, the (spent) catalyst must be removed from the crude reaction mixture which complicates both the workup of the product and recycling of the catalyst. The field of heterogeneous catalysis, in which catalysts are bound to a solid support, can be viewed as a field within solid-supported chemistry. Solid-supported chemistry is an enabling technology in combinatorial organic chemistry. It stands at the basis of solid-

supported nucleic acid and peptide synthesis. This and the related "catch-and-release" strategy have been thoroughly explored by Ley and Baxendale.[22] Over the years, many solid supports for attachments of catalysts have been investigated, such as polymeric materials (e.g. polystyrene) and silica. Several strategies have been devised, such as polymer brushes, monoliths, and cartridges filled with polymeric particles.

One of the best known solid-supported catalysts is palladium on carbon (Pd/C). Ouchi et al. used a commercially available flow reactor to achieve partial or full reduction of ethyl nicotinate. The reactor worked with an HPLC-like column with an internal volume of 12 mL, which was filled with the catalyst material. By passing the starting material over this column together with H_2 at elevated temperatures, the authors were able to obtain almost 2 kg of product per day.[25] Workup in this case was easy as only the volatile solvent had to be removed from the otherwise pure reaction yield.

Contrary to the well-known Pd/C catalyst which is bound onto the carbon support by non-covalent interactions, covalent attachment of other catalysts onto solid supports is often not trivial. Several solid supports have been used in continuous flow such as monoliths, (polymeric) nanocoatings, and microparticles (see Figure 5).[26] Glass or polymeric monoliths typically do not allow re-use of the chip, as the monolith will be fixed in place. The use of (polymeric) nanocoatings on the inner walls of the microchannel has been explored by the group of Verboom. Ricciardi et al. demonstrated the beneficial effect of neighbouring hydroxyl groups on the catalytic performance of sulfonic acid-containing polymer brushes.[27] These brushes are built up from two different monomers, 3-sulfopropyl methacrylate and 2-hydroxyethyl methacrylate. When 2-hydroxyethyl methacrylate was substituted with hydroxyl-free methyl methacrylate, the catalytic activity and stability dropped considerably. This also demonstrates the importance of (local) surface chemistry.
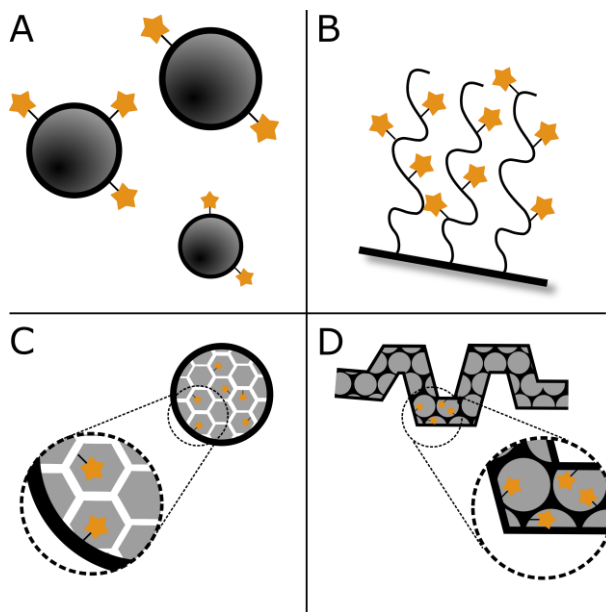
Figure 5: Types of solid supports. The star represents a catalyst. **A:** Monolayers on beads (polymeric or otherwise), **B:** polymer brushes on surfaces, **C:** mesoporous silica, with pores running through the material and **D:** monolithic solid support inside of a microchannel.

Nanocoatings of monolayers often do not give enough catalyst loading, unless when used in very specific cases. For the 1,2,3-triazole formation from azides and alkynes a copper tube was successfully used as the catalyst *and* reactor.[28] For most other catalysts, polymer brushes instead of monolayers are necessary to generate enough surface area and to ensure sufficient catalyst loading. Work by Costantini et al. showed that their polymer brush performed 150 times better than a monolayer of catalyst.[29] The preparation of polymer brushes in microfluidic devices, however, is not trivial as characterization requires breaking of the device and the catalyst loading is not very high.[29] This leads to long residence times and low reagent concentrations. Munirathinam et al. generated brushes of poly(glycidyl methacrylate) on the walls of their microreactor device. Subsequently, piperazine was attached *via* nucleophilic ring-opening of the epoxide moiety. This catalyst was then used in the Knoevenagel reaction between benzaldehyde (20–50 µM) and malonitrile (60 mM) at 90 °C and 5 bar pressure. Despite these forcing conditions the catalytic polymer brush was

stable for several days and led to good conversion of benzaldehyde. However, a thousand-fold excess of malonitrile was necessary to drive the reaction forward. Knoevenagel reactions with other active methylene compounds were investigated, but residence times had to be increased from 4 to 52 min to achieve good conversion, which is ten times slower compared to the same catalytic support using TBD as base.[29, 30] The rate of the Knoevenagel reaction is known to be solvent dependent.[29] However, the polymer brush needs to swell to expose enough catalyst, which limits the choice of solvent. The use of acetonitrile proved a reasonable compromise.

Work by Gill et al. shows the increased activity of a cobalt-catalyst for the hydrolytic kinetic resolution of epichlorohydrin when the catalyst is attached to polymer brushes on silica.[31] The cobalt-catalyst is thought to operate via a dual activation pathway where one Co^{III} site binds to the epoxide and another to the incipient hydroxide. The same catalyst, used homogeneously at 0.01% loading, gave less conversion than the solid-supported Co^{III} catalyst. The authors attribute this to the higher probability of site-site interaction in the polymer brush, basically deriving from an increase in the local concentration. These examples highlight the importance of careful tuning of surface composition and chemistry.

In this thesis, a packed-bed microreactor was used. For the microreactors, both monoliths and (polymeric) nanocoatings on the wall of the microreactor were deemed unsuitable as they do not allow flexible exchange of catalyst. The packed-bed microreactor chip was designed with microparticles as the solid-support in mind. This material is kept in a reservoir located on the microchip, through which the solvent with reagents is passed. The solid-supported catalyst is held in place by a frit yet can be removed after the flow reaction. The solid support must be of a specific size to prevent small particles from passing the frit and clogging of the channel downstream. A potential drawback of this packed-bed approach is that the packing of the particles is less than optimal due to differences in particles size. This imperfect packing may lead to uncontrolled fluid dynamics and stagnant zones, broadened residence times, reduced heat transfer coefficients, and formation of hot

or cold spots, effectively negating one of the advantages of microreactor technology (homogeneous reaction conditions).[32] The packed bed used in this thesis is relatively small (less than 300 μm in height). The microparticles are sieved before use to an appropriate size range. This sieving is done by hand, using metallic mesh sieves and decreases the difference between the largest and smallest particles. The packed bed will therefore be isothermal and the microreactor will keep its beneficial characteristics.[33] Several materials can be used for the microparticles, but typically polystyrene[34, 35] and silica[36, 37] are used.

Examples of packed-bed catalysis in flow are e.g. provided by Wiles and Watts, who demonstrate the use of gallium triflate, a strong Lewis acid, supported on polystyrene beads for the continuous flow Strecker reaction.[38] Starting from ketones and amines, they were able to produce up to tens of milligrams per hour (typically 50 mg h^{-1}) of material with excellent purity.

Alza et al. showed the use of L-proline-derived catalysts attached to a polystyrene support for continuous flow Mannich reactions.[34] The authors developed three closely related solid-supported proline catalysts and found that the presence of a 1,2,3-triazole moiety had a beneficial effect on the rate of the aldol reaction between a preformed imine and an aldehyde in *N*-dimethylformamide (DMF). DMF turned out to be the best solvent for this reaction, as it could efficiently swell the polymeric supports. However, DMF is a poor choice from a synthetic chemistry standpoint, as it is difficult to remove from the crude.

Nevertheless, it is known that polymeric supports are limited in solvent scope, as not all solvents equally swell the material to expose enough surface area. On the other hand, if the material swells too much, there is a chance of blocking the microreactor.[39] Often a balance has to be found between a good solvent for the support and a good solvent for the reaction. The limited solvent compatibility of polymeric materials can be reduced by synthesizing cross-linked polymer particles, however, we chose to avoid polymeric particles altogether. Instead, this thesis focuses on the application of mesoporous silica as a catalyst support.

Mesoporous silica is silica with pores having a diameter between 2 and 50 nm. The pores run through the entire length of the material and the silica does not need to swell to expose a large surface area, giving it a wider solvent compatibility. The most commonly used morphologies are MCM-41 and SBA-15, both of which have been used in this thesis.

Regardless of the solid support used, catalysts must be covalently attached to ensure the longevity and durability of the solid-supported catalyst. Several methods exists for attachment of organic monolayers onto oxide materials. During the course of this thesis we developed a novel method for the covalent modification of mesoporous silica.[40, 41]

Click chemistry

An ideal strategy to covalently attach catalysts to solid supports is click chemistry. Click chemistry is a concept in organic chemistry, best explained by the following excerpt from Kolb et al.:

"The reaction must be *modular, wide in scope*, give *very high yields*, generate only *inoffensive byproducts* that can be removed by non-chromatographic methods, and be *stereospecific* (but not necessarily enantioselective). The required process characteristics include *simple reaction conditions* (ideally, the process should be insensitive to oxygen and water), *readily available starting materials and reagents*, the use of *no solvent or a solvent that is benign* (such as water) *or easily removed*, and *simple product isolation.* Purification–if required–must be by non-chromatographic methods, such as crystallization or distillation, and the product must be stable under physiological conditions."[42]

The best known example of click chemistry was independently discovered by the laboratories of Sharpless and Meldal in 2002.[43, 44] The 1,3-dipolar cycloaddition between a 1,3-dipole and a dipolarophile was discovered in early twentieth century and was further explored in the 1960s by German chemist Rolf Huisgen. Rediscovered in the beginning of the twenty-first century, the 1,3-dipolar

cycloaddition of terminal alkynes (dipolarophile) and azides (1,3-dipole) catalyzed by copper is now one of the most ubiquitous reaction in organic chemistry.
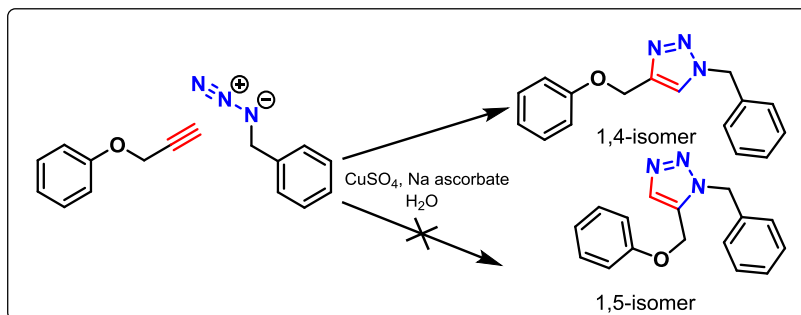

Figure 6. The copper-catalyzed 1,3-dipolar cycloaddition forms exclusively the 1,4-regioisomer of the 1,2,3-triazole, connecting both fragments. The 1,5-isomer is not formed under Cu^I-catalyzed conditions.

The reaction as investigated by Huisgen required heating the reactants at reflux and gave both the 1,4- and 1,5-regioisomer. However, in the presence of a suitable Cu^I source the reaction yields exclusively the 1,4-isomer of 1,2,3-triazole at room temperature (see Figure 6). The azide and alkyne are easily introduced into synthetic targets and mostly unreactive towards other functional groups. Furthermore, the reaction tolerates ambient conditions and is high yielding with no by-products. Given these properties, the copper-catalyzed azide-alkyne cycloaddition (CuAAC) is an ideal reaction for a wide variety of tasks and has made its way into materials science for end-group functionalization of polymers, modification of polymeric microparticles, ligation of larger molecules, bioconjugation, and dendrimer synthesis.[45-48] Despite other click chemistries being available, CuAAC is still in use today, with the work of Leibfarth et al. being a beautiful example of exploiting the CuAAC reaction to synthesize perfect, sequence-defined oligomers.[49]

Although CuAAC is a powerful technique, the use of copper impedes its application. Cu^I can be toxic and is a known catalyst. Residual Cu^I could interfere with solid-supported catalysis and is undesirable.

Soon after the discovery of CuAAC click chemistry, another long-forgotten reaction was resurrected: the thiol-ene reaction.[50] Thiols can react with terminal alkenes (and alkynes) under free-radical conditions forming stable thio-ether bonds (see Figure 7).[51] Thiol-ene click has been used in the synthesis of dendrimers, polymer coupling, and modification of mesoporous silica.[41, 45, 52] An initiator such as azobisisobutyronitrile (AIBN) is the source of radicals. The reaction proceeds with anti-Markovnikov stereochemistry. Use of a photo-initiator such as 2,2-dimethoxy-2-phenylacetophenone (DMPA) to provide radicals allows precise tuning of the timing and location of the reaction (photolithography). Another advantage is that no copper is used in the coupling reaction.
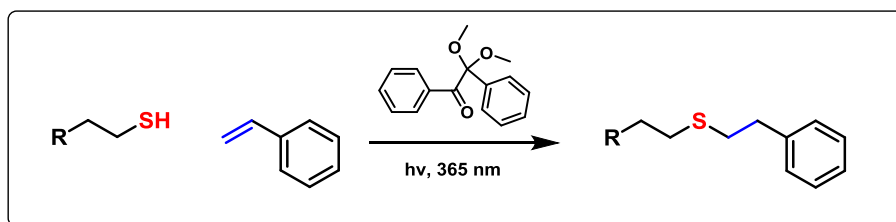

Figure 7. Typical photo-initiated free-radical thiol-ene coupling reaction, yielding a stable thio-ether linkage. 2,2-Dimethoxy-2-phenylacetophenone is used as the photo-initiator.

Expanding upon the click chemistry concept, more "click" reactions and transformations have since been identified. Reactions like strain-promoted azide-alkyne click chemistry (SPAAC) and inverse-electron demand Diels-Alder (IEDDA) reaction between tetrazines and strained alkenes have gained considerable attention.[53, 54] These fast click reactions (tetrazine–*trans*-cyclooctene IEDDA is among the fastest click-reactions known) require no external catalyst, making them very suitable for use in biological systems and materials where copper is not tolerated, such as biomedical applications or living systems.

Aim of the research

This thesis focuses on the application of catalysis in continuous flow. Methods for covalent immobilization of organic molecules (i.e., catalysts) on glass-like solid supports are investigated, as well as the use of these solid-supported materials in continuous flow. Heterogeneous and homogeneous catalysis in continuous flow are investigated for organic synthesis and polymer chemistry.

Outline of this thesis

In this thesis, the use of novel surface functionalization techniques is explored for the covalent attachment of catalysts onto solid supports. Both solid-supported and unsupported catalysis are examined in continuous flow for the synthesis of small molecules and polymers.

Silicon carbide (SiC) is a chemically inert and very robust material and is being used as a material for microreactors. Controlling the surface chemistry can be done by heating HF-etched surfaces in neat 1-alkenes for prolonged times. Functionalization of modified surfaces was mainly done through attachment of a labile acid fluoride onto the surface. It was therefore desirable to speed up the covalent modification of SiC and to introduce new functionalization strategies. In **chapter 2**, we show the covalent surface modification of SiC using 1-alkenes and 1,ω-dialkenes under microwave irradiation.

Mesoporous silica is another interesting catalyst support. This type of porous silica exists in many shapes and sizes but all of them share a common property: they have a large surface area per gram and are relatively chemically inert. Direct attachment of catalysts on mesoporous silica is not possible and therefore covalent surface modification is necessary. **Chapter 3** describes a new post-synthesis surface modification technique whereby the surface silanols react with 1,ω-alkenes, leaving the surface terminated with hydrophobic alkene groups. Those alkene groups can then be further modified using thiol-ene click chemistry.

Heterogeneous catalysis and continuous flow is a powerful albeit difficult combination. Solid-supported catalysts can potentially block microchannels and destroy microreactors. Furthermore, some microreactor setups are not compatible with (in)organic acids. However, acid catalysis has found widespread use in organic chemistry and has proven to be of significant interest. A solid-supported sulfonic acid is synthesized from mercaptopropyl-terminated mesoporous silica and investigated for the protection and deprotection of alcohols in **chapter 4**.

Due to their excellent heat transfer capabilities microreactors are well suited for exothermic polymerizations. Microreactors give precise control over residence time and the ability to quench the polymerization in a timely manner. The extremely rapid and sensitive ring-opening polymerization of L-lactide, catalyzed by 1,5,7-triazabicyclo[4.4.0]dec-5-ene, could benefit from these advantages. **Chapter 5** describes our efforts towards exploiting the characteristics of microreactor technology and organocatalysis for this ring-opening polymerization.

At the end of this thesis, **chapter 6** critically summarizes the results of this body of work and gives directions for future research.

References

[**1**] P. J. Nieuwland, K. Koch, N. van Harskamp, R. Wehrens, J. C. van Hest, F. P. Rutjes. Flash chemistry extensively optimized: high-temperature Swern-Moffatt oxidation in an automated microreactor platform. *Chem. - Asian J.* **2010,** *5* (4), 799-805.

[**2**] J. P. McMullen, K. F. Jensen. Integrated microreactors for reaction automation: new approaches to reaction development. *Annu. Rev. Anal. Chem.* **2010,** *3*, 19-42.

[**3**] P. Watts, C. Wiles. Micro reactors: a new tool for the synthetic chemist. *Org. Biomol. Chem.* **2007,** *5* (5), 727-732.

[**4**] S. G. Newman, L. Gu, C. Lesniak, G. Victor, F. Meschke, L. Abahmane, K. F. Jensen. Rapid Wolff–Kishner reductions in a silicon carbide microreactor. *Green Chem.* **2014,** *16* (1), 176-180.

[**5**] R. Srinivasan, I. M. Hsing, P. E. Berger, K. F. Jensen, S. L. Firebaugh, M. A. Schmidt, M. P. Harold, J. J. Lerou, J. F. Ryley. Micromachined reactors for catalytic partial oxidation reactions. *AlChE J.* **1997,** *43* (11), 3059-3069.

[**6**] G. M. Greenway, S. J. Haswell, D. O. Morgan, V. Skelton, P. Styring. The use of a novel microreactor for high throughput continuous flow organic synthesis. *Sens. Actuators, B* **2000,** *63* (3), 153-158.

[**7**] C. Wiles, P. Watts, S. J. Haswell, E. Pombo-Villar. The aldol reaction of silyl enol ethers within a micro reactor. *Lab Chip* **2001,** *1* (2), 100-101.

[**8**] X. Fu, S. Liu, X. Ruan, H. Yang. Research on staggered oriented ridges static micromixers. *Sens. Actuators, B* **2006,** *114* (2), 618-624.

[**9**] A. D. Stroock, S. K. W. Dertinger, A. Ajdari, I. Mezić, H. A. Stone, G. M. Whitesides. Chaotic Mixer for Microchannels. *Science* **2002,** *295* (5555), 647-651.

[**10**] B. P. Mason, K. E. Price, J. L. Steinbacher, A. R. Bogdan, D. T. McQuade. Greener Approaches to Organic Synthesis Using Microreactor Technology. *Chem. Rev.* **2007,** *107* (6), 2300-2318.

[**11**] I. R. Baxendale, J. Deeley, C. M. Griffiths-Jones, S. V. Ley, S. Saaby, G. K. Tranmer. A flow process for the multi-step synthesis of the alkaloid natural product oxomaritidine: a new paradigm for molecular assembly. *Chem. Commun.* **2006,** (24), 2566-2568.

[**12**] A. R. Bogdan, S. L. Poe, D. C. Kubis, S. J. Broadwater, D. T. McQuade. The Continuous-Flow Synthesis of Ibuprofen. *Angew. Chem., Int. Ed.* **2009,** *48* (45), 8547-8550.

[**13**] M. D. Hopkin, I. R. Baxendale, S. V. Ley. A flow-based synthesis of Imatinib: the API of Gleevec. *Chem. Commun.* **2010,** *46* (14), 2450-2452.

[**14**] J. P. McMullen, K. F. Jensen. Rapid Determination of Reaction Kinetics with an Automated Microfluidic System. *Org. Process Res. Dev.* **2011,** *15* (2), 398-407.

[**15**] J. Sedelmeier, S. V. Ley, I. R. Baxendale, M. Baumann. KMnO$_4$-Mediated Oxidation as a Continuous Flow Process. *Org. Lett.* **2010,** *12* (16), 3618-3621.

[**16**] B. List, R. A. Lerner, C. F. Barbas. Proline-Catalyzed Direct Asymmetric Aldol Reactions. *J. Am. Chem. Soc.* **2000,** *122* (10), 2395-2396.

[**17**] B. List. Proline-catalyzed asymmetric reactions. *Tetrahedron* **2002,** *58* (28), 5573-5590.

[**18**] H. Hiemstra, H. Wynberg. Addition of aromatic thiols to conjugated cycloalkenones, catalyzed by chiral ß-hydroxy amines. A mechanistic study of homogeneous catalytic asymmetric synthesis. *J. Am. Chem. Soc.* **1981,** *103* (2), 417-430.

[**19**] A. J. A. Cobb, D. M. Shaw, D. A. Longbottom, J. B. Gold, S. V. Ley. Organocatalysis with proline derivatives: improved catalysts for the asymmetric Mannich, nitro-Michael and aldol reactions. *Org. Biomol. Chem.* **2005,** *3* (1), 84-96.

[**20**] F. Giacalone, M. Gruttadauria, P. Agrigento, R. Noto. Low-loading asymmetric organocatalysis. *Chem. Soc. Rev.* **2012,** *41* (6), 2406-2447.

[**21**] M. Wiesner, J. D. Revell, H. Wennemers. Tripeptides as Efficient Asymmetric Catalysts for 1,4-Addition Reactions of Aldehydes to Nitroolefins–A Rational Approach. *Angew. Chem.* **2008,** *120* (10), 1897-1900.

[**22**] R. C. Pratt, B. G. G. Lohmeijer, D. A. Long, R. M. Waymouth, J. L. Hedrick. Triazabicyclodecene: A Simple Bifunctional Organocatalyst for Acyl Transfer and Ring-Opening Polymerization of Cyclic Esters. *J. Am. Chem. Soc.* **2006,** *128* (14), 4556-4557.

[**23**] A. P. Dove, H. Li, R. C. Pratt, B. G. G. Lohmeijer, D. A. Culkin, R. M. Waymouth, J. L. Hedrick. Stereoselective polymerization of *rac-* and *meso-*lactide catalyzed by sterically encumbered *N*-heterocyclic carbenes. *Chem. Commun.* **2006,** (27), 2881-2883.

[**24**] A. P. Dove. Organic Catalysis for Ring-Opening Polymerization. *ACS Macro Lett.* **2012,** *1* (12), 1409-1412.

[**25**] T. Ouchi, C. Battilocchio, J. M. Hawkins, S. V. Ley. Process Intensification for the Continuous Flow Hydrogenation of Ethyl Nicotinate. *Org. Process Res. Dev.* **2014,** *18* (11), 1560-1566.

[**26**] A. Kirschning, W. Solodenko, K. Mennecke. Combining enabling techniques in organic synthesis: continuous flow processes with heterogenized catalysts. *Chem. Eur. J.* **2006,** *12* (23), 5972-5990.

[**27**] R. Ricciardi, R. Munirathinam, J. Huskens, W. Verboom. Improved catalytic activity and stability using mixed sulfonic acid- and hydroxy-

bearing polymer brushes in microreactors. *ACS Appl. Mater. Interfaces* **2014,** *6* (12), 9386-9392.

[**28**] A. R. Bogdan, N. W. Sach. The Use of Copper Flow Reactor Technology for the Continuous Synthesis of 1,4-Disubstituted 1,2,3-Triazoles. *Adv. Synth. Catal.* **2009,** *351* (6), 849-854.

[**29**] F. Costantini, W. P. Bula, R. Salvio, J. Huskens, H. J. G. E. Gardeniers, D. N. Reinhoudt, W. Verboom. Nanostructure Based on Polymer Brushes for Efficient Heterogeneous Catalysis in Microreactors. *J. Am. Chem. Soc.* **2009,** *131* (5), 1650-1651.

[**30**] R. Munirathinam, J. Huskens, W. Verboom. Piperazine-Containing Polymer Brush Layer as Supported Base Catalyst in a Glass Microreactor. *J. Flow Chem.* **2014,** *4* (3), 135-139.

[**31**] C. S. Gill, K. Venkatasubbaiah, N. T. Phan, M. Weck, C. W. Jones. Enhanced cooperativity through design: pendant Co[III]-salen polymer brush catalysts for the hydrolytic kinetic resolution of epichlorohydrin (salen=N,N'-bis(salicylidene)ethylenediamine dianion). *Chem. Eur. J.* **2008,** *14* (24), 7306-7313.

[**32**] J. Wegner, S. Ceylan, A. Kirschning. Ten key issues in modern flow chemistry. *Chem. Commun.* **2011,** *47* (16), 4583-4592.

[**33**] A. Karim, J. Bravo, D. Gorm, T. Conant, A. Datye. Comparison of wall-coated and packed-bed reactors for steam reforming of methanol. *Catal. Today* **2005,** *110* (1-2), 86-91.

[**34**] E. Alza, C. Rodriguez-Escrich, S. Sayalero, A. Bastero, M. A. Pericas. A solid-supported organocatalyst for highly stereoselective, batch, and continuous-flow Mannich reactions. *Chem. Eur. J.* **2009,** *15* (39), 10167-10172.

[**35**] A. Bogdan, D. T. McQuade. A biphasic oxidation of alcohols to aldehydes and ketones using a simplified packed-bed microreactor. *Beilstein J. Org. Chem.* **2009,** *5*, 17.

[**36**] C. Wiles, P. Watts. Parallel synthesis in an EOF-based micro reactor. *Chem. Commun.* **2007,** (46), 4928-4930.

[**37**] N. Nikbin, P. Watts. Solid-Supported Continuous Flow Synthesis in Microreactors Using Electroosmotic Flow. *Org. Process Res. Dev.* **2004,** *8* (6), 942-944.

[**38**] C. Wiles, P. Watts. Solid-Supported Gallium Triflate: An Efficient Catalyst for the Three-Component Ketonic Strecker Reaction. *ChemSusChem* **2012,** *5* (2), 332-338.

[**39**] N. T. S. Phan, D. H. Brown, P. Styring. A facile method for catalyst immobilisation on silica: nickel-catalysed Kumada reactions in mini-continuous flow and batch reactors. *Green Chem.* **2004,** *6* (10), 526-532.

[**40**] S. P. Pujari, L. Scheres, A. T. M. Marcelis, H. Zuilhof. Covalent Surface Modification of Oxide Surfaces. *Angew. Chem., Int. Ed.* **2014,** *53* (25), 6322-6356.

[**41**] S. A. van den Berg, J. Tu, K. M. Sliedregt, A. Kros, T. Wennekes, H. Zuilhof. Clickable Mesoporous Silica via Functionalization with 1,ω-Alkenes. *Adv. Mater. Interfaces* **2014,** *1* (3), 1300061/1300061-1300061/1300061/1300065.

[**42**] H. C. Kolb, M. G. Finn, K. B. Sharpless. Click Chemistry: Diverse Chemical Function from a Few Good Reactions. *Angew. Chem., Int. Ed.* **2001,** *40* (11), 2004-2021.

[**43**] V. V. Rostovtsev, L. G. Green, V. V. Fokin, K. B. Sharpless. A Stepwise Huisgen Cycloaddition Process: Copper(I)-Catalyzed Regioselective "Ligation" of Azides and Terminal Alkynes. *Angew. Chem.* **2002,** *114* (14), 2708-2711.

[**44**] C. W. Tornøe, C. Christensen, M. Meldal. Peptidotriazoles on Solid Phase: [1,2,3]-Triazoles by Regiospecific Copper[I]-Catalyzed 1,3-Dipolar Cycloadditions of Terminal Alkynes to Azides. *J. Org. Chem.* **2002,** *67* (9), 3057-3064.

[**45**] P. Antoni, M. J. Robb, L. Campos, M. Montanez, A. Hult, E. Malmström, M. Malkoch, C. J. Hawker. Pushing the Limits for Thiol−Ene and CuAAC Reactions: Synthesis of a 6th Generation Dendrimer in a Single Day. *Macromolecules* **2010,** *43* (16), 6625-6631.

[**46**] M. Meldal. Polymer "Clicking" by CuAAC Reactions. *Macromol. Rapid Commun.* **2008,** *29* (12-13), 1016-1051.

[**47**] A. S. Goldmann, L. Barner, M. Kaupp, A. P. Vogt, C. Barner-Kowollik. Orthogonal ligation to spherical polymeric microparticles: Modular approaches for surface tailoring. *Prog. Polym. Sci.* **2012,** *37* (7), 975-984.

[**48**] A. S. Goldmann, M. Glassner, A. J. Inglis, C. Barner-Kowollik. Post-Functionalization of Polymers via Orthogonal Ligation Chemistry. *Macromol. Rapid Commun.* **2013,** *34* (10), 810-849.

[**49**] F. A. Leibfarth, J. A. Johnson, T. F. Jamison. Scalable synthesis of sequence-defined, unimolecular macromolecules by Flow-IEG. *Proc. Natl. Acad. Sci. U. S. A.* **2015,** *112* (34), 10617-10622.

[**50**] C. E. Hoyle, C. N. Bowman. Thiol–Ene Click Chemistry. *Angew. Chem., Int. Ed.* **2010,** *49* (9), 1540-1573.

[**51**] R. Hoogenboom. Thiol–Yne Chemistry: A Powerful Tool for Creating Highly Functional Materials. *Angew. Chem., Int. Ed.* **2010,** *49* (20), 3415-3417.

[**52**] M. A. Caipa Campos, J. M. Paulusse, H. Zuilhof. Functional Monolayers on Oxide-Free Silicon Surfaces via Thiol–ene Click Chemistry. *Chem. Commun.* **2010,** *46* (30), 5512-5514.

[**53**] J. Yang, J. Šečkutė, C. M. Cole, N. K. Devaraj. Live-Cell Imaging of Cyclopropene Tags with Fluorogenic Tetrazine Cycloadditions. *Angew. Chem., Int. Ed.* **2012,** *51* (30), 7476-7479.

[**54**] J. M. Baskin, J. A. Prescher, S. T. Laughlin, N. J. Agard, P. V. Chang, I. A. Miller, A. Lo, J. A. Codelli, C. R. Bertozzi. Copper-free click chemistry for dynamic in vivo imaging. *Proc. Natl. Acad. Sci. U. S. A.* **2007,** *104* (43), 16793-16797.

Chapter 2

Microwave-Assisted Formation of Organic Monolayers from 1-Alkenes on Silicon Carbide

Abstract. The rate of formation of covalently linked organic monolayers on HF-etched silicon carbide (SiC) is greatly increased by microwave irradiation. Upon microwave treatment for 60 min at 100 °C (60W), 1-alkenes yield densely packed, covalently attached monolayers on flat SiC surfaces, a process that typically takes 16 h at 130 °C under thermal conditions. This approach was extended to SiC microparticles. The monolayers were characterized by X-ray photoelectron spectroscopy and static water contact angle measurements. The microwave-assisted reaction is compatible with terminal functionalities, such as alkenes that enable subsequent versatile "click" chemistry reactions, further broadening the range and applicability of chemically modified SiC surfaces.

Introduction

Silicon carbide (SiC) is a material which is characterized by a combination of high mechanical robustness and chemical inertness, while additionally being biocompatible.[1-7] SiC is known for its use as structural material, as an abrasive, and more recently as a large-band gap semiconductor for high-performance microelectronic devices. The biocompatibility of SiC makes this material suitable as scaffold in a variety of biomedical applications.[4, 5, 7-9] The resulting highly versatile application of this material would thus be further enhanced by the ability to tune its surface properties, for instance using nanocoatings in the form of covalently bound monolayers. The chemical robustness of SiC, however, also hampers its functionalization with such coatings.[10] Consequently, only a few strategies exist to covalently apply monolayers on SiC, such as functionalization via silane chemistry[8] and radical-mediated attachment of 2,2'-azobis(isobutyronitrile).[11] Another strategy allows photochemical grafting of alkenes.[9, 12] Finally, our group pioneered the thermal grafting of alkenes and alkynes onto SiC.[13, 14] First, the oxide overlayer on SiC surfaces is removed by treating the surface with hydrofluoric acid (HF). Etching with HF also generates surface hydroxyl groups.[15] Alkenes react with these surface hydroxyl groups at relatively high temperatures (130–150 °C) by Markovnikov addition of surface hydroxyls to the C=C double bond, leading to densely packed monolayers (Scheme 1).[10] Rosso et al. showed that the chemical stability of these monolayers on SiC far exceeded those on silicon, silicon nitride and gold, as demonstrated by refluxing them at pH = -0.3 which left the monolayers intact.[13] In addition, the thermal stability of such monolayers is quite high (most of a C_{18} monolayer is still present at 280 °C).[16] In spite of their stability, the generation of these monolayers by current methods usually requires long reaction times to reach completion (16–24 h). To circumvent these long reaction times, and to expand the toolbox for SiC functionalization, we aimed to take advantage of another feature of SiC, namely its ability to efficiently absorb microwaves.[17, 18] The usefulness of microwaves for monolayer attachment has previously been demonstrated on flat Si(111) surfaces and porous hydrogen-terminated silicon.[19-21] We hypothesized that

microwave irradiation might also speed up the attachment of monolayers onto SiC significantly, due to localized heating of the SiC surface.
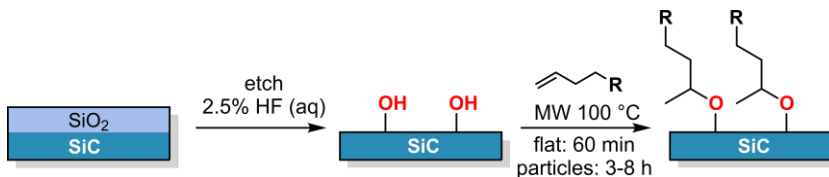
Scheme 1. Microwave-assisted formation of covalently linked organic monolayers onto SiC.

Results and Discussion

The contact angle increases with reaction time and already after 45 min the maximum contact angle of 106° is obtained (Figure 1A), matching reported contact angles indicative of disordered, but densely packed organic monolayers on SiC.[13] In order to get a detailed view of monolayer formation, the contribution of the Si-$\underline{C}$ (carbon from the substrate) and $\underline{C}$-C + $\underline{C}$-O (carbon from organic monolayer) carbon atoms were studied using XPS C1s narrow scans (Figure 1B). The ratio of ($\underline{C}$-C + $\underline{C}$-O)/Si-$\underline{C}$ increased with reaction time, indicating the formation of an organic monolayer. Overexposure to microwaves may lead to formation of multilayers as well. With reaction times above 60 min, no substantial change was observed in the carbon content from the organic monolayer, indicative of the completion of the attachment reaction. IRRAS measurements on modified substrates showed a CH_3 stretching band at 2960 cm^{-1}, and antisymmetric and symmetric stretching bands of CH_2 at 2924 and 2853 cm^{-1}, respectively (see Appendix 1, Figure S1). Such values are characteristic of disordered SiC-bound monolayers.[13]
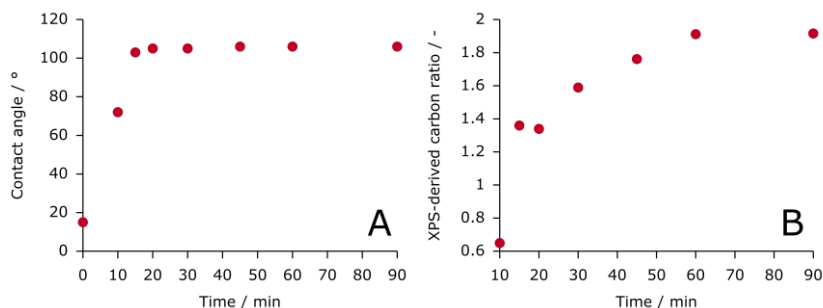
Figure 1. Microwave-assisted formation of a covalently bound 1-hexadecene-derived monolayer on SiC at 100 °C. **A:** Development of the static water contact angle (±1°). **B:** XPS-derived ($\underline{C}$-C +$\underline{C}$-O)/Si-$\underline{C}$ ratio versus reaction time (min).

The effect of reaction temperature on monolayer formation was studied by reacting HF-etched SiC surfaces with 1-hexadecene for 60 min at different temperatures. The static water contact angle reaches a plateau of 106° at reaction temperatures > 80 °C (see Appendix 1, Figure S8). In line with the XPS-observed increase of the carbon content up to 100 °C, the optimum reaction conditions for formation of high-quality alkene-derived organic monolayers on SiC surfaces under microwave irradiation were found to be 60 min at 100 °C. This is appreciably faster and milder than previously obtained for non-microwave-assisted heating (16 h at 160 °C; rate enhancement roughly 2-4 orders of magnitude, dependent on the SiC substrate).[14, 22]

In order to more directly study the effect of microwave assistance, two parallel experiments on SiC surfaces were carried out using 1-hexadecene for 60 min at 100 °C, respectively with and without microwave assistance (Figure 2). XPS C1s narrow scans show that monolayer formation is essentially complete after 1 h when employing microwave irradiation, whereas conventional thermal heating results in a much lower carbon attachment. The precise mechanism by which monolayers attach to SiC under the presently studied conditions is not known, but we tentatively attribute this significant rate enhancement to the efficient microwave absorption of SiC.
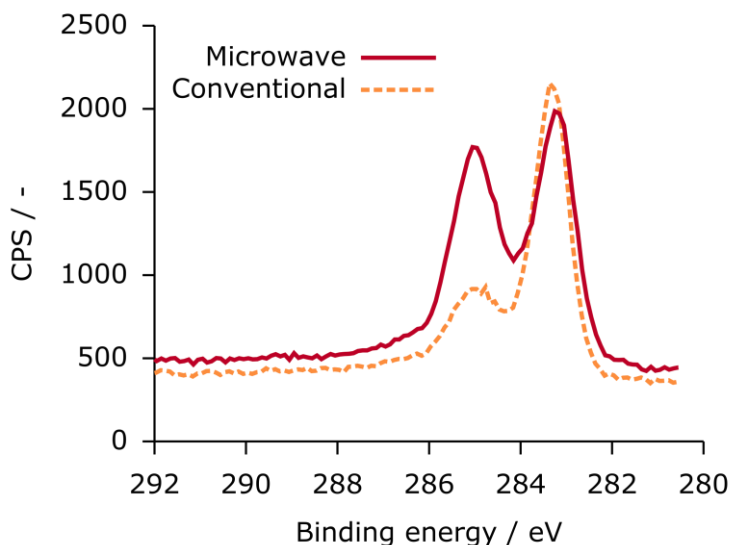
Figure 2. XPS C1s spectra displaying the efficacy of microwave-assisted heating on the formation of 1-hexadecene-derived monolayers onto SiC (100 °C, 60 min). Microwave assistance: solid red; conventional heating: dashed orange.

To further explore the scope of the microwave-assisted monolayer attachment, we turned to bi-functional monolayers and subsequent modifications. While with a few functional groups – such as epoxide and chlorine substituted alkenes – this procedure yielded highly disordered attachment chemistry (likely with substantial 'upside-down' attachment), ω-functionalized-1-alkenes with vinyl (CH=CH$_2$) moieties attached smoothly and in a regular fashion. Therefore the attachment of a range of 1,ω-dialkenes, especially 1,11-dodecadiene, was examined in more detail. These reactions allow subsequent surface-bound chemistry, especially thiol-ene click reactions, which can for instance be used to create patterned surfaces.[23, 24] Click-chemistry approaches are ideal follow-up reactions, due to their mild reaction conditions.[25]

Two SiC surfaces were modified under microwave assistance with 1,11-dodecadiene to give alkene-terminated surfaces. The resulting static water contact angle was found to be 92°, slightly below the contact angle of 96° reported for thermally

coupled tetradecadiene-modified Si(111).[26] The XPS C1s narrow scan spectrum (see Appendix 1, Figure S5) showed a large contribution from the attached carbon – since this was larger than expected for a monolayer, such as was strictly found for 1-hexadecene (*vide supra*), this likely indicates the formation of a covalently linked multilayer. Such multilayer formation has been observed before for UV-induced grafting of alkenes onto TiO_2.[27]

Subsequently, 1,11-dodecadiene-modified SiC surfaces were subjected to thiol-ene click chemistry using *1H,1H,2H,2H*-perfluorodecanethiol and DMPA as a photoinitiator under UV irradiation (365 nm; 120 min at room temperature). A conversion of 43% ± 2% was found for this substantially sized thiol (see SI for calculation). This value is lower than observed for thiol-ene click reactions on Si(111).[26] A potential discrepancy in calculation of this conversion might arise from the assumption that a monolayer is present, whereas XPS clearly shows multilayer formation on the SiC surface. Nevertheless, the modification is effective, as shown by the increase in the static water contact angle from 92° to 107°.

In the next step, the scope of the MW-assisted surface modification was extended to commercially available SiC microparticles. Prior to modification with 1,ω-dialkenes, SiC particles (microgrits and microspheres) were activated in aqueous HF (2.5%) for 12 min. Freshly etched particles were reacted with 1,ω-dialkenes under microwave irradiation. SiC microparticles require higher MW power (> 80 W) and longer reaction times (3–8 h) than flat SiC films to covalently attach an organic monolayer (Table S1). This may be related to the porosity and shape of the particles (Figure 3A), as previously found by Fernández-Rosas et al.[28] Nevertheless these conditions are substantially faster and milder than needed for non-microwave-assisted modification of SiC microparticles (65 h at 130 °C).
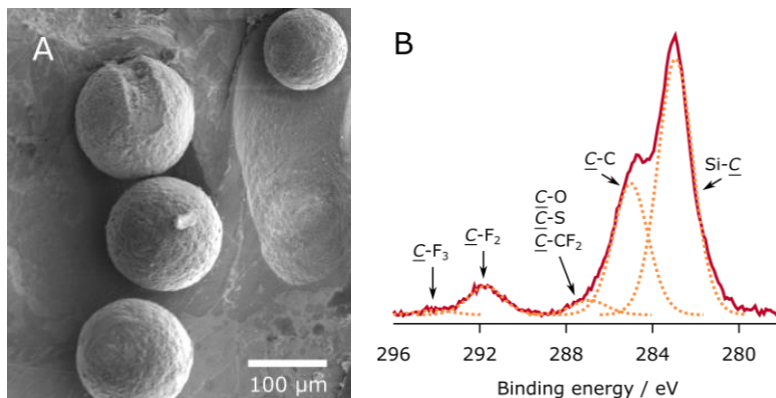
Figure 3. **A:** SEM image of SiC microspheres after thiol-ene functionalization. **B:** C1s narrow scan of 1,11-dodecadiene-functionalized SiC microspheres after thiol-ene coupling of *1H,1H,2H,2H*-perfluorodecanethiol.

XPS-derived thicknesses (Appendix 1, Table S2) suggest that surface modification of SiC microgrits with 1,7-octadiene produces multilayers (estimated length of 1,7-octadiene monolayer = 0.9 nm), whereas grafting 1,11-dodecadiene to microgrits and microspheres generates organic layers with thicknesses closer to a monolayer length (estimated to be 1.3 nm).[13] No sign of SiO_2 was found in XPS spectra after modification of microparticles. Subsequently, thiol-ene click reaction to ω-vinyl-functionalized SiC microgrits and microspheres was performed using *1H,1H,2H,2H*-perfluorodecanethiol and AIBN as radical initiator at 80 °C for 18 h[29] (Appendix 1, Table S3; Figure 3A; for SEM images with higher magnification, showing the surface morphology in detail, see Appendix 1, Figure S13-S15). The high-resolution C 1s XPS spectrum confirms the successful attachment of the fluorothiol to 1,11-dodecadiene-modified SiC microspheres, as seen by the peaks at 291.7 and 294.1 eV, which correspond to $-CF_2-$ and to $-CF_3$ groups, respectively (Figure 3B). The XPS-derived thickness had increased from 1.3 to 1.8 nm after thiol-ene functionalization.

An initial assessment of the hydrolytic stability of the grafted layers on the microspheres, analogous to what has previously been done for flat SiC surfaces,[14, 16] was carried out by immersing the fluorothiol-functionalized SiC microspheres in

PBS buffer (pH = 7.4) and in trifluoroacetic acid (TFA)-spiked trifluoroethanol (pH = 2) for one week. The F/Si ratio from the survey XPS spectrum decreased only ≈ 18% and ≈ 22% after exposure to PBS buffer and to TFA spiked trifluoroethanol respectively, confirming the high stability of SiC-bound monolayers, as this loss likely results predominantly from thio-ether cleavage.

Conclusion

Microwave assistance of the monolayer formation using 1-alkenes on silicon carbide surfaces speeds up the reaction to form densely packed monolayers, by two to four orders of magnitude. This methodology was also successfully extended to commercially available SiC microgrits and microspheres. Furthermore, by using 1,ω-dialkenes, this reaction permits easy access to "clickable" monolayers on SiC materials with complex structures. This will allow tuning and further covalent bio-functionalization of the surface and thereby unlock new applications for this material, which is currently under investigation.

Materials & Methods

Materials. Acetone (semiconductor grade VLSI PURANAL Honeywell 17617), tetrahydrofuran (Sigma-Aldrich, CHROMASOLV® Plus, for HPLC, ≥99.9%, inhibitor-free) *1H,1H,2H,2H*-perfluorodecanethiol (Sigma-Aldrich, 98%), 2,2-dimethoxy-phenylacetophenone (Sigma-Aldrich, 99%), 2,2′-Azobis-2-methylpropionitrile (Sigma-Aldrich, solution 0.2 M in toluene) and Milli-Q water (resistivity 18.3 MΩ cm) were used as received. Dichloromethane (CH_2Cl_2, Sigma-Aldrich, > 99.8%) was purified over aluminum oxide under argon using a Pure Solv 400 solvent purification system (Innovative Technology, Amesbury, USA). Hydrofluoric acid (HF, Merck, 40%) was diluted with deionized water to get a 2.5% solution. (Warning: hydrofluoric acid is an extremely corrosive acid: HF readily penetrates human skin, allowing it to destroy soft tissues and decalcify bone, and should be handled with extreme care!) Stoichiometric polycrystalline 3C-SiC films (thickness 183 nm, surface roughness determined with AFM 2.1 ± 0.2 nm)

were prepared by chemical vapor deposition (CVD) on Si(100).[30] SiC microgrits (CARBOREX F280, d_{s50} = 36.5 ± 1.5 μm) were obtained from Washington Mills Electro Minerals (Manchester, UK). SiC microspheres (d_{50} = 128 μm, total pore volume by Hg extrusion porosimetry = 0.46 mL/g) were provided by SICAT Catalyst (Willstät, Germany). 1-Hexadecene, 1,7-octadiene and 1,11-dodecadiene (Aldrich) were distilled under reduced pressure before use.

Preparation of Monolayers on HF-etched SiC. Pieces of SiC (1 × 1 cm) wafers were first rinsed several times with acetone (p.a. grade). These samples were sonicated for 5 min in acetone and then dried with a stream of inert gas. The samples were further cleaned using air plasma (Harrick PDC-002 setup) for 5 min. Subsequently, SiC substrates were etched in 2.5% aqueous HF solution for 2 min. After etching, the samples were thoroughly rinsed with Milli-Q water and finally blown dry with a stream of argon. These freshly etched and dried surfaces were then quickly transferred into a microwave reaction vial, which was charged with 2 mL of alkene inside an Ar filled glovebox and sealed with a crimp cap (see Appendix 1, Figure S16). The reaction vessel, containing a SiC surface or SiC particles and neat alkene, was allowed to react in the microwave (MW) system (Model CEM Discover, CEM Corporation, Charlotte, NC, USA) at a specific temperature and time at 60 W maximum microwave power. The microwave automatically adjusted the power output to maintain the set temperature (optimal conditions: 100 °C). After a set time (optimal conditions: 60 min), the modified samples were removed from the reaction vessel and immediately rinsed extensively with acetone and DCM, sonicated for 5 min in DCM to remove physisorbed molecules, and blown dry using a stream of argon. The modified surfaces were directly subjected to surface characterization unless specified otherwise.

SiC particles (microspheres and microgrits) were etched by immersion in 2.5% aqueous HF solution according to the following procedure: 1.5 min immersion in HF 2.5% solutions + 1 min sonication in HF 2.5% + 7.5 min immersion in HF 2.5% solution, rinsing with deionized water, sonication for 10 seconds in deionized water, rinsing in THF + 2 seconds sonication in THF, filtering and finally rinsing with

CH$_2$Cl$_2$, 2 seconds sonication and drying with a membrane pump at 50 °C for > 48 h.

Freshly activated SiC particles (100 mg) were loaded into a MW reaction vessel containing 1.5 mL of alkene inside an Ar filled glove box and reacted in the MW system at 150 W power at a defined temperature and time. Afterwards modified particles were rinsed thoroughly with DCM, dried and stored in glove box until further modification.

Thiol-ene click reaction

The thiol-ene reaction on flat SiC was performed using DMPA as photosensitizer, whereas the thiol-ene reaction on particles was performed using AIBN as a thermally-initiated radical source. This is because the SiC particles are not UV transparent, which is required for thiol-ene reactions using DMPA.

Flat SiC: One 1,11-dodecadiene-modified SiC surface was added to a solution of *1H,1H,2H,2H*-perfluorodecanethiol (0.13 mL, 0.45 mmol), 2,2-dimethoxy-phenylacetophenone (25 mg, 0.098 mmol) in DCM (2 mL). This solution was irradiated with 365 nm UV light for 120 min. The sample was taken out, rinsed extensively with DCM, sonicated in DCM and dried using a stream of nitrogen.

SiC particles: 20 mg of SiC microparticles (microgrits or microspheres) were added to the reaction flask containing AIBN (0.5 mL of 2M solution in toluene, 1 mmol) and *1H,1H,2H,2H*-perfluorodecanethiol (0.43 mL, 1.5 mmol) under continuous flow of Ar. The heterogeneous mixture was kept under Ar and heated at 80 °C for 18 h. The mixture was then cooled down to room temperature and diluted with DCM. Finally, the modified SiC particles were rinsed thoroughly with DCM, dried and stored in a glove box.

Monolayer Characterization

Contact Angle Measurements. Contact angle measurements were performed on a Krüss DSA 100 contact angle goniometer with an automated drop dispenser and image video capture system. The static contact angles of three small droplets of 3.0 μL volume of liquid, dispensed on modified silicon carbide surfaces with a microliter syringe with stainless steel needle (diameter = 0.51 mm), were determined using a Tangent 2 fitting model. The digital drop images were processed by the image analysis system, which calculated both the left and right contact angles from the drop shape with an accuracy of ±1.0°.

X-ray Photoelectron Spectroscopy (XPS). XPS measurements were performed using a JPS-9200 photoelectron spectrometer (JEOL, Japan). A monochromatic Al Kα X-ray source (hν = 1486.7 eV) at 12 kV and 20 mA and an analyzer pass energy of 10 eV were used. The base pressure in the chamber during measurements was 3×10^{-7} Torr, and spectra were collected at room temperature. The take-off angle φ (angle between sample and detector) of 80° is defined with a precision 1°. The typical sample size was 1×1 cm. XPS analysis of SiC particles was done in the same equipment using a twin-beam X-ray source (AlKα, 1436.2 eV) operated at 10 kV and 15 mA. All XPS spectra were evaluated using the CasaXPS software (version 2.3.15).

Calculation of thiol-ene click conversion. By taking a well-defined surface (Si(111)) with a monolayer derived from $C_{16}F_{17}$, we calculated the ratio of the F 1s peaks. Both samples were measured under the same conditions in the XPS instrument. The ratio was calculated by taking the area under the F 1s peak of the thiol-ene clicked SiC monolayer, divided by the area under the F 1s peak of the Si(111)-$C_{16}F_{17}$ monolayer. Because the fluorine-containing parts of both monolayers are on top of each monolayer, we can ignore electron attenuation effects, making it a fair comparison. Assuming equal monolayer density, this gives a value relative to the "ideal" fluorine containing monolayer, which in this case corresponded to approximately 43% of the F1s peak of a Si(111)-$C_{16}F_{17}$ monolayer.

Scanning Electron Microscopy (SEM). SEM images were captured using a field emission Auger microprobe (JAMP-9500F, JEOL Tokyo) operated at 10 kV with working distance fixed at 27 mm. Previous to SEM analysis the samples were coated with Au in a JEOL JFC-1300 Auto Fine Coater (Jeol Ltd., Tokyo, Japan).

Characterization of SiC microparticles. SEM images of freshly etched microgrits and microparticles are shown in Figure S5 and Figure S6 (see Appendix 1), respectively. XPS survey scans from freshly etched SiC particles display an oxygen content of 10.7% and 9.8% for microgrits and microspheres, respectively. These values are slightly higher than those reported for SiC films (~8%).[14, 31] In addition a small amount of F was observed in both materials (microgrits, 1.3%; microspheres 0.8%). High-resolution C1s spectra contained one peak at ~283 eV that belongs to Si–C (inorganic C) and Si-_C_-O$_x$ (oxycarbide species) at ~284 eV. Narrow scan data of the Si2p region show for both type of particles the peak corresponding to the bulk SiC at ~100 eV and a smaller signal at ~102 eV assigned to the silicon oxycarbide layer (Si-_C_-O$_x$) produced by the HF treatment. No contribution due to SiO$_2$ was detected at 103–104 eV.

XPS-derived thickness calculation. Thicknesses of layers on SiC particles were calculated from XPS electron attenuation using the following equation[31]

$$t = \lambda_{CH} \cos\theta \ln(1 + \frac{I_{CH}\rho_S\lambda_S}{I_S\rho_{CH}\lambda_{CH}})$$

where λ_{CH} = 2.8 nm is the attenuation length of C1s photoelectrons in alkyl monolayers,[32] and λ_S = 2.35 nm corresponds to the attenuation length of C1s photoelectrons in SiC.[33] θ is the takeoff angle between the surface plane and the detector and I_{CH} (_C_–C + _C_=C + _C_–O) and I_S (Si–_C_) are the intensities of the C1s narrow scan XPS signal from the organic film and from the substrate respectively. The ρ_{CH} and ρ_S are the elemental densities of carbon in the monolayer and in the SiC substrate and were estimated at 0.054 and 0.08 mol cm^{-3}, respectively.

The calculation of thicknesses of monolayers on microparticles and microgrits does not take into account effects of the particle size and shape. As noted by Sheng and Sutherland[34], for particles with a diameter < 1 micron, the application of the formula above leads to an overestimation of the thicknesses. The particles used in this study have much larger diameters (30 to 100 micron) and as such this effect will be smaller, yet we cannot fully rule out some degree of overestimation of the thicknesses. The data in Table S2 (see Appendix 1), however, does allow for comparison between particle samples.

Stability test of modified particles. Particles were immersed in PBS buffer (pH 7.4) or in trifluoroacetic acid (TFA) spiked trifluoroethanol (pH 2) for one week. After this time, the particles were rinsed extensively with Milli-Q water, THF and DCM, filtered and stored in a glovebox until XPS analysis.

References

[**1**] S. Sundararajan, B. Bhushan. Micro/Nanotribological Studies of Polysilicon and SiC Films for MEMS Applications. *Wear* **1998,** *217*, 251-261.

[**2**] W. J. Choyke, H. Matsunami, G. Pensl, *Silicon Carbide, Recent Major Advances*. Springer: Berlin, 2003.

[**3**] C. Sella, J. C. Martin, J. Lecoeur, A. Le Chanu, M. F. Harmand, A. Naji, J. P. Davidas. Biocompatibility and Corrosion Resistance in Biological Media of Hard Ceramic Coatings Sputter Deposited on Metal Implants. *Mater. Sci. Eng., A* **1991,** *139*, 49-57.

[**4**] S. Santavirta, M. Takagi, L. Nordsletten, A. Anttila, R. Lappalainen, Y. T. Konttinen. Biocompatibility of Silicon Carbide in Colony Formation Test In Vitro. *Arch. Orthop. Traum. Surg.* **1998,** *118*, 89-91.

[**5**] A. de Carlos, J. P. Borrajo, J. Serra, P. Gonzalez, B. Leon. Behaviour of MG-63 Osteoblast-Like Cells on Wood-Based Biomorphic SiC Ceramics Coated With Bioactive Glass. *J. Mater. Sci.: Mater. Med.* **2006,** *17* (6), 523-529.

[**6**] A. J. Rosenbloom, D. M. Sipe, Y. Shishkin, Y. Ke, R. P. Devaty, W. J. Choyke. Nanoporous SiC: A Candidate Semi-Permeable Material for Biomedical Applications. *Biomed. Microdevices* **2004,** *6* (4), 261-267.

[**7**] S. F. Cogan, D. J. Edell, A. A. Guzelian, Y. P. Liu, R. Edell. Plasma-Enhanced Chemical Vapor Deposited Silicon Carbide as an Implantable Dielectric Coating. *J. Biomed. Mater. Res., Part A* **2003,** *67A* (3), 856-867.

[**8**] E. H. Williams, A. V. Davydov, A. Motayed, S. G. Sundaresan, P. Bocchini, L. J. Richter, G. Stan, K. Steffens, R. Zangmeister, J. A. Schreifels, M. V. Rao. Immobilization of Streptavidin on 4H–SiC for Biosensor Development. *Appl. Surf. Sci.* **2012,** *258* (16), 6056-6063.

[**9**] G. Qin, R. Zhang, B. Makarenko, A. Kumar, W. Rabalais, J. M. Lopez Romero, R. Rico, C. Cai. Highly Stable, Protein Resistant Thin Films on SiC-Modified Silicon Substrates. *Chem. Commun.* **2010,** *46* (19), 3289-3291.

[**10**] S. P. Pujari, L. Scheres, A. T. M. Marcelis, H. Zuilhof. Covalent Surface Modification of Oxide Surfaces. *Angew. Chem., Int. Ed.* **2014,** *53* (25), 6322-6356.

[**11**] M. Iijima, H. Kamiya. Surface Modification of Silicon Carbide Nanoparticles by Azo Radical Initiators. *J. Phys. Chem. C* **2008,** *112* (31), 11786-11790.

[**12**] M. Steenackers, I. D. Sharp, K. Larsson, N. A. Hutter, M. Stutzmann, R. Jordan. Structured Polymer Brushes on Silicon Carbide. *Chem. Mater.* **2010,** *22* (1), 272-278.

[**13**] M. Rosso, A. Arafat, K. Schroën, M. Giesbers, C. S. Roper, R. Maboudian, H. Zuilhof. Covalent Attachment of Organic Monolayers to Silicon Carbide Surfaces. *Langmuir* **2008,** *24* (8), 4007-4012.

[**14**] S. P. Pujari, L. Scheres, T. Weidner, J. E. Baio, M. A. Stuart, C. J. van Rijn, H. Zuilhof. Covalently Attached Organic Monolayers onto Silicon Carbide From 1-Alkynes: Molecular Structure and Tribological Properties. *Langmuir* **2013,** *29* (12), 4019-4031.

[**15**] S. Dhar, O. Seitz, M. D. Halls, S. Choi, Y. J. Chabal, L. C. Feldman. Chemical Properties of Oxidized Silicon Carbide Surfaces upon Etching in Hydrofluoric Acid. *J. Am. Chem. Soc.* **2009,** *131* (46), 16808-16813.

[**16**] N. S. Bhairamadgi, S. P. Pujari, F. G. Trovela, A. Debrassi, A. A. Khamis, J. M. Alonso, A. A. Al Zahrani, T. Wennekes, H. A. Al-Turaif, C. van Rijn, Y. A. Alhamed, H. Zuilhof. Hydrolytic and Thermal Stability of Organic Monolayers on Various Inorganic Substrates. *Langmuir* **2014,** *30* (20), 5829-5839.

[**17**] C. O. Kappe. Unraveling the Mysteries of Microwave Chemistry Using Silicon Carbide Reactor Technology. *Acc. Chem. Res.* **2013,** *46* (7), 1579-1587.

[**18**] J. M. Kremsner, C. O. Kappe. Silicon Carbide Passive Heating Elements in Microwave-Assisted Organic Synthesis. *J. Org. Chem.* **2006,** *71* (12), 4651-4658.

[**19**] R. Boukherroub, A. Petit, A. Loupy, J.-N. Chazalviel, F. Ozanam. Microwave-Assisted Chemical Functionalization of Hydrogen-Terminated Porous Silicon Surfaces. *J. Phys. Chem. B* **2003,** *107* (48), 13459-13462.

[**20**] W. Sun, C. Qian, M. L. Mastronardi, M. Wei, G. A. Ozin. Hydrosilylation Kinetics of Silicon Nanocrystals. *Chem. Commun.* **2013,** *49* (97), 11361-11363.

[**21**] A. Petit, M. Delmotte, A. Loupy, J.-N. Chazalviel, F. Ozanam, R. Boukherroub. Microwave Effects on Chemical Functionalization of Hydrogen-Terminated Porous Silicon Nanostructures. *J. Phys. Chem. C* **2008,** *112* (42), 16622-16628.

[**22**] The reaction proceeds truly smoothly on some SiC substrates, but noticably slower on others (from different batches, typically produced by CVD methods), despite identical preactivion steps (HF etching) and resulting XPS spectrum. We have not found the source of this variation.

[**23**] C. Wendeln, S. Rinnen, C. Schulz, H. F. Arlinghaus, B. J. Ravoo. Photochemical Microcontact Printing by Thiol−Ene and Thiol−Yne Click Chemistry. *Langmuir* **2010,** *26* (20), 15966-15971.

[**24**] C. E. Hoyle, C. N. Bowman. Thiol–Ene Click Chemistry. *Angew. Chem., Int. Ed.* **2010,** *49* (9), 1540-1573.

[**25**] J. E. Moses, A. D. Moorhouse. The Growing Applications of Click Chemistry. *Chem. Soc. Rev.* **2007,** *36* (8), 1249-1262.

[**26**] M. A. Caipa Campos, J. M. Paulusse, H. Zuilhof. Functional Monolayers on Oxide-Free Silicon Surfaces via Thiol–ene Click Chemistry. *Chem. Commun.* **2010,** *46* (30), 5512-5514.

[**27**] R. Franking, R. J. Hamers. Ultraviolet-Induced Grafting of Alkenes to TiO2 Surfaces: Controlling Multilayer Formation. *J. Phys. Chem. C* **2011,** *115* (34), 17102-17110.

[**28**] E. Fernández-Rosas, A. Baldi, E. Ibañez, L. Barrios, S. Novo, J. Esteve, J. A. Plaza, M. Duch, R. Gómez, O. Castell, C. Nogués, C. Fernández-Sánchez. Chemical Functionalization of Polysilicon Microparticles for Single-Cell Studies. *Langmuir* **2011,** *27* (13), 8302-8308.

[**29**] L. M. Campos, K. L. Killops, R. Sakai, J. M. J. Paulusse, D. Damiron, E. Drockenmuller, B. W. Messmore, C. J. Hawker. Development of Thermal and Photochemical Strategies for Thiol−Ene Click Polymer Functionalization. *Macromolecules* **2008,** *41* (19), 7063-7070.

[**30**] C. S. Roper, V. Radmilovic, R. T. Howe, R. Maboudian. Single-Source Chemical Vapor Deposition of SiC Films in a Large-Scale Low-Pressure CVD Growth, Chemical, and Mechanical Characterization Reactor. *J. Electrochem. Soc.* **2006,** *153* (8), C562-C566.

[**31**] M. Rosso, M. Giesbers, A. Arafat, K. Schroën, H. Zuilhof. Covalently Attached Organic Monolayers on SiC and Si_xN_4 Surfaces: Formation Using UV Light at Room Temperature. *Langmuir* **2009,** *25* (4), 2172-2180.

[**32**] C. L. A. Lamont, J. Wilkes. Attenuation Length of Electrons in Self-Assembled Monolayers of *n*-Alkanethiols on Gold. *Langmuir* **1999,** *15* (6), 2037-2042.

[**33**] M. Krawczyk, L. Zommer, A. Kosiński, J. W. Sobczak, A. Jablonski. Measured Electron IMFPs for SiC. *Surf. Interface Anal.* **2006,** *38* (4), 644-647.

[**34**] E. Sheng, I. Sutherland. A quantitative XPS study of spherically shaped powders coated with an overlayer. *Surf. Sci.* **1994,** *314* (3), 325-330.

Chapter 3

Clickable Mesoporous Silica via Functionalization with 1,ω-Alkenes

Abstract. Tuning the surface properties of mesoporous silica is desirable for many applications, such as catalysis. We present a new modification method of calcined mesoporous silica, based on the thermal grafting of 1,7-octadiene. This easy method generates a high loading of terminal alkenes. We show that the modified surface is directly available for thiol-ene click chemistry, which enables a wide variety of molecules to be attached to this alkene-functionalized mesoporous silica.

Introduction

Mesoporous silica has attracted considerable attention in several areas of chemistry, such as in catalysis,[1, 2] drug delivery,[3-22] chromatography,[23] and purification of waste water.[24] Several methods exist to covalently attach an organic moiety to this material, such as co-condensation[25, 26] and post-synthesis grafting of organosilanes,[27, 28] alcohols,[29, 30] Grignard reagents,[31-33] and monosilazanes.[34] These methods each have one or more drawbacks that potentially limit functionalization and application of mesoporous silica, such as incomplete removal of templating agent, oligomer formation and subsequent pore blockage, the need to control the amount of water for reliable condensation, and/or harsh conditions.[27, 28, 30, 31, 34-36] We report here a novel route to functionalize the surface of mesoporous silica using alkene chemistry that is straightforward and potentially overcomes pore blockage.

Our group is investigating mesoporous silica as a solid support for catalysts. We envisaged a two-step strategy to covalently attach complex molecules to mesoporous silica. First, a well-defined monolayer is introduced onto the surface of mesoporous silica. This monolayer must contain a terminal moiety that allows further covalent attachment of polar or apolar molecules under high-yielding and mild reaction conditions. Click reactions are ideally suited, because of mild reaction conditions and large functional group tolerance. Recent examples of click chemistry for surface functionalization include azide-alkyne cycloadditions,[37-42] Staudinger ligation,[43, 44] tetrazine-cyclopropene reverse electron-demand Diels-Alder reactions[45] and thiol-ene[46-49] and thiol-yne radical couplings.[50-52]

Thiol-based radical coupling has recently established itself as a versatile, mild, high-yielding and easy technique in materials chemistry.[50-52] Our group has shown the use of thiol-ene[46] and thiol-yne[52] click chemistry to functionalize alkene-terminated monolayers on oxide-free silicon. In addition, we have demonstrated that 1-alkenes can form covalently attached monolayers on fused silica using ultra-violet light;[53] for a review, see Pujari et al.[54] However, this method cannot be used for mesoporous

silica as this material is not UV transparent at the required wavelength, so therefore a new approach was needed.
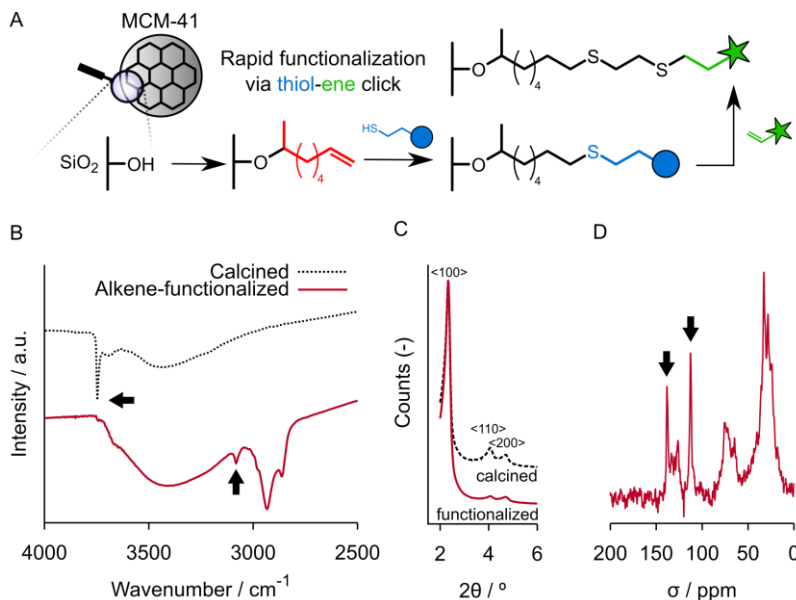

Figure 1. A: Overview of functionalization route of mesoporous silica with 1,7-octadiene, and subsequent versatile thiol-ene click reactions for highly functionalized silica. **B:** IR spectra of calcined (black line) and alkene-functionalized (red line) mesoporous silica. Arrows indicate silanol Si-OH stretch at 3740 cm^{-1} and vinylic C-H stretch at 3081 cm^{-1}. **C:** XRD spectra of calcined (dashed black) and alkene-functionalized (solid red) mesoporous silica, showing Bragg diffraction peaks characteristic of MCM-41-type silica. **D:** Solid-state ^{13}C NMR of alkene-functionalized mesoporous silica. Arrows indicate peaks belonging to vinyl carbons at 138 and 112 ppm.

In this paper, we present a new, straightforward and general method for the covalent functionalization of mesoporous silica based on this alkene chemistry (see Figure 1a). A thermal reaction with 1,7-octadiene was used to functionalize mesoporous silica with alkene moieties, which enables surface-bound thiol-ene coupling. The structure and loading of these functionalized nanomaterials was determined by X-ray photoelectron spectroscopy (XPS), solid-state ^{13}C NMR, FTIR, thermal gravimetric analysis (TGA) and X-ray diffraction (XRD). Finally, we show the versatility of alkene-terminated mesoporous silica by using multiple thiol-ene click

reactions to allow facile attachment of a complex molecule, namely quinine (Figure 2).

Results and Discussion

Calcined mesoporous silica was reacted with neat 1,7-octadiene at 100 °C for 24 h under argon to yield alkene-functionalized silica that showed a distinct vinylic C-H stretch at 3081 cm^{-1} in its infrared spectra (see Figure 1b).

In previous work, our group showed that covalent attachment of alkenes onto fused-silica slides using ultraviolet light occurs via Markovnikov addition involving surface silanols.[53] The sharp signal at 3740 cm^{-1} present in calcined, unfunctionalized mesoporous silica was attributed to isolated silanol stretching[55] and proved strongly decreased in the IR spectra of the functionalized silica, indeed suggesting a mode of attachment involving surface silanol groups. Mischki et al. have previously shown that the thermal addition of silanols across alkenes occurs, at least to some degree, via an acid-catalyzed Markovnikov addition mechanism.[56] We tentatively attributed the upcoming shoulder at 2970 cm^{-1} in the C-H region in the IR spectrum of 1,7-octadiene-functionalized mesoporous silica to the presence of a methyl group (Figure 1b), which suggests the presence of Markovnikov addition products under thermal conditions as well. This reaction is likely to be catalyzed by the acidity of isolated silanols, which have a pK_a of around 2.[57] To further confirm the presence of Markovnikov addition products, we functionalized mesoporous silica with 11-fluoro-1-undecene. Deconvolution of the peaks in the C-H region of 11-fluoro-1-undecene-functionalized mesoporous silica resulted in four contributions at 2860, 2908, 2934 and 2970 cm^{-1} (see Appendix 2, Figure S1), clearly displaying the methyl C-H stretching vibration at 2970 cm^{-1} which is absent in the spectrum of pure 11-fluoro-1-undecene. At present, however, we cannot rule out the presence of anti-Markovnikov addition products, although the reasonably low temperature of this reaction favors Markovnikov addition.[56]

XRD spectra of calcined and 1,7-octadiene-functionalized mesoporous silica show Bragg diffraction peaks corresponding to intact pores (see Figure 1c). The approximate pore diameter was calculated using a literature procedure, by subtracting the approximate wall thickness (10 Å) from the distance between pore centers, giving a value of 33.7 Å for both samples.[58]

To obtain a more detailed picture of the structure on the resulting particles, we performed solid-state ^{13}C NMR analysis of 1,7-octadiene-functionalized mesoporous silica. Specifically, we were interested in finding out to which degree the thermal treatment in the presence of silica induced isomerization and formation of a thermodynamically more stable internal alkene. The ^{13}C NMR data clearly showed the presence of terminal double bond carbon atoms visible at 138 and 112 ppm (see Figure 1c). The signal at 24 ppm was tentatively attributed to a methyl group, which supports a Markovnikov addition mechanism of 1,7-octadiene to surface silanols. The smaller signal at 127 ppm possibly indicates some isomerization to internal alkenes, but only for a small subset of terminal double bonds.[59] The proportion of internal alkenes in *cis* and *trans* conformation has not been established, however this is of little consequence as the *cis* isomer will rapidly isomerize to the slower reacting *trans* isomer under thiol-ene click reaction conditions.[60]

C1s XPS data of 1,7-octadiene-functionalized mesoporous silica showed a main peak at 285.0 eV and a shoulder at 287.5 eV, with a peak ratio of 7 : 1 (see Appendix 2, Figure S2). This is in line with formation of one C-O bond as implied by covalent Markovnikov addition of one of the alkene functional groups, and the obtained XPS energies matched those obtained with DFT calculations of the C1s energies of the indicated structure.[61] This result also implies that surface-attached alkenes do not react again to form "loops" in significant amounts, as the ratio of C-C : C-O would otherwise shift towards 6 : 2. Altogether, these measurements strongly suggested the formation of a methyl group upon functionalization of mesoporous silica with 1-alkenes, and a Markovnikov addition mechanism taking place, at least to an appreciable degree, under thermal conditions.

Thermal gravimetric analysis of 1,7-octadiene-functionalized mesoporous silica allowed for calculation of the organic content. Analysis showed a slow decrease in weight without sharp transitions over a large temperature range (200 to 900 °C). The overall weight loss was 23% and corresponds to a loading of 2.7 mmol/(g SiO$_2$) that rivals the loading of conventional organosilane-based functionalization methods, and compares favorably to the Grignard method.
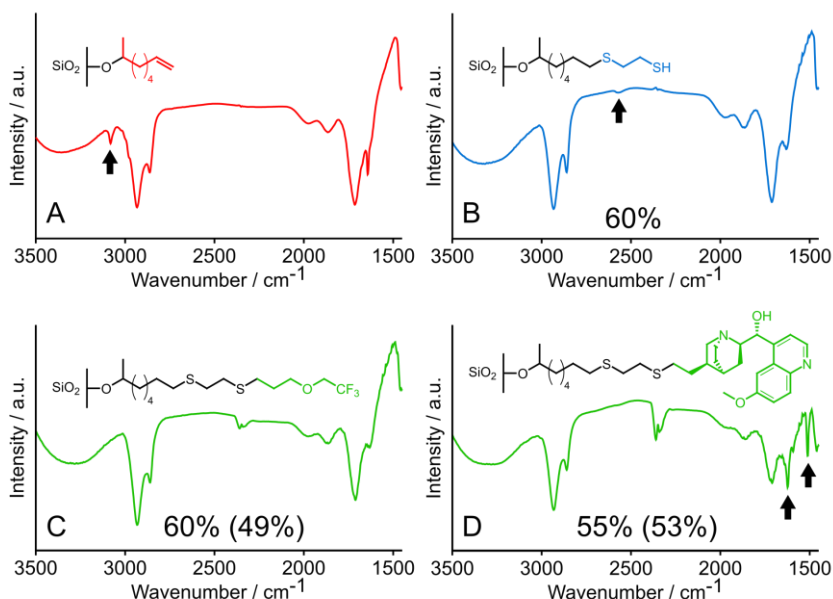

Figure 2. FTIR spectra of functionalized mesoporous silica with the corresponding structures as inset, with arrows indicating peaks discussed in text. **A:** 1,7-Octadiene-functionalized **B:** after thiol-ene click reaction of 1,7-octadiene-functionalized silica with 1,2-ethanedithiol. **C** and **D:** after thiol-ene click reaction of 1,2-ethanedithiol-functionalized silica with 3-(2,2,2-trifluoroethoxy)prop-1-ene (**C**) and quinine (**D**), respectively. Percentages indicate XPS-derived conversions of first and second (in parentheses) thiol-ene click reaction.

The formation of mesoporous silica covalently functionalized with terminal alkene moieties allows investigation of the potential of thiol-ene click chemistry to further modify mesoporous silica. To this aim, 1,7-octadiene-functionalized mesoporous silica was reacted with *1H,1H,2H,2H*-perfluorodecanethiol in the presence of a radical initiator, while irradiating with 365 nm UV light. The C1s XPS data for the

product indicated a yield of 60% for the thiol-ene click reaction. In line with this, the IR spectrum for this and all other clicked thiols showed no detectable vinyl C-H peak at 3081 cm^{-1}.

Thermal gravimetric analysis of the obtained silica showed a weight loss of 43%, which indicated that this material contains 0.95 mmol perfluorodecanethiol/(g SiO$_2$). This translated into in a yield of 35% for the thiol-ene click reaction. The difference in the yield calculated from the TGA and XPS results suggests that the monolayer at the inner pores of the material is not converted as efficiently, which may be due to steric hindrance inside the relatively small pores.

To extend the range of molecules that can be attached to include alkenes, 1,7-octadiene-functionalized mesoporous silica was reacted with 1,2-ethanedithiol to give thiol-terminated silica. The IR spectrum of 1,2-ethanedithiol-functionalized mesoporous silica (see Figure 2b) showed a weak absorption due to S-H stretching at 2550 cm^{-1}, while no vinylic C-H peak at 3081 cm^{-1}, belonging to the parent material, was detected. After washing with THF, *n*-hexane and dichloromethane, the thiol-terminated silica was reacted immediately with either 3-(2,2,2-trifluoroethoxy)prop-1-ene or quinine (Figure 2c and d, respectively). IR and XPS measurements confirmed that these subsequent thiol-ene reactions worked. In the case of reaction with quinine, after thorough washing of the silica, the IR spectrum displayed characteristic peaks for quinine (see Figure 2d; arrows indicate peaks at 1622 and 1512 cm^{-1}) yet did not show any residual vinylic peak at 3081 cm^{-1}, indicating covalent attachment to the silica via the H$_2$C=CH- bond of quinine. XPS analysis allowed for an estimation of the yields of these surface-bound thiol-ene click reactions, which were around 50%. Thermal gravimetric analysis showed a modest weight loss of 30% for these quinine-functionalized materials, indicating that probably the inner part of pores react less efficiently. These modest yields are possibly due to the layer thickness in comparison to the pore diameter. The layer thickness of quinine-functionalized silica was estimated by measuring the length of the energy-minimized structure. The approximate length of this structure (Figure 2d) is 25 Å, which is in the same size range as the pore diameter (33.7 Å). Thus, steric

hindrance is expected to play a role in these relatively small pores. Functionalization of mesoporous silica with larger pores is currently under investigation.
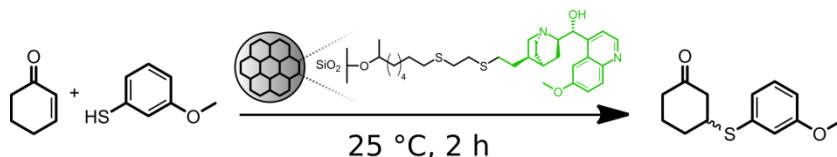
Scheme 1. Catalytic activity of quinine-modified mesoporous silica in the thio-Michael addition reaction.

Overall, however, the three operationally simple and generally applicable reaction steps allowed the covalent attachment of a complex molecule to mesoporous silica.

Quinine-functionalized mesoporous silica was tested for catalytic activity in the thio-Michael addition of 3-methoxythiophenol to 2-cyclohexen-1-one (see Scheme 1).[62] Without catalyst, no conversion was observed within 2 h under these reaction conditions. Addition of 1 mol% of quinine resulted in full conversion to the thio-Michael addition product, according to ^{1}H NMR. Addition of 12 mg quinine-functionalized mesoporous silica (approximately 1 micromol quinine; see Appendix 2) gave 75% conversion in 2 h, which showed that the covalently attached quinine is catalytically active. A further experiment even showed that the quinine-functionalized silica is similarly active compared to its soluble counter-part.[63] Furthermore, an added benefit of this solid-supported catalyst is easy workup by filtration and initial experiments also showed recyclability. To make use of these properties, we filled a fritted glass capillary with $\approx$ 1 mg of the quinine-functionalized silica. A 0.1 M solution of 2-cyclohexen-1-one and 3-methoxythiophenol in CDCl$_3$ was pumped via microfluidic connections through this capillary at 5 µL/min. After collecting the output for 60 min, conversion was measured by ^{1}H NMR, yielding quantitative conversion of 3-methoxythiophenol. This demonstrates that the quinine-functionalized silica can also be used under continuous flow conditions. Use and further development of these and related materials for surface-bound organocatalysis are currently ongoing.

Conclusion

In summary, 1-alkenes can be used for the facile covalent functionalization of mesoporous silica, with high loadings that are comparable to or better than other methods. This allows the one-step modification of mesoporous silica with functionalized alkenes such as 1,7-octadiene. In addition, surface-bound thiol-ene click reactions were demonstrated on 1,7-octadiene-functionalized mesoporous silica, allowing the attachment of thiols using thiol-ene click chemistry. In case dithiols are used, complex alkenes such as quinine can be attached in a second follow-up thiol-ene click reaction. Quinine-functionalized mesoporous silica was shown to be catalytically highly active in the thio-Michael addition reaction. This approach opens up a wide range of extremely mild and versatile functionalizations of mesoporous silica, which is currently under investigation.

Materials and Methods

Materials. 1,7-Octadiene (99.4% (GC-MS)), *1H,1H,2H,2H*-perfluorodecanethiol (97%), 1,2-ethanedithiol (98%), 3-methoxythiophenol (98%), 2-cyclohexen-1-one (> 98%), 2,2-dimethoxy-2-phenylacetophenone (DMPA, 99%), undec-10-en-1-ol (98%), 18-crown-6 (99%), methanesulfonyl chloride (> 99%), potassium fluoride (> 99.0%) and 2,2,2-trifluoroethanol (> 99%) were purchased from Sigma-Aldrich. Allyl bromide (> 98.0%) was purchased from Fluka. Tetrahydrofuran (THF) (99%) and *n*-hexane (> 95%) were purchased from VWR. Dichloromethane (Sigma-Aldrich, > 99.8%) was purified using a Pure Solv 400 solvent purification system (Innovative Technology, Amesbury, USA).

11-Fluoro-1-undecene,[64] 3-(2,2,2-trifluoroethoxy)prop-1-ene[65] and mesoporous silica[3] were prepared according to literature procedures.

Modification of mesoporous silica. In a typical experiment, mesoporous silica (200 mg) was cleaned by calcination at 500 °C for 6 h. The resulting powder was transferred to an oven-dried, 50 mL round-bottomed flask, fitted with Teflon sleeves and a reflux condenser, and put under an argon atmosphere. 1,7-Octadiene was

degassed by sparging with argon for 1.5 h, and 5.0 mL (34 mmol) was added to the silica. The resulting suspension was heated in an oil bath at 100 °C for 24 h under argon. After this time, the slurry was allowed to cool to room temperature, after which it was diluted with THF and transferred onto a fritted glass funnel. The functionalized mesoporous silica was rinsed successively with 10 mL THF, 10 mL *n*-hexane, and 10 mL dichloromethane before allowing it to dry overnight at room temperature.

Thiol-ene click chemistry. In a typical experiment, DMPA (12 mg, 47 mmol), *1H,1H,2H,2H*-perfluoro-decanethiol (100 μL, 349 μmol) and 1.0 mL dichloromethane were added to 57 mg of alkene-terminated mesoporous silica. The suspension was sparged for 2 min using argon and then irradiated for 120 min using a 6W 365 nm UV lamp placed at a distance of 3 cm. After this time, the powder was transferred onto a fritted glass funnel and rinsed with dichloromethane (10 mL). The powder was dried for 2 h under vacuum before further analysis.

The thiol-ene click reaction with 1,2-ethanedithiol was performed in a similar way as above, but the workup was a bit more elaborate to avoid exposure to 1,2-ethanedithiol. The fritted glass funnel was put on a Büchner flask filled with aqueous sodium hypochlorite. The vacuum hose of the Büchner flask was connected to a wet scrubber filled with aqueous sodium hypochlorite. Vacuum was applied carefully and the silica was rinsed extensively with tetrahydrofuran and dichloromethane. After rinsing and drying on the fritted funnel, the silica was quickly transferred to a new vial for the subsequent thiol-ene click reaction with quinine.

Characterization. Transmission infrared spectra were taken with a Bruker Tensor 27 FTIR spectrometer, equipped with an MCT detector cooled with liquid nitrogen. This setup was combined with a Hyperion 2000 microscope accessory, using a sodium chloride crystal as support for the powders. XPS spectra were obtained using a Jeol JPS-9200 and a twin-beam X-ray source (AlKα, 1436.2 eV) operating at 10 kV and 15 mA. Spectra were processed using CasaXPS 2.3.15. A Shirley-type

background subtraction was used for peak integration. Thermal gravimetric analysis (TGA) was performed on a PerkinElmer Pyris STA6000, heating from 30 to 900 °C at a rate of 10 °C min^{-1}. Powders were dried at 120 °C for 16 h prior to thermal gravimetric analysis. X-ray diffraction measurements were performed on a Panalytical X'Pert Pro diffractometer using nickel-filtered Cu Kα radiation (λ = 0.1541 nm, tube settings 40 kV and 40 mA). Solid-state CP/MAS ^{13}C spectra were obtained using a Bruker DMX400 spectrometer equipped with a 4 mm triple-resonance CP/MAS probe at a spinning frequency of 10.5 kHz.

Quinine-catalyzed thio-Michael addition. A stock solution of 3-methoxy-thiophenol (0.35 mL, 2.8 mmol) and 2-cyclohexen-1-one (0.30 mL, 3.1 mmol) was made in 6 mL CDCl$_3$. This solution was divided over three vials. To one of the vials was added quinine-modified mesoporous silica (12 mg, approximately 0.001 mmol). To another vial was added quinine (3.2 mg, 0.01 mmol). The remaining vial served as blank. The three vials were shaken in an incubator at 25 °C for 2 h. Conversion was determined by ^{1}H NMR analysis.

Quinine-catalyzed thio-Michael addition in flow. A stock solution of 3-methoxy-thiophenol (9.6 μL, 0.08 mmol) and 2-cyclohexen-1-one (10. 0 μL, 0.1 mmol) was made in 1 mL CDCl$_3$. This solution was pumped through a glass capillary containing ≈ 1 mg of the quinine-functionalized silica. After equilibration for 10 min, the output was collected for 60 min. Conversion was determined by ^{1}H NMR analysis.

Approximation of quinine loading on mesoporous silica. The approximate loading of quinine-functionalized mesoporous silica was estimated as follows: TGA showed a weight loss of 30% for the quinine-functionalized silica. This means that per gram of quinine-functionalized silica, the silica host weighs 700 mg. This 700 mg would contain 0.7 · 2.7 mmol g^{-1} = 1.9 mmol alkene-chains, which weighs 1.9 · 110 = 208 mg. Of the 300 mg organic content, 92 mg is due to the dithiol and the quinine. Assuming that the conversion of the dithiol click reaction is the same as the conversion of the perfluorodecanethiol click reaction, namely 35%, this means that

one gram of quinine-functionalized silica contains $1.9 \cdot 0.35 = 0.67$ mmol dithiol; this weighs 63 mg. This leaves $300 - 208 - 63 = 29$ mg of organic content due to the quinine, which is 0.089 mmol per gram of quinine-functionalized mesoporous silica. Running a quinine-catalyzed reaction with 12 mg quinine-functionalized mesoporous silica resulted in a conversion of 75% after 2 h. Running a quinine-catalyzed reaction with a similar amount of quinine (1 micromol), we obtained 68% conversion by ^{1}H NMR, confirming that our estimation is valid.

References

[**1**] H.-T. Chen, B. G. Trewyn, J. W. Wiench, M. Pruski, V. S. Y. Lin. Urea and Thiourea-Functionalized Mesoporous Silica Nanoparticle Catalysts with Enhanced Catalytic Activity for Diels–Alder Reaction. *Top. Catal.* **2009,** *53* (3-4), 187-191.

[**2**] S. L. Hruby, B. H. Shanks. Acid–base cooperativity in condensation reactions with functionalized mesoporous silica catalysts. *J. Catal.* **2009,** *263* (1), 181-188.

[**3**] F. Porta, G. E. M. Lamers, J. I. Zink, A. Kros. Peptide modified mesoporous silica nanocontainers. *Phys. Chem. Chem. Phys.* **2011,** *13* (21), 9982-9982.

[**4**] F. Porta, G. E. M. Lamers, J. Morrhayim, A. Chatzopoulou, M. Schaaf, H. den Dulk, C. Backendorf, J. I. Zink, A. Kros. Folic Acid-Modified Mesoporous Silica Nanoparticles for Cellular and Nuclear Targeted Drug Delivery. *Adv. Healthc. Mater.* **2013,** *2* (2), 281-286.

[**5**] P. Nadrah, F. Porta, O. Planinsek, A. Kros, M. Gaberscek. Poly(propylene imine) dendrimer caps on mesoporous silica nanoparticles for redox-responsive release: smaller is better. *Phys. Chem. Chem. Phys.* **2013,** *15* (26), 10740-10748.

[**6**] S. Angelos, E. Johansson, J. F. Stoddart, J. I. Zink. Mesostructured silica supports for functional materials and molecular machines. *Adv. Funct. Mater.* **2007,** *17* (14), 2261-2271.

[**7**] M. Liong, S. Angelos, E. Choi, K. Patel, J. F. Stoddart, J. I. Zink. Mesostructured multifunctional nanoparticles for imaging and drug delivery. *J. Mater. Chem.* **2009,** *19* (35), 6251-6257.

[**8**] J. Blechinger, A. A. Torrano, R. Herrmann, A. T. Bauer, S. W. Schneider, A. Reller, C. Brauchle. Uptake Kinetics, Uptake Pathways and Cytotoxicity of SiO_2-Nanoparticles Interacting with HeLa and HUVEC Cells. *Biophys. J.* **2011,** *100* (3), 469-469.

[**9**] V. Cauda, A. Schlossbauer, T. Bein. Bio-degradation study of colloidal mesoporous silica nanoparticles: Effect of surface functionalization with organo-silanes and poly(ethylene glycol). *Microporous Mesoporous Mat.* **2010,** *132* (1-2), 60-71.

[**10**] F. Feil, V. Cauda, T. Bein, C. Brauchle. Direct Visualization of Dye and Oligonucleotide Diffusion in Silica Filaments with Collinear Mesopores. *Nano Lett.* **2012,** *12* (3), 1354-1361.

[**11**] N. M. Khashab, A. Trabolsi, Y. A. Lau, M. W. Ambrogio, D. C. Friedman, H. A. Khatib, J. I. Zink, J. F. Stoddart. Redox- and pH-Controlled Mechanized Nanoparticles. *Eur. J. Org. Chem.* **2009,** (11), 1669-1673.

[**12**] Z. X. Li, J. C. Barnes, A. Bosoy, J. F. Stoddart, J. I. Zink. Mesoporous silica nanoparticles in biomedical applications. *Chem. Soc. Rev.* **2012,** *41* (7), 2590-2605.

[**13**] Y. S. Lin, C. P. Tsai, H. Y. Huang, C. T. Kuo, Y. Hung, D. M. Huang, Y. C. Chen, C. Y. Mou. Well-ordered mesoporous silica nanoparticles as cell markers. *Chem. Mater.* **2005,** *17* (18), 4570-4573.

[**14**] J. Lu, M. Liong, J. I. Zink, F. Tamanoi. Mesoporous silica nanoparticles as a delivery system for hydrophobic anticancer drugs. *Small* **2007,** *3* (8), 1341-1346.

[**15**] J. M. Rosenholm, E. Peuhu, L. T. Bate-Eya, J. E. Eriksson, C. Sahlgren, M. Linden. Cancer-Cell-Specific Induction of Apoptosis Using Mesoporous Silica Nanoparticles as Drug-Delivery Vectors. *Small* **2010,** *6* (11), 1234-1241.

[**16**] E. Ruiz-Hernandez, A. Baeza, M. Vallet-Regi. Smart Drug Delivery through DNA/Magnetic Nanoparticle Gates. *ACS Nano* **2011,** *5* (2), 1259-1266.

[**17**] A. Schlossbauer, S. Warncke, P. M. E. Gramlich, J. Kecht, A. Manetto, T. Carell, T. Bein. A Programmable DNA-Based Molecular Valve for Colloidal Mesoporous Silica. *Angew. Chem., Int. Ed.* **2010,** *49* (28), 4734-4737.

[**18**] I. Slowing, B. G. Trewyn, V. S. Y. Lin. Effect of surface functionalization of MCM-41-type mesoporous silica nanoparticles on the endocytosis by human cancer cells. *J. Am. Chem. Soc.* **2006,** *128* (46), 14792-14793.

[**19**] I. Slowing, J. L. Vivero-Escoto, B. G. Trewyn, V. S. Y. Lin. Mesoporous silica nanoparticles: structural design and applications. *J. Mater. Chem.* **2010,** *20* (37), 7924-7937.

[**20**] M. Vallet-Regi, E. Ruiz-Hernandez. Bioceramics: From Bone Regeneration to Cancer Nanomedicine. *Adv. Mater.* **2011,** *23* (44), 5177-5218.

[**21**] M. Vallet-Regi, I. Izquierdo-Barba, M. Colilla. Structure and functionalization of mesoporous bioceramics for bone tissue regeneration and local drug delivery. *Philos. Trans. R. Soc. A-Math. Phys. Eng. Sci.* **2012,** *370* (1963), 1400-1421.

[**22**] J. Zhang, Z. F. Yuan, Y. Wang, W. H. Chen, G. F. Luo, S. X. Cheng, R. X. Zhuo, X. Z. Zhang. Multifunctional Envelope-Type Mesoporous Silica Nanoparticles for Tumor-Triggered Targeting Drug Delivery. *J. Am. Chem. Soc.* **2013,** *135* (13), 5068-5073.

[**23**] A. Katiyar, S. Yadav, P. G. Smirniotis, N. G. Pinto. Synthesis of ordered large pore SBA-15 spherical particles for adsorption of biomolecules. *J. Chromatogr. A* **2006,** *1122* (1-2), 13-20.

[**24**] X. Feng. Functionalized Monolayers on Ordered Mesoporous Supports. *Science* **1997,** *276* (5314), 923-926.

[**25**] F. Hoffmann, M. Cornelius, J. Morell, M. Fröba. Silica-based mesoporous organic-inorganic hybrid materials. *Angew. Chem., Int. Ed.* **2006,** *45* (20), 3216-3251.

[**26**] M. Etienne, B. Lebeau, A. Walcarius. Organically-modified mesoporous silica spheres with MCM-41 architecture. *New J. Chem.* **2002,** *26* (4), 384-386.

[**27**] S. Kumari, B. Malvi, A. K. Ganai, V. K. Pillai, S. Sen Gupta. Functionalization of SBA-15 Mesoporous Materials using "Thiol–Ene Click" Michael Addition Reaction. *J. Phys. Chem. C* **2011,** *115* (36), 17774-17781.

[**28**] J. J. Cras, C. A. Rowe-Taitt, D. A. Nivens, F. S. Ligler. Comparison of chemical cleaning methods of glass in preparation for silanization. *Biosens. Bioelectron.* **1999,** *14* (8-9), 683-688.

[**29**] C. Pathmamanoharan, A. P. Philipse. Preparation of Small Alkane-Grafted Silica Particles (for SAXS and SANS Studies) from Aqueous Commercial Sols. *J. Colloid Interface Sci.* **1994,** *165* (2), 519-521.

[**30**] G. C. Ossenkamp, T. Kemmitt, J. H. Johnston. Toward Functionalized Surfaces through Surface Esterification of Silica. *Langmuir* **2002,** *18* (15), 5749-5754.

[**31**] A. Ramírez, L. Sierra, B. Lebeau, J.-L. Guth. Formation of Si–H groups during the functionalization of mesoporous silica with Grignard reagents. *Microporous Mesoporous Mat.* **2007,** *98* (1-3), 115-122.

[**32**] K. Yamamoto, T. Tatsumi. Organic functionalization of mesoporous molecular sieves with Grignard reagents. *Microporous Mesoporous Mat.* **2001,** *44-45*, 459-464.

[**33**] S. Angloher, J. Kecht, T. Bein. Metal−Organic Modification of Periodic Mesoporous Silica: Multiply Bonded Systems. *Chem. Mater.* **2007,** *19* (23), 5797-5802.

[**34**] T. Deschner, Y. Liang, R. Anwander. Silylation Efficiency of Chorosilanes, Alkoxysilanes, and Monosilazanes on Periodic Mesoporous Silica. *J. Phys. Chem. C* **2010,** *114* (51), 22603-22609.

[**35**] J. Kecht, T. Bein. Functionalization of colloidal mesoporous silica by metalorganic reagents. *Langmuir* **2008,** *24* (24), 14209-14214.

[**36**] J. H. Clark, D. J. Macquarrie. Catalysis of liquid phase organic reactions using chemically modified mesoporous inorganic solids. *Chem. Commun.* **1998,** (8), 853-860.

[**37**] C. Haensch, T. Erdmenger, M. W. M. Fijten, S. Hoeppener, U. S. Schubert. Fast Surface Modification by Microwave Assisted Click Reactions on Silicon Substrates. *Langmuir* **2009,** *25* (14), 8019-8024.

[**38**] T. Lummerstorfer, H. Hoffmann. Click Chemistry on Surfaces: 1,3-Dipolar Cycloaddition Reactions of Azide-Terminated Monolayers on Silica. *J. Phys. Chem. B* **2004,** *108* (13), 3963-3966.

[**39**] A. Schlossbauer, D. Schaffert, J. Kecht, E. Wagner, T. Bein. Click Chemistry for High-Density Biofunctionalization of Mesoporous Silica. *J. Am. Chem. Soc.* **2008,** *130* (38), 12558-12559.

[**40**] R. Manova, T. A. van Beek, H. Zuilhof. Surface Functionalization by Strain-Promoted Alkyne–Azide Click Reactions. *Angew. Chem., Int. Ed.* **2011,** *50* (24), 5428-5430.

[**41**] J. Nakazawa, T. D. P. Stack. Controlled Loadings in a Mesoporous Material: Click-on Silica. *J. Am. Chem. Soc.* **2008,** *130* (44), 14360-14361.

[**42**] P. Riente, J. Yadav, M. A. Pericàs. A Click Strategy for the Immobilization of MacMillan Organocatalysts onto Polymers and Magnetic Nanoparticles. *Org. Lett.* **2012,** *14* (14), 3668-3671.

[**43**] E. Saxon, J. I. Armstrong, C. R. Bertozzi. A ''Traceless'' Staudinger Ligation for the Chemoselective Synthesis of Amide Bonds. *Org. Lett.* **2000,** *2* (14), 2141-2143.

[**44**] M. Köhn, R. Breinbauer. The Staudinger Ligation—A Gift to Chemical Biology. *Angew. Chem., Int. Ed.* **2004,** *43* (24), 3106-3116.

[**45**] J. Yang, J. Šečkutė, C. M. Cole, N. K. Devaraj. Live-Cell Imaging of Cyclopropene Tags with Fluorogenic Tetrazine Cycloadditions. *Angew. Chem., Int. Ed.* **2012,** *51* (30), 7476-7479.

[**46**] M. A. Caipa Campos, J. M. J. Paulusse, H. Zuilhof. Functional monolayers on oxide-free silicon surfaces via thiol-ene click chemistry. *Chem. Commun.* **2010,** *46* (30), 5512-5514.

[**47**] A. T. Dickschat, F. Behrends, M. Buhner, J. Ren, M. Weiss, H. Eckert, A. Studer. Preparation of bifunctional mesoporous silica nanoparticles by orthogonal click reactions and their application in cooperative catalysis. *Chem. Eur. J.* **2012,** *18* (52), 16689-16697.

[**48**] Y. Kotsuchibashi, M. Ebara, T. Aoyagi, R. Narain. Fabrication of doubly responsive polymer functionalized silica nanoparticles via a simple thiol–ene click chemistry. *Polym. Chem.* **2012,** *3* (9), 2545.

[**49**] M. L. Chen, J. Zhang, Z. Zhang, B. F. Yuan, Q. W. Yu, Y. Q. Feng. Facile preparation of organic-silica hybrid monolith for capillary hydrophilic liquid chromatography based on "thiol-ene" click chemistry. *J. Chromatogr. A* **2013,** *1284*, 118-125.

[**50**] M. J. Kade, D. J. Burke, C. J. Hawker. The power of thiol-ene chemistry. *J. Polym. Sci., Part A: Polym. Chem.* **2010,** *48*, 743-750.

[**51**] J. Zhang, Y. Chen, M. A. Brook. Facile Functionalization of PDMS Elastomer Surfaces Using Thiol–Ene Click Chemistry. *Langmuir* **2013**.

[**52**] N. S. Bhairamadgi, S. Gangarapu, M. A. Caipa Campos, J. M. J. Paulusse, C. J. M. van Rijn, H. Zuilhof. Efficient Functionalization of

Oxide-Free Silicon(111) Surfaces: Thiol–yne versus Thiol–ene Click Chemistry. *Langmuir* **2013,** *29* (14), 4535-4542.

[**53**] J. ter Maat, R. Regeling, M. Yang, M. N. Mullings, S. F. Bent, H. Zuilhof. Photochemical Covalent Attachment of Alkene-Derived Monolayers onto Hydroxyl-Terminated Silica. *Langmuir* **2009,** *25* (19), 11592-11597.

[**54**] S. P. Pujari, L. Scheres, A. T. M. Marcelis, H. Zuilhof. Covalent Surface Modification of Oxide Surfaces. *Angew. Chem., Int. Ed.* **2013**.

[**55**] S. A. Mirji, S. B. Halligudi, N. Mathew, V. Ravi, N. E. Jacob, K. R. Patil. Adsorption of methanol on Si(100)/SiO$_2$ and mesoporous SBA-15. *Colloids Surf., A* **2006,** *287* (1-3), 51-58.

[**56**] T. K. Mischki, R. L. Donkers, B. J. Eves, G. P. Lopinski, D. D. M. Wayner. Reaction of Alkenes with Hydrogen-Terminated and Photooxidized Silicon Surfaces. A Comparison of Thermal and Photochemical Processes. *Langmuir* **2006,** *22* (20), 8359-8365.

[**57**] J. M. Rosenholm, T. Czuryszkiewicz, F. Kleitz, J. B. Rosenholm, M. Lindén. On the Nature of the Brønsted Acidic Groups on Native and Functionalized Mesoporous Siliceous SBA-15 as Studied by Benzylamine Adsorption from Solution. *Langmuir* **2007,** *23* (8), 4315-4323.

[**58**] M. Grün, I. Lauer, K. K. Unger. The synthesis of micrometer- and submicrometer-size spheres of ordered mesoporous oxide MCM-41. *Adv. Mater.* **1997,** *9* (3), 254-257.

[**59**] P. M. Słomkiewicz. Isomerization of linear alkenes on Amberlyst 15. *Appl. Catal., A* **2006,** *301* (2), 232-240.

[**60**] T. M. Roper, C. A. Guymon, E. S. Jönsson, C. E. Hoyle. Influence of the alkene structure on the mechanism and kinetics of thiol-alkene photopolymerizations with real-time infrared spectroscopy. *J. Polym. Sci., Part A: Polym. Chem.* **2004,** *42* (24), 6283-6298.

[**61**] M. Giesbers, A. T. M. Marcelis, H. Zuilhof. Simulation of XPS C1s Spectra of Organic Monolayers by Quantum Chemical Methods. *Langmuir* **2013,** *29* (15), 4782-4788.

[**62**] K. A. Fredriksen, T. E. Kristensen, T. Hansen. Combined bead polymerization and Cinchona organocatalyst immobilization by thiol–ene addition. *Beilstein J. Org. Chem.* **2012,** *8*, 1126-1133.

[**63**] Performing the homogenous reaction with 1 micromol of quinine resulted in a conversion of 68% in 2 h.

[**64**] Q.-Y. Sun, L. C. P. M. de Smet, B. van Lagen, M. Giesbers, P. C. Thüne, J. van Engelenburg, F. A. de Wolf, H. Zuilhof, E. J. R. Sudhölter. Covalently Attached Monolayers on Crystalline Hydrogen-Terminated Silicon: Extremely Mild Attachment by Visible Light. *J. Am. Chem. Soc.* **2005,** *127* (8), 2514-2523.

[**65**] J. A. S. Smith, B. J. Brisdon, S. A. Brewer, C. R. Willis. Synthesis of model organosiloxanes containing perfluoroetheroside-chains. *J. Mater. Chem.* **2000,** *10* (8), 1765-1769.

Chapter 4

Continuous-Flow Alcohol Protection and Deprotection Reactions Catalyzed by Silica-Supported Sulfonic Acid

Abstract. Alcohol protection and deprotection reactions, catalyzed by solid-supported sulfonic acid, have been investigated under continuous flow conditions. Primary, secondary, benzylic and phenolic alcohols can be protected under these conditions by tetrahydropyranyl and several silyl ether moieties, generating synthetically useful amounts of material in short time. Furthermore, the described setup can be used to deprotect protected alcohols and be used in selective protection reactions. Because the solid-supported acid catalyst is continually re-used in a packed-bed approach, workup is greatly simplified and in most cases only solvent removal is necessary, while reaching high turn-over numbers.

Introduction

Flow chemistry has been an emerging technology in the past decade, allowing access to non-conventional process windows, in turn enabling new reactions or improving existing methodologies.[1] The combination of solid-supported catalysts and continuous flow is a logical step and has been applied successfully in a number of cases.[2, 3] Purification of the crude reaction mixture is simplified because removal of the catalyst is not necessary. The catalyst remains in the packed bed of the microreactor and is therefore continually recycled.

The field of solid-supported catalysis in continuous flow is relatively new. Several solid supports have been used in continuous flow, including silica, polymer beads and polymer brushes.[4-6] Examples of catalysts include solid-supported Lewis and Brønsted acids in an electro-osmotic flow reactor and sulfonic acid and 1,5,7-triazabicyclo[4.4.0]dec-5-ene grafted onto polymer brushes anchored to microchannel walls.[7-9] Brønsted acids, such as sulfonic acids, are especially versatile catalysts as they catalyze a wide variety of reactions, such as esterifications, condensations and hydrolyses. Verboom and co-workers employed polymer brushes modified with sulfonic acid groups and demonstrated a synergistic effect of neighboring hydroxyl groups on several acid-catalyzed reactions, such as the deprotection of benzaldehyde dimethyl acetal to form benzaldehyde and the deprotection of benzyl THP ether to benzyl alcohol.[8] However, the reactions in that study were carried out at relatively low concentrations (10 to 30 mM), complicating their further development for production of relevant amounts.

Because of their frequent use in organic synthesis it is of significant interest to study acid-catalyzed alcohol protection reactions.[10] To make this of practical interest for use in flow, a high reaction efficacy needs to be obtained at relatively high concentrations (typically 1 M of alcohol). Common alcohol protection groups are, for instance, tetrahydropyranyl and trimethylsilyl groups. In batch chemistry, a wide variety of catalysts has been successfully applied to alcohol trimethylsilyl ether protection reactions.
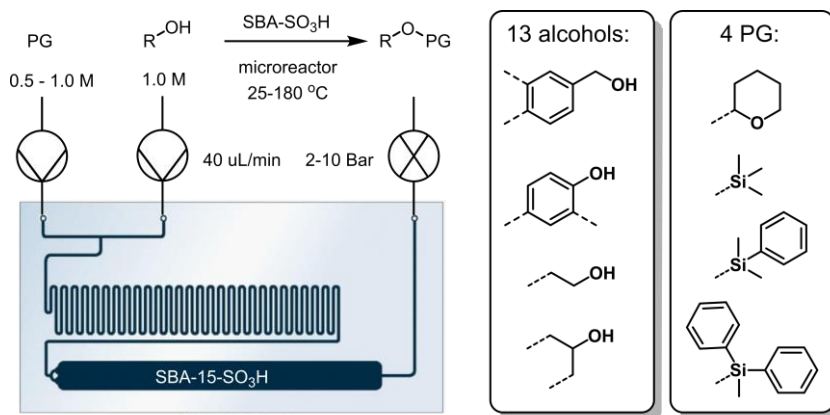
Scheme 1. Left: schematic setup of the flow reactor with mesoporous silica acid catalyst, showing the reactions that are performed in this microreactor. The microreactor used in this work consists of a meandering channel (5 μL volume) and a packed bed (35 μL volume when empty). **Right:** Substrate scope of the reactions.

For instance, Atghia and co-workers used montmorillonite clay to catalyze the trimethylsilylation of alcohols in good yields and relatively short reactions times.[11] Fu *et al.* show both the protection and deprotection of alcohols using 1,1,1,3,3,3-hexamethyldisilazane (HMDS) and montmorillonite clay.[12] Saidi and Azizi demonstrate the use of solid $LiClO_4$ for the same reaction under solvent-free conditions.[13] The reaction is also known to be catalyzed by silica-supported sulfonic acids.[14] We hypothesized that it would be possible to conduct these reactions in continuous flow using solid-supported sulfonic acids. Mesoporous SBA-15 silica was chosen as a solid support because silica, unlike polymeric materials, does not need to swell to expose a large surface area, giving it a wider solvent compatibility.

In this work, we report alcohol protection reactions, carried out in a commercially available continuous-flow system (Chemtrix Labtrix Start) using a solid-supported sulfonic acid catalyst. We investigated four alcohol protection and deprotection reactions (tetrahydropyranylation and silylations) in this setup on a variety of alcohols at high concentrations (1 M alcohol; see Scheme 1). Additionally, we studied the role of the catalyst in more detail and its use for selective alcohol

protection and deprotection reactions. The data presented in this work shows that using this packed-bed flow setup and catalyst it is possible to access synthetically relevant amounts of various types of protected alcohols in a short time.

Results and Discussion

Tetrahydropyranylation of alcohols in continuous flow. The protection of benzyl alcohol **1** to the tetrahydropyranyl derivative **1a** (see Scheme 1) was chosen as the first model reaction to allow comparison of our setup with previously published work.[7] The packed-bed microreactor (see Scheme 1) was filled with silica-supported sulfonic acid. Using 1.5 equivalents of 3,4-dihydro-*2H*-pyran (DHP) and a total flow rate of 20 μL/min, the conversion of benzyl alcohol was > 98% at reaction temperatures ranging from 25 to 75 °C, and nearly pure **1a** was formed. Increasing the flow rate to 80 μL/min still gave good conversion of benzyl alcohol (> 98% as measured by GC). Next, the amount of DHP was lowered to equimolar amounts at a flow rate of 40 μL/min; this retained the same high conversion. Encouraged by these results, a scale-out was performed at a benzyl alcohol concentration of 2 M, a flow rate of 60 μL/min and a temperature of 35 °C. The output of the microreactor was collected for 20 min and after evaporation of solvent gave 0.23 g nearly pure THP-protected benzyl alcohol. Small amounts of byproduct (≈ 2%) were detected by GC, which are tentatively ascribed to DHP oligomerization. These byproducts were easily removed by automated silica column chromatography (gradient from 0% to 10% ethyl acetate in petroleum ether). This result can be extrapolated to a productivity of 0.69 g product per hour, which is fourteen times higher than previously reported by Wiles et al. for a comparable setup (50 mg/h of **1a** in an electro-osmotic flow reactor with four parallel channels).[7]

We next investigated the scope of this tetrahydropyranylation protection reaction with a selection of alcohols. The primary alcohol 10-undecen-1-ol gave full conversion under similar conditions as benzyl alcohol. For a sterically more demanding secondary alcohol, *endo*-borneol **3**, high conversions (85–90%) could still be achieved, but required a slightly elevated temperature (optimal temperature

75 °C; see Appendix 4, Figure S1). This is in line with results reported previously by others.[15]

During these experiments, the packed bed acquired a darker color, which had no negative influence on the overall conversion of the reaction, but hinted at DHP oligomerization. The packed bed could be re-used for at least five reactions over several days, without need to replace the silica, and on average turn-over numbers of 200 were obtained in the scaled-out reaction.

Trimethylsilylation of alcohols in continuous flow. For a second model reaction, the formation of trimethylsilyl ethers was investigated as an example of another relevant common alcohol protection group. We assessed that trimethylsilylation through an acid-catalyzed reaction of alcohols with 1,1,1,3,3,3-hexamethyldisilazane (HMDS) would be a good candidate for evaluation in flow chemistry, as this method is atom efficient: one molecule of HMDS is able to trimethylsilylate two hydroxyl groups, generating only gaseous NH_3 as a byproduct.

Table 1. Optimization of the model reaction: Formation of trimethylsilyl ether **1b** from benzyl alcohol and HMDS. Solvent in all cases was dichloromethane.

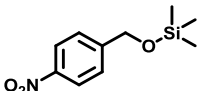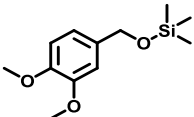| Entry	Temperature (°C)	Flow rate (µL/min)	HMDS (eq)	Conversion (%)
1	25	20	1	75[a,b]
2	50	20	1	93[a,b]
3	75	20	1	99[a,b]
4	50	20	0.6	> 99[c,d]
5	50	40	0.6	98[c,d]
6	60	40	0.6	> 99[c,d]
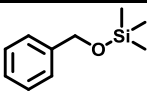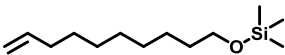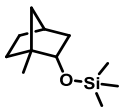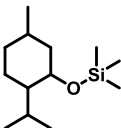
[a]Relative peak area of product versus total peak area of product plus starting material, as determined by GC-MS. [b]Amount of catalyst in packed bed was 4.0 mg. [c]Amount of catalyst in packed bed was 5.8 mg. [d]Conversion determined using internal standard.
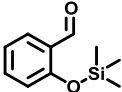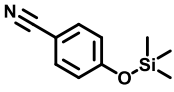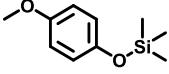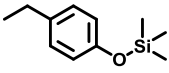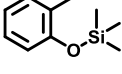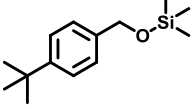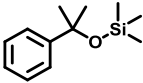
Benzyl alcohol **1** was reacted with HDMS in dichloromethane under continuous flow conditions (see Scheme 1) to give the trimethylsilyl ether derivative **1b**. Using an excess of HMDS, the reaction proceeded to approximately 75% conversion at room temperature with a flow rate of 20 µL/min. Increasing the temperature to 50 °C gave near-quantitative conversion of benzyl alcohol. Lowering the amount of

HMDS to 0.6 equivalents with respect to benzyl alcohol and using more catalyst in the packed bed resulted again in near-quantitative conversion (Table 1, entry 5). Doubling the flow rate to 40 μL/min resulted in residual benzyl alcohol, however, this was solved by increasing the temperature to 60 °C, to yield **1b** at a rate of 210 mg/h.

Table 2. Investigation of substrate scope for the trimethylsilylation of alcohols in continuous flow under optimized reaction conditions (60 °C, flow rate 40 μL/min, 1 M alcohol, 0.6 eq HMDS, solvent: dichloromethane).

Entry	Product		[HMDS] (M)	Yield (mg)[a]
1	**1b**		0.6	102 (94%)[b]
2	**2b**		0.6	140 (93%)[b]
3	**3b**		0.6	124 (93%)[b]
4	**4b**		0.6	128 (93%)[b]
5	**5b**		0.6	132 (98%)[b]
6	**6b**		0.51	45 (94%)[b,c]

7	**7b**		0.6	n.i. (99%)[d]
8	**8b**		0.75	n.i. (90%)[e]
9	**9b**		0.51	110 (95%)[b]
10	**10b**		0.51	108 (95%)[b]
11	**11b**		0.50	35 (96%)[c,e]
12	**12b**		0.50	46 (96%)[c,e]
13	**13b**		0.50	n.i. (10%)[e]

[a]Isolated yield in % in parentheses. [b]No starting material was observed by GC-MS. [c]Scale-out performed for 10 min. [d]Concentration of salicylaldehyde was 0.5 M, conversion by GC-MS was 99%. [e]Conversion as determined by ^{1}H NMR. n.i = not isolated.

With these optimized reaction conditions in hand, we set out to investigate the applicability of this protection reaction on various alcohols. Under these optimized conditions in the flow setup, the reaction quantitatively yields the trimethylsilyl ether derivative of primary, secondary and benzylic alcohols. Even sterically demanding secondary alcohols such as *endo*-borneol and menthol (Table 2, entries 3 and 4) were quantitatively converted. For the trimethylsilylation of 3,4-dimethoxybenzyl alcohol, a total flow rate of 80 μL/min still gave > 99% conversion

by GC. To assess the practical applicability, a scale-out of the process was next investigated by collecting the output of each flow reaction for 30 min and isolating the product by evaporation of the solvent (Table 2). Phenolic alcohols can also be converted to the trimethylsilyl ether derivative. Under the optimal conditions found for benzyl alcohol, activated phenols **9** and **10** were quantitatively converted to their trimethylsilyl ether derivative. Deactivated phenols, on the other hand, are less reactive and require more forceful conditions (see Table 2, entries 7 and 8). When using 0.75 equivalents of HMDS, 4-cyanophenol was protected as its trimethylsilyl ether in 90% conversion. The tertiary alcohol **13** proved to be unreactive under the optimized reaction conditions, furnishing only 10% conversion as measured by ^{1}H NMR. Salicylaldehyde proved to be a challenging case as the optimized reaction conditions for benzyl alcohol only gave approximately 50% conversion. Upon decreasing the concentration of salicylaldehyde to 0.5 M (using 1.0 equivalents of HMDS; Table 2, entry 7), conversion was quantitative, but a small amount ($\approx 2–3\%$) of byproduct was observed. On the other hand, at 1.0 M salicylaldehyde concentration, conversion was improved considerably by increasing the concentration of HMDS, but byproducts still appeared. This result is comparable to the batch reaction which, after 1 h, contained a similar amount of byproduct, yet also showed significant degradation of product.

These results show that for most alcohols this operationally simple reaction permits efficient trimethylsilylation of alcohols under continuous flow conditions. The output can be collected and the products can be isolated by simple evaporation of solvent. The continuous flow protocol delivers much shorter reaction times, as the residence time is approximately 30 s at 40 μL/min. This compares very favorably to batch, where the protection of these alcohols typically takes at least 60 min.[14]

Dimethylphenylsilylation of alcohols under continuous flow conditions. In literature, there are only few reports describing the use of disilazanes other than HMDS for alcohol silylation, yet different silazanes would allow for a larger scope of silyl protecting groups. Therefore, the possibility of introducing other silyl ethers using this sulfonic acid-catalyzed reaction under continuous flow conditions was

investigated. Commercially available 1,1,3,3-tetramethyl-1,3-diphenylsilazane (TMDPS), upon reaction with an alcohol, protects the alcohol as a dimethylphenyl silyl ether (DMPS).[16] Like most silyl ethers, DMPS ethers can be cleaved with a fluoride anion source, but interestingly it can also be selectively removed in presence of a TMS ether with lithium/naphthalene.[17, 18] Benzyl alcohol **1** was reacted with TMDPS under continuous flow conditions to give the corresponding silyl ether **1c** with approximately 73% conversion at 60 °C and 40 μL/min flow rate (Table 3, entry 1). This decrease in conversion is most likely due to the increased steric bulk of TMDPS versus HDMS. Increasing the temperature to 110 °C gave full conversion and an isolated yield of 94%.

Next, the reaction was optimized with respect to reactant stoichiometry. Because of the relatively high pressures in the flow setup at this elevated temperature and to improve solubility of starting materials, the solvent was also switched from dichloromethane to acetonitrile. The concentration of TMDPS was lowered to 0.52 M and the reaction was performed at 110 °C and 125 °C (Table 3, entries 4 and 5).
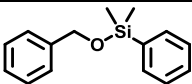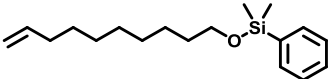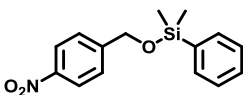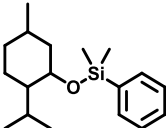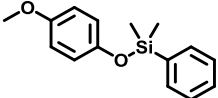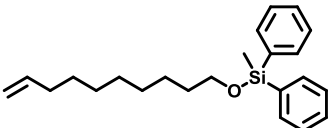
Table 3. Optimization of the model reaction, performed using 1 M benzyl alcohol and 40 μL/min total flow rate.

Entry	Temperature (°C)	[Benzyl alcohol] (M)	[TMDPS] (M)	Conversion (%)[a]
1	60	0.99	0.60	73[b]
2	100	0.99	0.60	97[b]
3	110	0.99	0.60	> 99[b]
4	110	1.01	0.52	> 99[c]
5	125	1.01	0.52	> 99[c]

[a]Relative peak area of product versus total peak area of product plus starting material, as determined by GC-MS. [b]Amount of catalyst in packed bed was 7.4 mg; solvent is dichloromethane. [c]Amount of catalyst in packed bed was 7.6 mg; solvent is acetonitrile.

Gratifyingly, both conditions yielded full conversion of benzyl alcohol, with no detectable amounts of starting materials. Finally, this model DMPS silylation reaction was scaled out under these optimized conditions for 30 min, giving 135 mg (94%) of dimethylphenylsilyl ether **1c** in good purity after evaporation of solvent.

Table 4. Investigation of the scope of the flow-through alcohol-protection reaction with 1,1,3,3-tetramethyl-1,3-diphenylsilazane (TMDPS). Solvent was acetonitrile unless noted otherwise.

Entry	Product		Yield (mg)[a]
1	**1c**		135 (94%)
2	**2c**		181 (99%)
3	**6c**		143 (83%)[b]
4	**4c**		125 (72%)[b]
5	**9c**		n.i. (86%)[c]
6	**2d**		n.i. (94%)[c,d]

[a]Isolated yield in parentheses. [b]After scale out and evaporation of solvent, product was dissolved and filtered over a short silica plug. [c]Conversion as determined by ^{1}H NMR. [d]Solvent was butyronitrile. n.i. = not isolated.

The reaction with TMDPS was also evaluated on other alcohols (Table 4). The silylation of menthol proved more challenging, but a conversion of ≈ 98% could still be reached at an elevated reaction temperature of 150 °C. A quantitative conversion could not be reached, but this may be due to small impurities in the menthol, corresponding to an unreactive isomer. A scale out of this reaction still afforded

125 mg of product in 72% yield and $> 95\%$ purity after 30 min collection, evaporation and removal of the small amount of unreacted material over a small plug of silica.

When employing the same reaction conditions for the protection of 4-methoxyphenol **9** (see Table 4, entry 5), an activated phenol, a conversion of 86% was measured by ^{1}H NMR. We attribute this moderate conversion to both the lower reactivity of the bulky disilazane and the lower nucleophilicity of phenols.

In these experiments, the silica-supported sulfonic acid in the packed bed could be re-used for at least four successive reactions, simplifying the procedure by not having to reload the packed bed.

Finally, the reaction between primary alcohol 10-undecen-1-ol **2** and commercially available 1,1,3,3-tetraphenyl-1,3-dimethyldisilazane was performed to give the diphenylmethylsilyl (DPMS) ether product **2d** (Table 4, entry 6). Due to the low solubility of this bulky disilazane in acetonitrile, the reaction solvent was switched to dry butyronitrile and the concentration of the disilazane was lowered to 0.125 M to prevent issues with precipitation of the tetraphenyldimethyldisilazane. Near-quantitative conversion of alcohol **2** (94%, ^{1}H NMR) to the desired diphenylmethylsilyl protected alcohol **3d** was obtained at a flow rate of 20 μL/min, a concentration of 0.25 M alcohol and a reaction temperature of 180 °C. This result shows that it is possible to react a primary alcohol with a very bulky disilazane under acid-catalyzed continuous flow conditions to allow for its protection as a bulky silyl ether with a stability that is intermediate between TMS and TBDMS.[16]

Influence of catalyst. During a control experiment without catalyst in a glass microreactor, partial conversion of benzyl alcohol to the trimethylsilyl ether product was observed. This prompted the further investigation into the influence of the catalyst by performing the reaction without catalyst, with unfunctionalized silica as potential catalyst and with the silica-supported sulfonic acid as catalyst. Somewhat surprisingly, the trimethylsilylation of benzyl alcohol with an excess of HMDS (0.75 equivalents; and temperature and residence time the same as in silica-catalyzed

reaction, 60 °C and 30 s, respectively) *without* any added catalyst, showed that benzyl alcohol was converted to the corresponding TMS ether with > 98% conversion. Surface silanols are known to be acidic[19] and might therefore also catalyze this reaction. However, they themselves may also be protected by silylation, therefore it was hypothesized that repetition of the reaction using the same glass microreactor should yield a progressively lower conversion, due to the decreased availability of silanols on the microchannel wall. This was indeed found to be the case. During the course of the reaction the number of silanols diminish as the silanols on the microchannel wall are silylated by reaction with HMDS. These silanols are not regenerated and therefore the conversion continues to decline. This 'wall-catalyzed' reaction was only observed for the most reactive substrate and disilazane species. For example, for the analogous uncatalyzed reaction of 3,4-dimethoxybenzyl alcohol **6** and 0.5 M HMDS a conversion of only 10% (GC-MS) was observed, which was only slightly increased by using more HMDS or the use of elevated temperatures (17% conversion at 100 °C). When the solid-supported sulfonic acid was employed, the conversion of 3,4-dimethoxybenzyl alcohol to the TMS ether was still > 99% at a flow rate of even 80 μL/min (reaction temperature of 60 °C and 0.5 equivalents HMDS with respect to the alcohol). This indicated that the sulfonic acid catalyst was indeed necessary to guarantee high conversions for all substrates.

These results prompted us to look more closely at the role of the silica support itself. The influence of the catalyst support on the reaction of 4-methoxyphenol with HMDS under acid-catalyzed flow conditions was examined. This activated phenol converted smoothly to its trimethylsilyl ether derivative when using the silica-supported sulfonic acid. When using regular flash silica (sieved to > 75 micrometer, typical loading in packed bed: 25 mg), however, a conversion of only 64% was obtained under otherwise identical conditions. Furthermore, from the GC-MS spectra of samples taken over at 10, 15 and 20 min, it can be seen that the conversion steadily decreases when regular silica is used, which is attributed to the decrease of free surface silanols by silylation (see Appendix 4, Figure S2). Under

these conditions, the acidic silanols on the silica surface become trimethylsilylated and are no longer available for acid catalysis.[20, 21] To investigate if this also affected the silica-supported sulfonic acid catalyst, we ran the trimethylsilylation of 4-(*tert*-butyl)benzyl alcohol **12** for 4 h at 30 °C. At this lower temperature, we did not expect full conversion and thus were able to more sensitively detect a decrease in conversion. Indeed, after 4 h on-stream, a small decrease in conversion to the product is observed, indicating partial deactivation of the sulfonic acid population (see Appendix 4, Figure S38). Nevertheless, scale-outs performed with the same packed bed after this period reached good conversion (> 95% as measured by ^{1}H NMR).

To substantiate essential role of the sulfonic acid on silica as a catalyst, we compared the reaction of menthol with TMDPS using flash silica and our silica-supported sulfonic acid. At temperatures of 60–100 °C silica-supported sulfonic acid indeed gave higher conversions of menthol than the regular flash silica (see Appendix 4, Figure S3 for the remaining % of menthol). Only at high reaction temperatures (135 °C), the conversion of menthol to menthol DMPS ether was nearly equal in both cases.

Nevertheless, these results do show that regular flash silica can act as an acid catalyst in flow chemistry. Its potential contribution to acid-catalyzed reactions with silica-based solid-supported catalysts, although hard to characterize, should always be taken into account.

Selective protection of hydroxyl groups. To investigate the potential of the acid-catalyzed reaction of disilazanes for the selective protection of alcohols, we performed several competition experiments. The first competition experiment was performed between a primary alcohol (10-undecen-1-ol) and a secondary alcohol (menthol). The dimethylphenyl silylation reaction was performed using a solution of equimolar amounts of starting alcohols (both 0.5 M) and 0.25 equivalents of TMDPS (0.5 equivalents of silyl groups). The reaction was performed at several temperatures, and full conversion of TMDPS was found at 90 °C using a flow rate of

40 µL/min. The reaction was selective for the protection of the primary alcohol, giving the silyl ether products in a 9 : 1 ratio (GC-MS). The primary alcohol reacts approximately sixteen times faster under these conditions (see Supporting Information for the calculation). The selectivity for the primary alcohol decreased slightly at higher reaction temperatures (7 : 1 at 135 °C).

Encouraged by these results, the attention was turned to compounds that contain two types of alcohols. Vanillyl alcohol contains both a benzylic and an activated phenolic alcohol. It was subjected to reactions using HMDS and TMDPS. For the protection of vanillyl alcohol with HMDS, preferentially the benzylic alcohol reacted (see Appendix 4, Figure S4), giving the mono-protected trimethylsilyl ether of the benzylic alcohol with 76% selectivity (^{1}H NMR). The reaction with TMDPS conducted at 120 °C again favored the benzylic position: the mono-protected trimethylsilyl ether of the benzylic alcohol was formed with 80% selectivity (^{1}H NMR) (see Appendix 4, Figure S5).

Finally, the selective trimethylsilyl ether protection of 3-(*tert*-butoxy)propane-1,2-diol, containing a primary and a secondary alcohol, was investigated. At a reaction temperature of 60 °C, the conversion was 81% and the mono-protected trimethylsilyl ether of the primary alcohol was obtained with 90% selectivity (as measured by ^{1}H NMR, see Appendix 4, Figure S6). A higher conversion could not be reached due to the hygroscopic nature of the starting compound: adventitious water will react with HMDS to give the hydroxy- or siloxane derivative.

These experiments show the possibility to protect one alcohol over another alcohol in flow. This would allow subsequent reactions to take place on the unprotected alcohol.

Deprotection of trimethylsilyl ether. Finally, the deprotection of these silyl ethers under continuous flow conditions was examined. Trimethylsilyl ethers are known to be acid-labile in protic solvents such as methanol. Trimethylsilyl borneol ether **3b** was dissolved in methanol and passed over the packed bed containing silica-supported sulfonic acid. Several reaction conditions were tested (see Table 5),

starting with a high concentration with a relatively fast flow speed. Surprisingly, this already gave > 97% conversion to the deprotected alcohol. Increasing the reaction temperature had a negative influence on the conversion. This could be due to a backward reaction occurring between trimethylsilyl methanol ether and the liberated alcohol. Lowering the concentration to 0.25 M and setting the reaction temperature to 30 °C gave the highest conversion (Table 5, entry 6 and 7).

Table 5. Results of deprotection of borneol trimethylsilyl ether in methanol under continuous flow conditions.

Entry	Concentration (M)	Flow rate (µL/min)	T (°C)	Conversion (%)[a]
1	0.5	40	60	98
2	0.5	20	60	98
3	0.25	20	60	> 99[b]
4	0.25	20	80	> 99[b]
5	0.25	20	100	> 99[b]
6	0.25	20	30	> 99[b]
7	0.25	40	30	99

[a]As measured by GC-MS. [b]No starting material was detected by GC-MS.

Using these conditions, the deprotection of 10-undecen-1-ol trimethylsilyl ether **2b,** 10-undecen-1-ol dimethylphenylsilyl ether **2c** and menthol dimethylphenylsilyl ether **4c** was tested. The deprotection of all these silyl ethers to the corresponding alcohols proceeded smoothly at 30 °C and a flow rate of 40 µL/min. Furthermore, for compounds **2c** and **4c**, the temperature could be lowered to 0 °C with no noticeable loss of conversion (see Appendix 4, Figure S7). This, however, precludes the selective deprotection of these silyl ethers, due to the lack of difference in reactivity under the tested conditions. Nevertheless, the ability to catalyze both protection and deprotection reactions increases the versatility of this setup. Alcohols can be protected in flow, followed by deprotection to regain the original hydroxyl functionality, all using the same silica-supported sulfonic acid catalyst.

Conclusion

The protection of alcohols by tetrahydropyranyl or a range of silyl moieties can be performed highly effectively using continuous flow reactions and silica-supported sulfonic acids, outperforming both catalyzed batch reactions and previously reported catalyzed flow reactions.

Synthetically relevant amounts of tetrahydropyranyl-, trimethylsilyl- and dimethylphenylsilyl-protected alcohols can be generated using a laboratory-scale flow reactor and silica-supported sulfonic acid. Upwards of 200 mg protected alcohol per hour can be produced using this flow setup. The protection reaction can be used on a broad scope of alcohols and for selective protection reactions, showing a selectivity for primary alcohols over secondary alcohols, and for benzylic alcohols over phenolic alcohols. The same silica-supported sulfonic acid can be used for deprotection reactions of silyl ethers, using methanol as the solvent. When employing relatively mild reaction conditions (30 °C and 0.25 M concentration) the reaction proceeded with > 98% conversion for the tested substrates. The silica-supported sulfonic acid catalyst could be re-used for at least five reactions over several days, without the need to remove it from the crude reaction mixture.

Materials and Methods

Materials. Dichloromethane (CH$_2$Cl$_2$, Sigma-Aldrich, > 99.8%) and tetrahydrofuran (THF, Sigma-Aldrich, > 99.8%) were purified using a Pure Solv 400 solvent purification system (Innovative Technology, Amesbury, USA). Acetonitrile (HPLC grade) and butyronitrile was dried over 3Å molsieves. All other starting materials were obtained from commercial sources and used as received.

Synthesis of silica-supported acid catalyst (SBA-SO$_3$H). This synthesis was based on the syntheses described by Stucky and co-workers.[22] In a 500 mL round-bottomed flask was 100 mL deionized water, 20 mL conc. HCl (37%) and P123 (triblock copolymer, average M$_w$ 5,800 g/mol; 4.05 g; 0.7 mmol) under argon atmosphere. After complete dissolution of the template, tetraethylorthosilicate

(TEOS; 8.4 g; 40.4 mmol) was added. A white precipitate formed. After another 45 min, (3-mercaptopropyl)trimethoxysilane (MPTMS; 0.64 g; 3.2 mmol) was added, together with 1 mL 50% (w/w) H_2O_2. This suspension was stirred at 35 °C for 20 h. After this time, the stirring bar was removed and the mixture was heated to 90 °C and kept at this temperature for 48 h. The suspension was filtered and rinsed with copious amounts of water and acetone. In order to extract the template, 2.0 g of the white powder was stirred under argon in a mixture of 900 mL ethanol and 25 mL conc. HCl at 75 °C. Using X-ray diffraction, a hexagonal ordering was confirmed for this material (Appendix 4, Figure S8). The material was sieved (200 - 400 mesh, 45–75 μm) and suspended in 10% (w/w) H_2SO_4. After 8 h, the powder was isolated by filtration, rinsed with water and THF and dried under vacuum.

General Experimental Methods. Flow experiments were performed in a Chemtrix Labtrix Start system, using a 3026 catalyst chip (Chemtrix BV, Geleen, The Netherlands). The catalyst chip was filled with a small amount of flash silica (SiliCycle, P60, sieved to > 75 μm) and 5–9 mg of SBA15-SO$_3$H (solid-supported sulfonic acid on mesoporous silica, sieved to 45–75 μm) and finally another small plug of flash silica. The plugs of regular flash silica serve as an additional frit to prevent small particles (which may dislodge from the SBA15-SO$_3$H) from clogging the microchannels downstream. The outside of the chip was cleaned and the packed bed was flushed with DCM or MeCN.

The residence time was calculated by taking a typical pore volume of mesoporous silica and multiplying by the loading, giving approximately 15 μL pore volume. Assuming that the remainder of the packed bed is taken up by silica, the total volume of the microreactor is 5 μL (volume of meandering channel, see Scheme 1) + 15 μL (pore volume of silica) ≈ 20 μL. Combined with a flow rate of 40 μL/min and a visual estimation during the flushing of the microreactor with solvent, the residence time is approximately 30 seconds.

Typical syntheses

Tetrahydropyranylation. A solution of benzyl alcohol (1 M) and DHP (1 M) were placed in 1 mL syringes on a syringe pump. These solutions were introduced at a flow rate of 20 μL/min (total flow rate 40 μL/min) into the microreactor (temperature typically 30 °C) where the packed bed contained solid-supported sulfonic acid. After equilibration (at least 5 min), the output was collected for 30 min. Solvent was removed *in vacuo* to give the tetrahydropyranyl-protected benzyl alcohol in 98% yield.

Trimethylsilylation. A solution of benzyl alcohol (1 M) and 1,1,1,3,3,3-hexamethyldisilazane (0.5 M) in dichloromethane were placed in 1 mL syringes on a syringe pump. These solutions were introduced at a flow rate of 20 μL/min (total flow rate 40 μL/min) into the microreactor (temperature 60 °C) where the packed bed contained solid-supported sulfonic acid. After equilibration (at least 10 min), the output was collected for 30 min. Solvent was removed *in vacuo* to give the trimethylsilyl ether derivative of benzyl alcohol in 94% yield.

Dimethylphenylsilylation. A solution of 10-undecen-1-ol (1 M) and 1,1,3,3-tetramethyl-1,3-diphenylsilazane (0.5 M) in acetonitrile were placed in 1 mL syringes on a syringe pump. These solutions were introduced at a flow rate of 20 μL/min (total flow rate 40 μL/min) into the microreactor (temperature 135 °C) where the packed bed contained solid-supported sulfonic acid. After equilibration (at least 10 min), the output was collected for 30 min. Solvent was removed *in vacuo* to give the dimethylphenyl ether derivative of 10-undecen-1-ol in 99% yield.

Uncatalyzed flow reactions were performed on the same Labtrix Start system using the 3023 microreactor chip (internal volume 10 μL).

References

[**1**] J. Wegner, S. Ceylan, A. Kirschning. Flow Chemistry - A Key Enabling Technology for (Multistep) Organic Synthesis. *Adv. Synth. Catal.* **2012,** *354* (1), 17-57.

[**2**] J. Wegner, S. Ceylan, A. Kirschning. Ten key issues in modern flow chemistry. *Chem. Commun.* **2011,** *47* (16), 4583-4592.

[**3**] A. Kirschning, W. Solodenko, K. Mennecke. Combining enabling techniques in organic synthesis: continuous flow processes with heterogenized catalysts. *Chem. Eur. J.* **2006,** *12* (23), 5972-5990.

[**4**] S. V. Ley, I. R. Baxendale, R. N. Bream, P. S. Jackson, A. G. Leach, D. A. Longbottom, M. Nesi, J. S. Scott, R. I. Storer, S. J. Taylor. Multi-step organic synthesis using solid-supported reagents and scavengers: a new paradigm in chemical library generation. *J. Chem. Soc., Perkin Trans. 1* **2000,** (23), 3815-4195.

[**5**] M. Benaglia, A. Puglisi, F. Cozzi. Polymer-Supported Organic Catalysts. *Chem. Rev.* **2003,** *103* (9), 3401-3429.

[**6**] M. A. Harmer, Q. Sun. Solid acid catalysis using ion-exchange resins. *Appl. Catal., A* **2001,** *221* (1–2), 45-62.

[**7**] C. Wiles, P. Watts. Parallel synthesis in an EOF-based micro reactor. *Chem. Commun.* **2007,** (46), 4928-4930.

[**8**] R. Ricciardi, R. Munirathinam, J. Huskens, W. Verboom. Improved catalytic activity and stability using mixed sulfonic acid- and hydroxy-bearing polymer brushes in microreactors. *ACS Appl. Mater. Interfaces* **2014,** *6* (12), 9386-9392.

[**9**] F. Costantini, W. P. Bula, R. Salvio, J. Huskens, H. J. G. E. Gardeniers, D. N. Reinhoudt, W. Verboom. Nanostructure Based on Polymer Brushes for Efficient Heterogeneous Catalysis in Microreactors. *J. Am. Chem. Soc.* **2009,** *131* (5), 1650-1651.

[**10**] R. D. Crouch. Selective deprotection of silyl ethers. *Tetrahedron* **2013,** *69* (11), 2383-2417.

[**11**] F. Shirini, M. Mamaghani, S. V. Atghia. A mild and efficient method for the chemoselective trimethylsilylation of alcohols and phenols and deprotection of silyl ethers using sulfonic acid-functionalized ordered nanoporous Na+-montmorillonite. *Appl. Clay Sci.* **2012,** *58*, 67-72.

[**12**] Z.-H. Zhang, T.-S. Li, F. Yang, C.-G. Fu. Montmorillonite Clay Catalysis XI[1]: Protection and Deprotection of Hydroxyl Group by Formation and Cleavage of Trimethylsilyl Ethers Catalysed by Montmorillonite K-10. *Synth. Commun.* **1998,** *28* (16), 3105-3114.

[**13**] N. Azizi, M. R. Saidi. Novel and Efficient Method for the Silylation of Hydroxyl Groups with Hexamethyldisilazane (HMDS) under Solvent-Free and Neutral Conditions. *Organometallics* **2004,** *23* (6), 1457-1458.

[**14**] D. Zareyeea, B. Karimi. A novel and highly efficient method for the silylation of alcohols with hexamethyldisilazane (HMDS) catalyzed by recyclable sulfonic acid-functionalized ordered nanoporous silica. *Tetrahedron Lett.* **2007,** *2007* (48), 1277-1280.

[**15**] F. Shirini, K. Marjani, H. T. Nahzomi. Silica Triflate as a New, Mild and Efficient Catalyst for Tetrahydropyranylation of Alcohols and Deprotection of Tetrahydropyranyl Ethers. *Phosphorus, Sulfur Silicon Relat. Elem.* **2007,** *182* (9), 2235-2240.

[**16**] S. E. Denmark, R. P. Hammer, E. J. Weber, K. L. Habermas. Diphenylmethylsilyl Ether (DPMS): A Protecting Group for Alcohols. *J. Org. Chem.* **1987,** *52* (1), 165-168.

[**17**] B. C. Milgram, B. B. Liau, M. D. Shair. Gram-Scale Synthesis of the A'B'-Subunit of Angelmicin B. *Org. Lett.* **2011,** *13* (24), 6436-6439.

[**18**] C. Behloul, D. Guijarro, M. Yus. Desilylation procedure via a naphthalene-catalysed lithiation reaction. *Tetrahedron* **2005,** *61* (28), 6908-6915.

[**19**] J. M. Rosenholm, T. Czuryszkiewicz, F. Kleitz, J. B. Rosenholm, M. Lindén. On the Nature of the Brønsted Acidic Groups on Native and Functionalized Mesoporous Siliceous SBA-15 as Studied by Benzylamine Adsorption from Solution. *Langmuir* **2007,** *23* (8), 4315-4323.

[**20**] C. Zapilko, R. Anwander. Size-Selective Surface Silylation of Cagelike Mesoporous Silica SBA-2 with Disilazane Reagents. *Chem. Mater.* **2006,** *18* (6), 1479-1482.

[**21**] W. Hertl, M. L. Hair. Reaction of Hexamethyldisilazane with Silica. *J. Phys. Chem.* **1971,** *75* (14), 2181-2185.

[**22**] D. Margolese, J. A. Melero, S. C. Christiansen, B. F. Chmelka, G. D. Stucky. Direct Syntheses of Ordered SBA-15 Mesoporous Silica Containing Sulfonic Acid Groups. *Chem. Mater.* **2000,** *12* (8), 2448-2459.

Chapter 5

Clickable Polylactic Acids by Fast Organocatalytic Ring-Opening Polymerization in Continuous Flow

Abstract. The use of microreactor technology for the ring-opening polymerization of L-lactide catalyzed by 1,5,7-triazabicyclo[4.4.0]dec-5-ene allows for rapid optimization of reaction parameters (reaction temperature and residence time). At moderate catalyst loading, good control over the polymerization is demonstrated by high conversion of monomer (> 95%) and low polydispersity (< 1.3) at residence times as low as 2 s. The polymerization gives higher conversion at lower reaction temperature. This metal-free, organocatalytic route yields well-defined poly(lactic acid) and the mild reaction conditions give access to bicyclononyne- and tetrazine-containing poly(lactic acid) amenable to click chemistry.

This chapter is submitted as:

"Clickable Polylactic Acids by Fast Organocatalytic Ring-Opening Polymerization in Continuous Flow", Sebastiaan A. van den Berg, Tom Wennekes, and Han Zuilhof. Submitted for publication.

Introduction

The use of continuous flow microreactors is an attractive method to improve the control over polymerization reactions due the exquisite control over reaction parameters. Nevertheless, microreactor technology is still sparsely used in polymer chemistry.[1] Recent advances have led to microstructured devices where extremely rapid mixing and precise control over temperature is possible. The excellent heat transfer and mixing properties are ideally suited for e.g. exothermic polymerizations.[1] In some cases, continuous flow allows the use of far less stringent conditions and simpler experimental procedures compared to batch, allowing higher temperatures and potentially dangerous reaction conditions to be used safely.[2, 3] Due to the small reaction volumes and short reaction times employed, fast screening of reaction conditions is possible with minimal reagent use.[4, 5] Once identified, optimal conditions can also be scaled up more reliably compared to batch as the advantageous mixing and heat transfer characteristics are largely maintained in larger flow set-ups. We are interested in the organocatalyzed ring-opening polymerization of L-lactide to produce poly(lactic acid) for biomedical and other applications and reasoned that this polymerization could benefit from the use of microreactors (see Figure 1).

To date, the use of continuous flow techniques has been reported for several types of polymerizations, including reversible addition−fragmentation chain-transfer (RAFT) polymerization,[6] atom-transfer radical polymerization (ATRP),[7, 8] living anionic[2, 3] and ring-opening polymerization.[4, 9, 10] Depending on the type of polymerization, improvement over batch comes from improved heat transfer or faster mixing. Iida et al. studied living anionic styrene polymerizations, initiated with *sec*-butyl lithium, in continuous flow.[3] Interestingly, they observed a dependence of the resulting molecular weight distribution on the channel geometry, especially when performing polymerizations that generated a highly viscous reaction medium. Microreactors with patterned channels performed better than the straight channel counterparts, possibly due to added passive mixing.
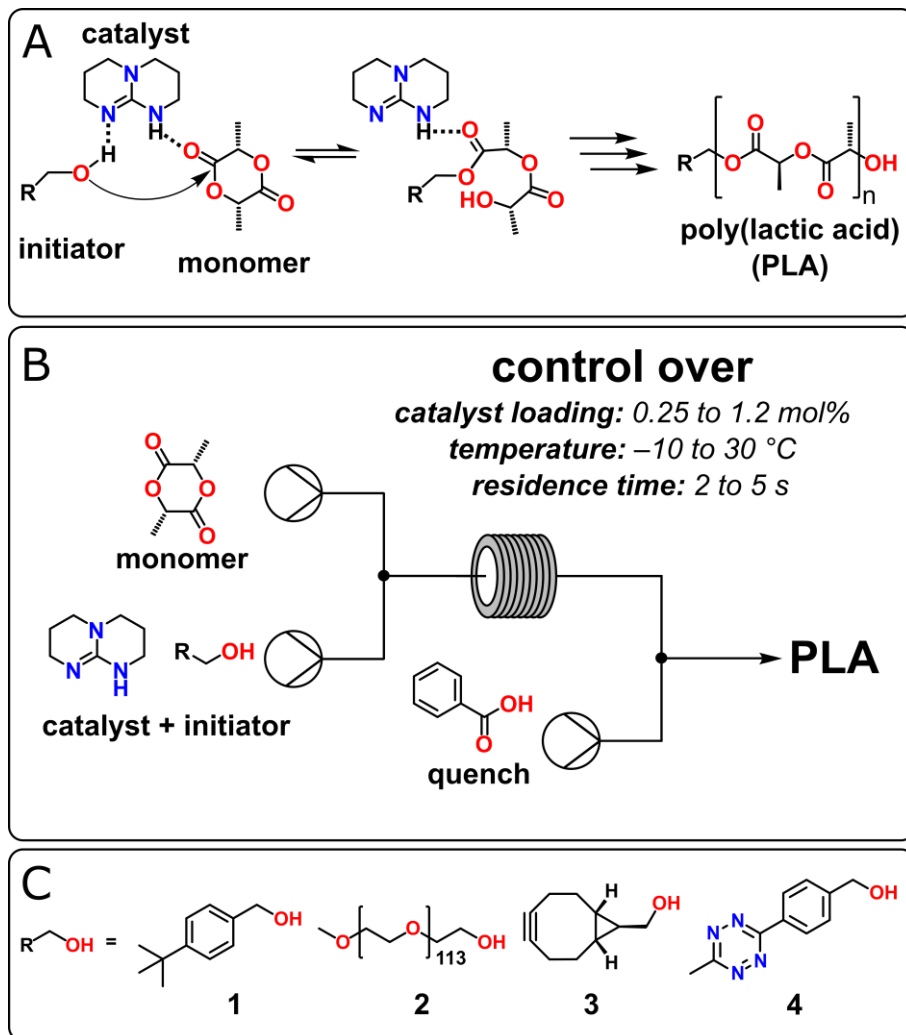
Figure 1. **A:** Mode of action of the TBD catalyst in the ring-opening polymerization of L-lactide: hydrogen bonding increases the nucleophilicity of the alcohol initiator[11] and starts polymer extension. **B:** The continuous flow organocatalytic polymerization of L-lactide is performed in a commercially available microreactor setup using a 1 μL internal volume glass microreactor chip. **C:** Alcohol initiators used in this study: 4-*tert*-butyl-benzyl alcohol **1**, PEG-5,000 **2**, *exo*-BCN-alcohol **3** and tetrazine **4**.

Tonhauser and coworkers also studied the living anionic polymerization of styrene.[2] When performed in a tubular stainless steel reactor, the anionic polymerization of styrene yielded very fast reactions (15 s in flow vs. 3 h in batch) at the expense of a broadened molecular weight distribution. By introducing functionalized epoxides into the microreactor via a separate channel, they were able to demonstrate precise *on-line* end-capping of the resulting polymers. Natalello and co-workers demonstrated the living anionic polymerization of styrene and 2-vinylpyridine (2VP). By using special micromixers in continuous flow, they were able to synthesize well-defined, high molecular weight PS and P2VP (polydispersity index (PDI) $\approx$ 1.05, M_n up to 149,000 g/mol for PS) at room temperature *vs* $-78\ °C$ in batch. Furthermore, the reaction time in flow was much shorter than in batch (< 25 s).[10]

Hornung et al. performed the first solution-phase RAFT polymerization of acrylates and acrylamides in continuous flow on a multi-gram scale.[6] Batch and flow modes of operation performed similarly, yielding in each case polymer with molecular weight up to 25,000 g/mol and polydispersities between 1.09 and 1.16.

Baeten and co-workers showed the elegant use of microreactors to quickly screen the cationic ring-opening polymerization of 2-oxazoline at temperatures well above the boiling point of the solvent. They were able to synthesize di- and triblock copolymers by linking two microreactor chips together. Despite its sensitivity to water, the polymerization in the microreactor proceeded rapidly and with minimal side-reactions.[4] The use of heterogeneous catalysts, on the other hand, had a negative influence on the control over the ATRP of methacrylate as Shen and co-workers showed. Using a solid-supported Cu(I) catalyst in flow gave a broader molecular weight distribution than when the same catalyst was used in batch. The authors attribute this to a broad residence time distribution of polymer chains in the flow reactor and the increase in viscosity of the medium. Due to the increased viscosity, polymer chains are hindered from entering the catalytic sites on the solid support. As a consequence, these chains are not deactivated fast enough, leading to uncontrolled polymer growth.[7] Poor PDI values are, however, not intrinsic to in-

flow polymer forming reactions, as e.g. elegantly shown by Leibfarth and co-workers. While strictly not a polymerization, they used flow-iterative exponential growth to generate sequence-defined, unimolecular oligomers (up to the octamer). Monomers contain orthogonally protected azides and alkynes and are coupled *via* the copper-catalyzed Huisgen 1,3-dipolar cycloaddition. The dimeric species is then reintroduced into the flow reactor, where half of the molecules are deprotected to reveal the alkyne and the other half to reveal the azide. Those dimers are then coupled to tetramers, and so on, leading to oligomers with extremely narrow PDI (<1.01 *vs* PS standards). The synthesis can be done in a sequence-defined manner, yielding perfectly alternating oligomers. Their synthesis is readily scaled, leading to 2.75 g/h.[12] Unfortunately, intermediates need to be chromatographed before the synthesis of the next oligomer, making the synthesis semi-automated. Furthermore, although individual yields are quantitative, the yields from the flow reactor are less than quantitative, which the authors attribute to the syringe pumps, inline liquid separator and solubility of the polymers in the aqueous phase. It does, however, present a glimpse into the future of polymer chemistry, where possibly sequence-defined polymer architectures can be synthesized at scale in flow.

Here we show that microreactors are also applicable to another type of homogeneously catalyzed polymerization reaction, namely the ring-opening polymerization of L-lactide to poly(lactic acid) (PLA), a popular bio-degradable and bio-compatible polyester derived from renewable resources. PLA is widely applied in packaging, disposable bottles and biomedical applications with an annual production of 185 kiloton in 2013, which is still increasing.[13, 14] Low-molecular weight PLA can be synthesized from a condensation reaction of 2-hydroxy propionic acid (lactic acid), however, the ring-opening polymerization (ROP) of cyclic lactide monomers gives access to the practically more useful polymers of high molecular weight.[13] The industrial synthesis of PLA currently relies heavily on metal catalysts such as $Sn(Oct)_2$ (tin (II) octate) at elevated temperatures. Other catalysts for the ROP of lactide have been investigated, including phosphines,[15] 4-dimethylaminopyridine,[16] organophosphates[17] and *N*-heterocyclic carbenes.[18] A

promising alternative is the organocatalyzed polymerization of L-lactide using amidine and guanidine bases.[19-21] Pratt et al. showed that 1,5,7-triazabicyclo[4.4.0]dec-5-ene (TBD) is a very potent organocatalyst for the ROP of cyclic esters.[16] The major drawback of TBD, however, is that besides catalyzing the ring-opening of cyclic esters, it also catalyzes the transesterification of the polyester backbone. This leads to an undesired increase in polydispersity (see Figure 1). In the presence of an excess of an alcohol, TBD can even be used to depolymerize PLA, generating esters of lactic acid.[22] To suppress transesterification, the polymerization is therefore quenched by manual addition of benzoic acid after a defined short reaction time. Other, less active catalysts such as DBU and thiourea derivates have been found to work well in batch. Continuous flow, however, presents an opportunity to utilize the high activity of TBD while suppressing transesterification by virtue of the excellent control over reaction parameters. Furthermore, TBD-catalyzed lactide polymerizations typically take less than 60 s to reach full conversion, even at low catalyst loadings (down to 0.1 mol% relative to monomer), making TBD an ideal candidate for flow-based optimization of this polymerization.[16] Using this procedure, Pratt et al. were able to obtain PLA with molecular weights up to 63,000 g/mol and a PDI of 1.1-1.2.[16] While highly attractive to further investigations, the sensitivity to water currently requires the polymerization to be performed in a glovebox.[16, 19] Furthermore, quenching of the polymerization by manual benzoic acid addition after the very short reaction times is not very reproducible. Taken together this limits the practical applicability of this method. We reasoned that application of the TBD-catalyzed ROP of L-lactide in continuous flow microreactors would allow for more control over this reaction, without the need for a glovebox, and give a better insight into the parameters controlling the polymerization. In microreactors, the mixing of reagents is fast (on the order of milliseconds) and the residence time before addition of a quenching agent can be precisely tuned. Finally, the temperature of the reaction can be adjusted quickly and maintained accurately. This allows for fast screening of reaction conditions with high reproducibility and a practical continuous production of PLA outside of the glovebox (see Figure 1).

In the light of biomedical applications of PLA and our ongoing research in this area, we were interested in obtaining PLA-based materials that could be functionalized efficiently with (bio)molecules through the use of click chemistry.[23-25] PLA chains have been shown to assemble into nanoparticles, which would enable their use as drug carriers by conjugating small bioactive molecules to the chain end.[26] Facile functionalization of a polymer chain end can be achieved by introducing a "clickable" moiety such as an alkyne or azide. The use of copper-catalyzed azide-alkyne cycloaddition (CuAAC) click chemistry for polymer functionalization has indeed been used extensively.[27] The metal-free, organocatalytic route towards PLA, however, begs for a copper-free alternative. The strain-promoted azide-alkyne cycloaddition (SPAAC) reaction and inverse electron demand Diels-Alder (IEDDA) reaction are good candidates for metal-free alternatives. SPAAC uses the inherent ring strain in cyclooctynes to react with azides in a copper-free manner.[28] One way to introduce this cyclooctyne moiety is by post-functionalization of the polymers, as shown by Boons and co-workers for poly(ethylene glycol)-*block*-poly(ε-caprolactone)[29]; this, however, introduces extra steps in the synthesis and purification of these materials. Therefore we hypothesized that cyclooctyne-derived alcohol **3** and tetrazine-derived alcohol **4** could be used as initiators, as this would allow for full incorporation of the clickable moiety in each polymer chain. There is some precedent for the use of strained alkynes, such as 4-dibenzocyclooctynol (DIBO), and tetrazines as clickable initiators for ROP, ATRP and RAFT polymerizations.[30-33]

Zheng et al. reported the use of DIBO as initiator for the ring-opening polymerization of poly(γ-benzyl-L-glutamate).[30] The polymerizations took 3 d, yielding materials with a PDI ranging from 1.14 to 1.29 with M_n up to 128,000 g/mol. From these polymers, they produced nanofibers, which could be further functionalized with azide-containing molecules in a modest 26% overall conversion.[30] Ledin et al. showed that a DIBO-derived initiator could be used for the RAFT polymerization of styrene.[31] The authors note that the presence of the strained alkyne in the DIBO-derived initiator had a negative impact on the polymerization.

To prevent side-reactions, the temperature of the reaction had to be lowered and the polymerization was stopped after 20 h at a mere 20% conversion. Wang et al. also used a DIBO-derived ATRP initiator to generate SPAAC-ready polystyrene. The styrene conversion was around 20%, which the authors tentatively attributed to side-reactions.[32] Furthermore, although the SPAAC reaction was copper-free, CuBr was used in the ATR polymerization of DIBO-PS. Other types of initiators that enable metal-free click chemistries have been used as well: Barker et al. used 5-norbornene-2-methanol as initiator for the ring-opening polymerization of L-lactide catalyzed by 1 mol% of 1,8-diazabicyclo[5.4.0]undec-7-ene (DBU). Using this norbornene group, the polymer chain ends could be ligated with tetrazine-containing molecules in an inverse electron-demand Diels-Alder reaction.[21, 34] All of these papers, however, either use copper in the synthesis of the polymer or face problems during the polymerization due to the presence of the strained alkyne. Likewise, using a tetrazine initiator in the synthesis of poly(valerolactone) under basic conditions gave rapid degradation of the tetrazine.[33]

In this chapter, we demonstrate the facile metal-free synthesis of well-defined PLA with a low PDI in continuous flow without the need for a protective atmosphere. The polymerization is performed with unprecedented short residence times, with optimal values as low as 2 s. Furthermore, we show for the first time the direct synthesis of SPAAC-ready PLA, initiated from the cyclooctyne-containing bicyclo[6.1.0]nonyne-derived alcohol **3,** and its click reaction with a set of azides. In addition, we also prepared the first example of tetrazine-containing PLA from tetrazine-derived alcohol **4** that can readily react with norbornenes and other tetrazine-click compatible reaction partners such as strained alkynes and alkenes.[33, 35] Scaling out in the microreactor chip under optimal reaction conditions leads to 200 mg per hour, which is easily purified by precipitation and can potentially be scaled up in industrial flow reactors. As toxic metals are completely avoided in the synthesis, our approach is ideally suited for synthesis of functional PLA materials for use in biomedical and other applications.

Results & Discussion

A series of experiments was performed in a continuous flow microreactor to study the effects of catalyst loading, residence time and temperature on the conversion of monomer and molecular weight distribution of the resulting PLA. We reasoned that a 1 μL microreactor chip would allow for the right residence time window and the quick screening of these reaction conditions. Four catalyst loadings were investigated (1.2, 0.5, 0.25 and 0.1 mol%). The ratio between monomer and initiator was kept constant at 80 : 1, thus targeting a degree of polymerization (DP) of 80 unless noted otherwise. The catalyst can be rapidly quenched by on-chip mixing of benzoic acid into the reaction stream at the end of the reaction zone, allowing precise control over the residence time. Quantitative conversion of monomer was easily achieved within seconds using 1.2 mol% of catalyst with respect to monomer, whereas the conversion was typically less than quantitative at catalyst loadings of 0.1–0.5 mol%. For example, with 0.5 mol% catalyst the monomer conversion was 91–100% with concomitant polydispersities between 1.24 and 1.52. A catalyst loading of 0.25 mol% was chosen to study the influence of temperature and residence time on the polymerization (Figure 2). Three different temperatures (−10, 10 and 30 °C) and four different residence times (2, 3, 4 and 5 s) were examined. The shortest residence time was chosen by taking the microreactor capabilities into account: even shorter residence times would need higher flow rates which could potentially damage the microreactor chip. At 0.25 mol% catalyst loading, the conversion ranged from 45 to 95% (see Figure 2, left). This broad range allowed us to clearly visualize the trends in conversion caused by the reaction parameters. Analysis by ^{1}H NMR yielded conversion and DP, whereas GPC was used to determine M_n (*vs* PS standards) and PDI. The data for 0.25 mol% catalyst is shown in Figure 2 (see Appendix 6 for tabulated data including other catalyst loadings). In these experiments the standard deviation in the given conversions is typically 5% or less (based on triplicate experiments; see Appendix 6, Figure S25 for detailed information).

We investigated the polymerization further by measuring the conversion at nine different temperatures at a fixed residence time (–10 to 30 °C, every 5 °C; 4 s) and calculating ΔH^0 from the Van 't Hoff plot (see Appendix 6, Figure S13). This value was found to be –20.8 kJ/mol and is in good agreement with the value of ΔH_p of –22.9 kJ/mol as previously reported by Duda et al.[36] This indicates that at this low catalyst loading, a thermodynamic equilibrium is reached even after these short 2–5 s residence times.
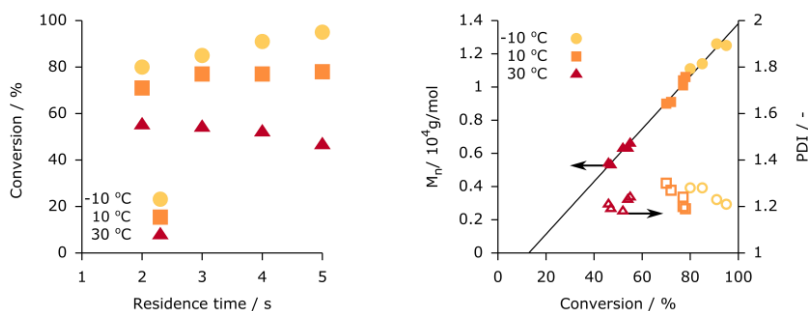
Figure 2. **Left:** Conversion of monomer at 0.25 mol% catalyst loading versus residence time. **Right:** M_n *vs* conversion follows a straight line, indicating a living polymerization. Catalyst loading: 0.25 mol%. Closed symbols denote M_n, open symbols denote PDI.

At higher catalyst loading (0.5 mol% w.r.t. monomer and up), the conversion of monomer is near-quantitative under all tested conditions. Monomer conversions reached $\geq$ 98.5% under all investigated conditions when using a fixed catalyst loading of 1.2 mol%, even at the shortest 2 s residence time. Residence times beyond 2 s only resulted in broadening of the molecular weight distribution (see Figure 3). This is in line with previous findings by Lohmeijer et al., who found that transesterification of the polymer backbone becomes more pronounced at high conversions.[16] The same dependence of PDI *vs* conversion is found for the polymerization of L-lactide using tin(II) octoate at 190 °C, which is also attributed to transesterification.[37] Despite this trend towards increased PDI at the high catalyst loading of 1.2 mol%, the use of the microreactor allowed for rapid screening toward optimal reaction parameters. A residence time of 2 s and a reaction temperature of

30 °C led to polymers with an acceptable PDI of 1.28 and M_n of 14,500 g/mol. This shows that control over the residence time, and thus the exact time when the catalyst is quenched, plays a crucial role in controlling this polymerization.
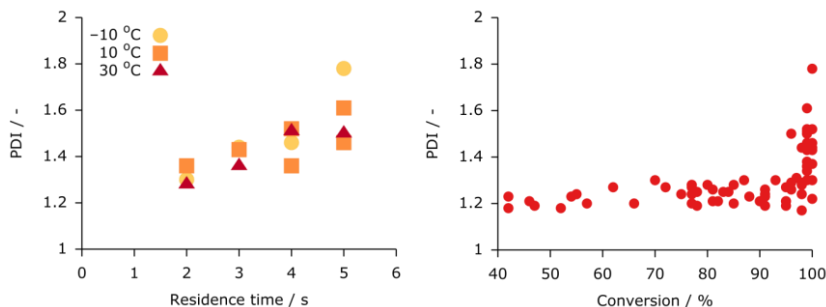

Figure 3. **Left:** Molecular weight distribution due to transesterification of the polymer backbone versus residence times. Catalyst loading 1.2 mol%; conversion at all residence times ≥ 98.5%. **Right:** Plot of PDI versus conversion for all experiments at a targeted DP of 80.

Broadening of the polymer weight distribution was less pronounced at lower catalyst loadings, because the transesterification process is slower at the less than quantitative conversion observed at these loadings and therefore has less influence. A transition can be seen in the case of 0.5 mol% catalyst loading. The increase in residence time leads to the conversion approaching 100% at −10 °C and a concomitant increase in PDI from 1.2 to 1.5 going from 2 to 5 s residence time. For 10 and 30 °C, where the conversions are 99% and 91–96%, respectively, the PDI decreases with respect to that observed at −10 °C, independent of residence time (see Figure 4). We tentatively attribute the typically higher polydispersities observed at lower temperatures to the higher conversions reached at these temperatures, which allows more transesterification to take place. Nevertheless, because reaction conditions could be rapidly screened, we identified optimal conditions at a catalyst loading of 0.25 mol%, being 5 s residence time and −10 °C; 95% conversion of monomer was reached. This gave PLA with an M_n of 12,500 g/mol and a PDI of 1.21 and demonstrates good control over the polymerization in the microreactor. This is especially noteworthy as all these results are obtained without the need to

perform the polymerization under an inert atmosphere, where this was deemed essential for all batch-based, TBD-catalyzed PLA polymerizations.[16, 38]
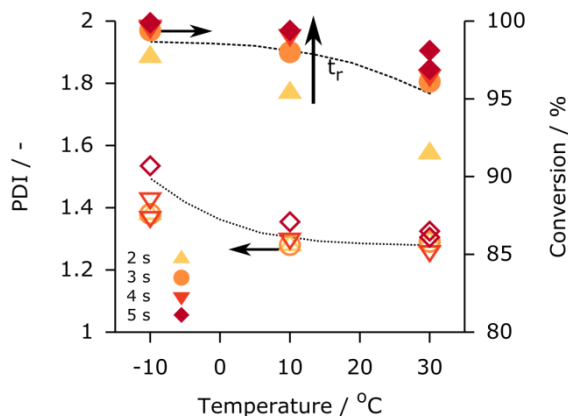

Figure 4. Monomer conversion (closed symbols) and resulting PDI values (open symbols) of TBD-catalyzed PLA formation versus reaction temperature (0.5 mol% TBD). Dashed lines only serve as a guide to the eye.

Higher degrees of polymerization (DP 160 and 240) can be obtained with the microreactor flow setup by adjusting the initiator-to-monomer ratio. The appropriate solutions of monomer (concentration kept at 1.6 M) and initiator were prepared for each targeted DP, using 0.01 M and 0.0067 M initiator for DP 160 and 240, respectively. For a DP of 160, at 0.6 mol% TBD relative to monomer, the polymerization showed very similar trends as for the polymerization targeting a DP of 80 at 0.5 mol% TBD. Conversion increased with increasing residence time (see Appendix 6, Figure S8) and the PDI of the resulting polymers was ≈ 1.2. Full conversion was found at a residence time of 5 s and temperature of –10 °C. The resulting PLA had a M_n of 22,000 g/mol, a PDI of 1.22, and analysis by ^{1}H NMR revealed the DP to be 169.

For a targeted DP of 240, the monomer concentration was kept constant at 1.6 M and the initiator concentration was lowered to 0.0067 M. Controlled variation of the residence time and catalyst loading showed that at 1.2 mol% TBD full conversion

was reached after 3 s at 10 °C (M_n 38,500 g/mol, PDI 1.29). Attempting to polymerize the monomer towards a DP of 240 at a lower catalyst loading (0.75 mol%) resulted in a 3 s residence time and −10 °C as optimal conditions: conversion was 87% and PDI was 1.17 (see Figure S9).

Batch polymerizations give lower conversion. Next we assessed how the polymerization performed in batch mode under the optimized conditions identified in the flow setup. Using oven-dried vials under nitrogen flow, the polymerization was conducted at room temperature (20 °C) with 0.5 mol% catalyst loading and was stopped after a reaction time of 3 s by manual addition of a benzoic acid solution. The resulting reaction mixtures were analyzed by ^{1}H NMR and GPC, showing $49 \pm 6\%$ conversion and PDI values of ≈ 1.2. Using the same stock solutions, the polymerization was performed in flow (at a temperature of 20 °C), giving 91% conversion at a residence time of 3 s and a similar PDI (1.2). This shows that greater control and conversion is achieved in flow without the need for a glovebox. A 30 min scale out under these conditions at 10 °C, followed by precipitation in diethyl ether, centrifugation and drying of the crude polymer, resulted in 64 mg of a white, fluffy polymer (93% yield, DP = 76, PDI 1.19). This extrapolates to > 120 mg of polymer per hour, demonstrating that even a microreactor can already produce useful amounts of well-defined polymer for research, whereas this can in principle be scaled up for commercial application in a mesoscale flow reactor.[39]

Monomer conversion increases upon lowering the reaction temperature. Interestingly, the general trend at these lower catalyst loadings (i.e. < 0.25 mol%) is that the conversion increases with decreasing reaction temperatures (see Figure 2, top). This phenomenon is also observed by Martello et al. for the polymerization of a lactone with TBD.[40] In the case of ring-opening polymerizations, the entropy decreases going from monomer to polymer.[36] The reaction is therefore driven by the exothermic enthalpic contribution from the release of ring strain. L-Lactide exhibits only moderate ring strain, which leads to an equilibrium between polymer and monomer. Duda et al. have reported that the monomer equilibrium concentration, $[M]_{eq}$, is higher at higher reaction temperatures, which matches our findings.[36]

Indeed, using the values for ΔH_p and ΔS_p^0, as determined by Duda et al. for PLA formation from L-lactide, the calculated Gibbs free energy of the polymerization, ΔG, is −12.1 kJ/mol at −10 °C versus −10.5 kJ/mol at 30 °C (see Appendix 6 for calculation). For higher catalyst loadings, the effect of temperature on the conversion is smaller. This may indicate that at certain catalyst loadings, the polymerization is under kinetic rather than thermodynamic control, due to the short residence times and rapid quenching of catalyst.

The livingness of this polymerization was investigated via a set of experiments. At 0.25 mol% catalyst loading and a reaction temperature of −10 °C, the plot of M_n versus conversion follows a straight line (see Figure 2, bottom). The conversion at −10 °C increased with increasing residence time, whereas the conversion at 10 °C leveled off after 3 s residence time (see Figure 2, top). At 30 °C, however, the conversion even decreased slightly at longer residence times. This clearly disagrees with the characteristics of a living polymerization. This lower conversion at longer residence times may be due to the competing depolymerization reaction that accelerates at higher temperatures, caused by the thermodynamic equilibrium between monomer and polymer. The depolymerization of PLA by transesterification is also catalyzed by TBD (see Figure 1) and can under certain circumstances compete with chain growth.

We investigated this further for both low and high catalyst loadings. At a catalyst loading of 0.1 mol% and a reaction temperature of −10 °C, the polymerization conditions were systematically varied for that loading and a targeted DP of 80. No polymeric product was, however, observed at 2–5 s residence time by direct precipitation of the microreactor output into diethyl ether. Increasing the residence time up to 30 s at a reaction temperature of −10 °C only gave oligomeric species (DP 8–12 as measured by ^{1}H NMR). The conversions for several residence times (up to 30 s) were determined using a microreactor with a larger internal volume (see Appendix 6, Figure S14) and showed that the conversion *decreased* with increasing residence time. We reason that there is not enough catalyst to properly start the

polymerization, while depolymerization negatively impacts polymer length at longer residence times.

At high catalyst loading (i.e. > 0.5 mol% for DP=80) the polymerization seems to be under kinetic control due to the timely addition of benzoic acid to quench TBD. The monomer equilibrium concentration is expected to be higher at higher temperatures, thus the polymerization was performed with 0.6 mol% TBD at 30 °C. For these conditions, the conversion was ≈ 98% for residence times up to 20 s, while longer residence times (i.e. 30 s or more) caused the conversion to drop again with a concomitant rise in PDI (see Appendix 6, Figure S24). We attribute this to the products of the polymerization being under kinetic control with residence times < 20 s, while the thermodynamic equilibrium is attained at longer residence times.

Preliminary results suggest that the catalyst efficacy is dependent on the concentration. The polymerization was performed at different residence times with 0.3 mol% TBD, 1.6 M monomer concentration and targeted DP of 80, at 30 °C. After this run, the solutions were diluted such that the concentrations of monomer, initiator and catalyst were halved. This two-fold decrease in concentration resulted in a four-fold decrease in conversion (see Appendix 6, Figure S23), which makes sense if the polymerization rate constant is dependent on both the monomer and catalyst concentration. Running the reaction at higher concentrations (e.g. 3.2 M) resulted in blockage of the microreactor chip due to precipitation of the monomer. Nevertheless, these results are in stark contrast with the results of Lohmeijer et al., who have been able to reach high conversions of monomer at very low loading (0.72 M monomer, 0.1 mol% catalyst).[16]

These and previously described data suggest that there is both a distinct low and high concentration regime for the ROP of L-lactide with respect to TBD-catalyst loading. At low catalyst loading (less than 0.2 equivalents of catalyst per initiator, or 0.25 mol% catalyst for a targeted DP of 80) the reaction appears to be thermodynamically controlled, the plot of conversion versus residence time is as shown in Figure 2 (top). At high catalyst loading (more than 0.4 equivalents of

catalyst per initiator, 0.5 mol% catalyst for a targeted DP of 80) and low residence time (10 s or less), the reaction appears to be under kinetic control, the same plot now resembling Figure S8 (see Appendix 6), and the timely addition of a quenching agent stops the reaction from reaching thermodynamic equilibrium.

Nevertheless, it should be emphasized that all the trends and optimal PLA polymerization conditions, described in the previous sections, could only be identified very rapidly thanks to the possibility of fast reaction condition screening in a microreactor.

Functionalized PLA production in flow using macro- and click chemistry-ready initiators. Having demonstrated that the ring-opening polymerization of L-lactide can be performed outside of the glovebox while maintaining good control over the process, we sought to add functionality to the resulting PLA polymer to increase the scope of its use in biomedical applications. PEG-PLA block copolymers are of interest for use in "stealthy" bio-compatible drug carriers.[26] Using commercially available polyethylene glycol monomethyl ether **2** (M_n 5,000 g/mol, PDI 1.04) as the initiator, the microreactor was used to quickly scan reaction conditions and generate PEG-PLA block copolymers in continuous flow.

At a catalyst loading of 1 mol%, a residence time of 2 s and 30 °C, 68% conversion of monomer was observed that increased to 96% conversion at a reaction temperature of −10 °C. The resulting PEG-PLA block copolymers had a PDI of 1.13 and 1.23, respectively (see Appendix 6, Figure S17). ^{1}H NMR measurements revealed that the composition of these two block copolymers was PEG_{113}-PLA_{54} and PEG_{113}-PLA_{70} (see Appendix 6, Figure S3 and S4, respectively). Quantitative monomer conversion could be achieved using a 4 s residence time at −10 °C, however, at the expense of a slightly higher PDI (1.32, DP of PLA block = 73).
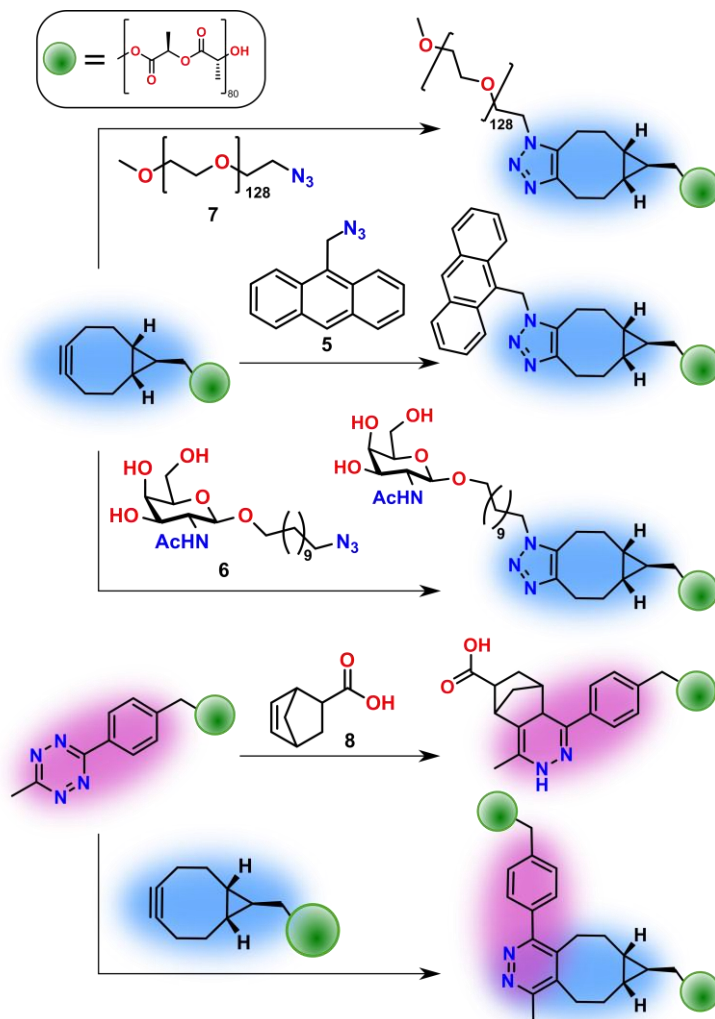
Figure 5: SPAAC with PEG-5,000-N3 (**7**), anthracene azide (**5**) and *N*-acetylgalactosamine derivative **6**, IEDDA with 5-norbornene-2-carboxylic acid (**8**) and finally IEDDA between BNC-PLA and tetrazine-PLA. [BCN moiety is highlighted in blue, tetrazine moiety highlighted in purple.]

Strain-release assisted click chemistries are, of course, a very versatile method to further functionalize PLA as it would allow for the facile and mild attachment of complex (bio)molecules without the involvement of any metal. We identified the metal-free strain-promoted azide-alkyne and tetrazine-norbornene click reactions as

fitting complements to our flow-based metal-free synthesis of PLA. As such, *exo*-BCN-derived alcohol **3** and tetrazine **4** were investigated as potential initiators and click handles (see Figure 1) at a targeted DP of 80 with 1 mol% catalyst loading.
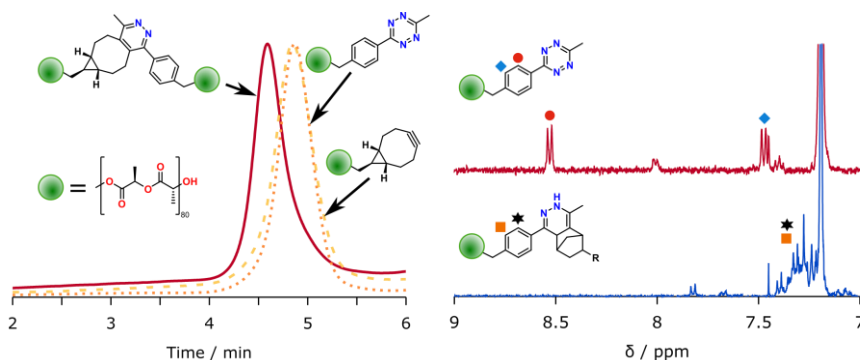
Figure 6. **Left:** GPC traces of BCN-PLA (dashed yellow) and tetrazine-PLA (dotted orange), both having DP = 80. The resulting clicked material (solid red) has M_n 27,000 g/mol and PDI 1.28. **Right:** Zoom of ^{1}H NMR of tetrazine-PLA before (top) and after (bottom) inverse electron demand Diels-Alder reaction with 5-norbornene-2-carboxylic acid.

After screening reaction conditions, the polymerization starting from *exo*-BCN-derived alcohol **3** was performed at a reaction temperature of −10 °C and 2 s residence time for 50 min. This yielded 150 mg of a white powder after centrifugation and drying (87%, M_n 17,500 g/mol and PDI 1.24). In order to assess if the strained alkyne survived the polymerization process, a SPAAC reaction was performed using 9-(azidomethyl)anthracene **5** for 6 h (see Scheme 1). After purification, ^{1}H NMR showed incorporation of the anthracene unit into the PLA, in a ratio of 1:164 (determined from the ratio of *H*-10 of the anthracene *vs* the backbone C-H protons of the PLA, matching the expected DP of 80) confirming the intact strained alkyne after polymerization (see Appendix 6, Figure S2). To demonstrate the feasibility of attaching biomolecules, we carried out the SPAAC reaction between *N*-acetylgalactosamine derivative **6** and BCN-PLA (see Figure 5). After 20 h in hexafluoroisopropanol, the clicked glycopolymer was purified by filtration and precipitation, and ^{1}H NMR confirmed full conversion of the BCN moiety (see Appendix 6, Figure S6).

By utilizing the BCN moiety on the BCN-PLA polymer, other polymeric materials containing an azide can be ligated, generating block copolymers as well. The SPAAC-ready BCN-PLA material was reacted with PEG-5,000-N$_3$ (**7**) for 24 h at room temperature in DCM. Analysis by GPC showed full conversion of the BCN-PLA starting material (see Appendix 6, Figure S18).

Analogously, we investigated tetrazine-linked alcohol **4** initiator for the ROP of L-lactide. Tetrazines are next-generation click chemistry handles, and are amenable to inverse electron demand Diels-Alder reaction which is among the fastest metal-free click reactions known. The use of tetrazines in synthesis is currently limited by their incompatibility with highly basic catalysts like DBU (and TBD) that cause them to degrade rapidly.[33] Methyl-substituted tetrazines such as **4** have been shown to be more stable than their hydrogen analogues.[41] Nevertheless, we found that exposure of **4** to TBD in batch reactions caused rapid degradation.[33] Based on the short residence times needed for the polymerization of L-lactide in flow, however, we postulated that the very brief contact time between tetrazine **4** and TBD would limit tetrazine degradation in our flow setup. The tetrazine-derived alcohol **4** was added to the monomer solution and used as an initiator, with the TBD catalyst in a separate syringe. This led to brightly colored polymeric material as the output of the microreactor. At a catalyst loading of 1 mol%, high conversions of monomer were found, yielding a DP of 80 while keeping the PDI below 1.3. The polymerization was scaled out under these optimized conditions for 50 min (reaction temperature −10 °C, residence time 2 s), giving 170 mg of a purple solid (98%, M$_n$ 17,000 g/mol, PDI 1.20) after purification by precipitation. ^{1}H NMR analysis revealed a degree of polymerization of 80 units and also confirmed the intact nature of the tetrazine moiety in the polymer. With this result we present the first example of tetrazine-terminated PLA, and show a distinct advantage of continuous flow microreactors over batch chemistry, as the short reaction time enables the use of the base-labile tetrazine initiator **4** without causing degradation. Next, a small amount of purified tetrazine-PLA material was reacted for 16 h with 5-norbornene-2-carboxylic acid. The color of the solution changed from pink to colorless and analysis by ^{1}H NMR

confirmed the complete consumption of the tetrazine handle (see Figure 6). The reaction of the tetrazine and norbornene subunits does not take place stereo- or regioselectively, leading to multiple products. This complicates analysis by ^{1}H NMR, and as such a norbornene-derived ester (see Appendix 6, Figure S8) was reacted with the tetrazine-terminated polymer. Unfortunately, no clear singlet of the 4-*tert*-butyl group was identified. This is again attributed to the different regioisomers. The reaction with *exo*-BCN **3** does lead to a single product (see Appendix 6, Figure S9). A comparative study showed that methyl-substituted 1,2,4,5-tetrazines react slower than their hydrogen counterparts, which is to be expected from the inverse-electron demand Diels-Alder reaction.[41] Future development and use of different tetrazines may lead to faster reaction kinetics.

Finally, the efficiency of the inverse electron demand Diels-Alder reaction and use of both clickable PLAs was investigated by reacting BCN-PLA and tetrazine-PLA to generate larger PLA. After 16 h at room temperature, analysis by ^{1}H NMR showed full consumption of BCN-PLA (see Appendix 6, Figure S7). GPC shows a material with M_n 27,000 g/mol and PDI 1.28 (see Figure 6). Facile precipitation yielded 70 mg of clicked polymeric product.

Conclusion

The organocatalyzed ring-opening polymerization of L-lactide under continuous flow conditions produces well-defined PLA (PDI ≈ 1.2) within seconds at low catalyst loadings (0.25–1.2%) and high conversions (95–100%) without the use of an inert atmosphere. Use of the microreactor allowed for a rapid extensive screening of reaction conditions for this polymerization. This revealed that longer residence times will typically give rise to higher conversions and a concomitantly broader molecular weight distribution due to transesterification of the polymer backbone by the catalyst (1,5,7-triazabicyclo[4.4.0]dec-5-ene; TBD). Polymers up to a DP of 240 (Mn 44,000 g/mol) have been synthesized in the same continuous flow reactor by adjusting the initiator-to-monomer ratio. This organocatalytic, metal-free continuous flow method is rapid and mild enough to allow the use of an initiator that contains a

PEG-5,000 chain, or a cyclooctyne or a base-labile tetrazine, without noticeable degradation of these moieties during the polymerization. The resulting BCN-PLA and tetrazine-PLA materials can then be readily functionalized with small (bio)molecules and large polymers bearing azides and norbornenes via SPAAC and inverse electron demand Diels-Alder click chemistry. Such functionalizations allow for an easy expansion of the scope of flow-based polymerizations for biomedical and other applications.

Materials & Methods

Tetrahydrofuran (THF, HiPerSolv CHROMANORM, VWR), 5-norbornene-2-carboxylic acid **8** (98%, mixture of en-do/exo, Sigma-Aldrich), methoxypolyethylene glycol azide **7** (Sigma-Aldrich, MW 5,000 g/mol) and polyethylene glycol monomethyl ether **2** (Sigma-Aldrich, MW 5,000 g/mol, PDI 1.04 as determined by GPC in THF vs PS standards) were used as received. Dichloromethane (CH_2Cl_2, Sigma-Aldrich, >99.8%) and toluene (Sigma-Aldrich, >99.8%) were purified over aluminum oxide under argon using a Pure Solv 400 solvent purification system (Innovative Technology, Amesbury, USA). (3S)-*cis*-3,6-Dimethyl-1,4-dioxane-2,5-dione (L-lactide, Aldrich, 98%) was recrystallized twice from dry toluene and dried under vacuum. Benzoic acid (Sigma-Aldrich, 99.5%) was used as received. 1,5,7-Triazabicyclo[4.4.0]dec-5-ene (TBD, Aldrich, 98%) was stored in a glovebox under argon atmosphere. 4-tert-Butylbenzyl alcohol **1** (Aldrich, 98%) was stored on 4 Å molsieves. ((1*R*,8*S*,9*r*)-bicyclo[6.1.0]non-4-yn-9-yl)methanol (*exo*-BCN-alcohol **3**)[28] and 9-(azidomethyl)anthracene[42] **5** were prepared according to literature procedures. (4-(6-methyl-1,2,4,5-tetrazin-3-yl)phenyl)methanol (tetrazine **4**) was prepared according to a literature procedure,[43] purified with dry column vacuum chromatography (heptane:ethyl acetate, 0% – 60%, 5% increase in ethyl acetate per fraction) and recrystallized from heptane:ethyl acetate (10:1). *N*-acetylgalactosamine **6** was prepared according to a modified literature procedure (see Appendix 6).[44]

Characterization. ^{1}H NMR experiments were performed on a Bruker Avance III 400 MHz spectrometer. The degree of polymerization for PLA initiated from 4-*tert*-butylbenzyl alcohol was determined by integrating the backbone protons at 5.15 ppm and the *tert*-butyl protons of the initiator at 1.32 ppm. Conversion was determined by integrating the monomer signals at 5.05 ppm and the polymer signals at 5.15 ppm. Molecular weight distribution was characterized by gel-permeation chromatography (GPC), performed using an Agilent 1200 LC system fitted with a PLgel 10 μm MIXED-D column. THF was used as a solvent and the system was calibrated using monodisperse polystyrene standards.

Typical polymerization of L-Lactide in continuous flow. In a glovebox, 14.5 mg TBD was weighed into a 25 mL volumetric flask. Outside of the glovebox, under a flow of nitrogen, 5 mL of a 0.1 M DCM solution of the initiator (4-*tert*-butylbenzyl alcohol) was added. The resulting suspension was sonicated for 5 min. Dry DCM was added to the 25 mL mark, and the solution was sonicated again for 5 min. Recrystallized L-lactide (2.3 g) was weighed in a 10 mL volumetric flask. Dry DCM was added to the 10 mL mark to get a 1.6 M monomer solution. Finally, benzoic acid (122 mg) was dissolved in 5 mL dry DCM. Three syringes were filled with initiator/catalyst, monomer and quench solution and loaded onto syringe pumps. The Chemtrix Labtrix system was fitted with a SOR 3221 chip (1 μL reactor volume, staggered oriented ridge mixers). The residence time was set by the flow rate of the syringe pumps; for a 2 s residence time, the first syringe pump (delivering the initiator/catalyst and monomer solutions) was set to 15 μL/min and the second syringe pump (delivering the benzoic acid quench solution) was set to 30 μL/min. Previous findings by Tonhauser et al. showed that flushing the reactor prior to the reaction may remove adventitious contaminants, such as water.[2] Water will act as a quenching agent, lowering the effective catalyst loading. Prior to collection of samples, the microreactor was flushed with the solutions for 20 min. After equilibration for 10 min at −10 °C, a sample was collected in a GC vial. After sample collection, the temperature was increased to 30 °C and again, the setup was equilibrated and a sample was taken. Finally, the temperature was decreased to

10 °C and a sample was taken after equilibration. This operation was repeated for other residence times, in random order. At each residence time, the three experiments at different temperatures where performed in random order.

Batch polymerization outside of glovebox. In the glovebox, 21.1 mg TBD was weighed into a 10 mL volumetric flask. Outside of the glovebox, 2 mL of a solution of 4-*tert*-butylbenzyl alcohol solution (0.1 M, 0.164 g in 10 mL DCM) and DCM was added to the 10 mL mark. A fresh monomer solution (1.6 M, 1.15 g in 5 mL DCM) was prepared. 0.2 mL of each solution was added to oven-dried vials under a nitrogen flow. The temperature in the lab was 20 °C. After 3 s, 0.5 mL of a benzoic acid solution (0.2 M, 0.23 g in 10 mL DCM) was added to quench the reaction. The solvent was removed by nitrogen flow. The conversion was measured using ^{1}H NMR. To compare these results with flow, the same solutions were used in the microreactor setup. The temperature was set to 20 °C, the same as in the lab. After an equilibration time of 20 min, the output was collected and analyzed by ^{1}H NMR after removal of solvent.

L-Lactide polymerization initiated from BCN-alcohol 3. As above, TBD (32 mg, 0.23 mmol) was weighed into a 10 mL volumetric flask inside the glovebox. To this flask was added *exo*-BCN-alcohol **3** (28 mg, 0.19 mmol). The polymerization in the microreactor was performed as above. After obtaining optimal reaction conditions, the output of the microreactor was collected for 50 min to yield 152 mg BCN-PLA.

L-Lactide polymerization initiated from tetrazine-alcohol 4. As above, TBD (27.0 mg, 0.19 mmol) was weighed into a 10 mL volumetric flask inside the glovebox. Under the above conditions (TBD and initiator in one flask), the tetrazine is not stable. Therefore, a new stock solution of L-lactide was made (1.15 g, 7.99 mmol) in 5 mL distilled DCM. To this flask was added tetrazine-derived alcohol **4** (20 mg, 0.10 mmol). The polymerization in the microreactor was performed as above. After obtaining optimal reaction conditions, the output of the microreactor was collected for 50 min to yield 171 mg tetrazine-PLA.

SPAAC reaction with azido-anthracene and BCN-PLA. To 12 mg of BCN-PLA (0.001 mmol) in DCM (1 mL) was added 9-(azidomethyl)anthracene **5** (5.5 mg, 0.024 mmol). This solution was stirred at rt for 6 h. After this time, the polymer was precipitated twice in diethyl ether and isolated by centrifuge at 5,000 rpm for 2 min. The resulting white precipitate was dried *in vacuo* and analyzed using GPC and ^{1}H NMR.

SPAAC reaction with PEG-5,000-azide and BCN-PLA. In a GC vial was 27 mg PEG-5000-azide (0.0054 mmol). To this was added 1.0 mL solution of BCN-PLA in DCM (0.005 mmol, M_n 28,000 g/mol, PDI 1.24) and the resulting solution was stirred at rt. After 24 and 48 h, samples were taken and analyzed using GPC.

SPAAC reaction with *N*-acetylgalactosamine derivative 6 and BCN-PLA. To 12 mg of BCN-PLA (0.001 mmol) in hexafluoroisopropanol (0.5 mL) was added *N*-acetylgalactosamine derivative **6** (3.0 mg, 0.037 mmol). This solution was stirred at rt for 20 h. After this time, the suspension was filtered over cotton and precipitated into diethyl ether. After isolation by centrifugation (5,000 rpm, 1 min), the resulting solid was redissolved in DCM and filtered again over cotton. The solvent was removed *in vacuo* and the resulting polymer was analyzed using ^{1}H NMR.

Inverse electron demand Diels-Alder reaction with tetrazine-PLA and 5-norbornene-2-carboxylic acid. To 15 mg purified tetrazine-PLA (0.0013 mmol) in 0.5 mL DCM was added five drops of 5-norbornene-2-carboxylic acid (**8**). The resulting purple solution was kept at rt for 16 h. After this time, the solution had turned colorless. The polymer was precipitated twice from diethyl ether and analyzed by ^{1}H NMR.

Inverse electron demand Diels-Alder reaction with tetrazine-PLA and BCN-PLA. To 50 mg BCN-PLA (0.004 mmol) was 47 mg tetrazine-PLA (0.004 mmol) and 1 mL DCM. The resulting solution was kept at rt for 16 h, purified by precipitation and analyzed with GPC and ^{1}H NMR.

References

[**1**] D. Wilms, J. Klos, H. Frey. Microstructured Reactors for Polymer Synthesis: A Renaissance of Continuous Flow Processes for Tailor-Made Macromolecules? *Macromol. Chem. Phys.* **2008,** *209* (4), 343-356.

[**2**] C. Tonhauser, D. Wilms, F. Wurm, E. B. Nicoletti, M. Maskos, H. Löwe, H. Frey. Multihydroxyl-Functional Polystyrenes in Continuous Flow. *Macromolecules* **2010,** *43* (13), 5582-5588.

[**3**] K. Iida, T. Q. Chastek, K. L. Beers, K. A. Cavicchi, J. Chun, M. J. Fasolka. Living anionic polymerization using a microfluidic reactor. *Lab Chip* **2008,** *9*, 339-345.

[**4**] E. Baeten, B. Verbraeken, R. Hoogenboom, T. Junkers. Continuous poly(2-oxazoline) triblock copolymer synthesis in a microfluidic reactor cascade. *Chem. Commun.* **2015,** *51* (58), 11701-11704.

[**5**] K. Geyer, J. D. Codee, P. H. Seeberger. Microreactors as tools for synthetic chemists-the chemists' round-bottomed flask of the 21st century? *Chem. Eur. J.* **2006,** *12* (33), 8434-8442.

[**6**] C. H. Hornung, C. Guerrero-Sanchez, M. Brasholz, S. Saubern, J. Chiefari, G. Moad, E. Rizzardo, S. H. Thang. Controlled RAFT Polymerization in a Continuous Flow Microreactor. *Org. Process Res. Dev.* **2011,** *15* (3), 593-601.

[**7**] Y. Shen, S. Zhu. Continuous atom transfer radical block copolymerization of methacrylates. *AIChE J.* **2002,** *48* (11), 2609-2619.

[**8**] C. Diehl, P. Laurino, N. Azzouz, P. H. Seeberger. Accelerated Continuous Flow RAFT Polymerization. *Macromolecules* **2010,** *43* (24), 10311-10314.

[**9**] S. Kundu, A. S. Bhangale, W. E. Wallace, K. M. Flynn, C. M. Guttman, R. A. Gross, K. L. Beers. Continuous flow enzyme-catalyzed polymerization in a microreactor. *J. Am. Chem. Soc.* **2011,** *133* (15), 6006-6011.

[**10**] A. Natalello, J. Morsbach, A. Friedel, A. Alkan, C. Tonhauser, A. H. E. Müller, H. Frey. Living Anionic Polymerization in Continuous Flow: Facilitated Synthesis of High-Molecular Weight Poly(2-vinylpyridine) and Polystyrene. *Org. Process Res. Dev.* **2014,** *18* (11), 1408-1412.

[**11**] L. Simón, J. M. Goodman. The Mechanism of TBD-Catalyzed Ring-Opening Polymerization of Cyclic Esters. *J. Org. Chem.* **2007,** *72* (25), 9656-9662.

[**12**] F. A. Leibfarth, J. A. Johnson, T. F. Jamison. Scalable synthesis of sequence-defined, unimolecular macromolecules by Flow-IEG. *Proc. Natl. Acad. Sci. U. S. A.* **2015,** *112* (34), 10617-10622.

[**13**] M. Jamshidian, E. A. Tehrany, M. Imran, M. Jacquot, S. Desobry. Poly-Lactic Acid: Production, Applications, Nanocomposites, and Release Studies. *Compr. Rev. Food Sci. Food Saf.* **2010,** *9* (5), 552-571.

[**14**] Institute for Bioplastics and Biocomposites: Material share of biopolymer production capacity. http://ifbb.wp.hs-hannover.de/downloads/content/Statistics/Market%20statistics/Production%20capacities/By%20material%20type/2013/Material%20share%20of%20biopolymer%20production%20capacity%20sorted%20by%20material%20grade%202013.png (August 25, 2015),

[**15**] A. P. Dove. Organic Catalysis for Ring-Opening Polymerization. *ACS Macro Lett.* **2012,** *1* (12), 1409-1412.

[**16**] R. C. Pratt, B. G. G. Lohmeijer, D. A. Long, R. M. Waymouth, J. L. Hedrick. Triazabicyclodecene: A Simple Bifunctional Organocatalyst for Acyl Transfer and Ring-Opening Polymerization of Cyclic Esters. *J. Am. Chem. Soc.* **2006,** *128* (14), 4556-4557.

[**17**] T. Saito, Y. Aizawa, K. Tajima, T. Isono, T. Satoh. Organophosphate-catalyzed bulk ring-opening polymerization as an environmentally benign route leading to block copolyesters, end-functionalized polyesters, and polyester-based polyurethane. *Polym. Chem.* **2015,** *6* (24), 4374-4384.

[**18**] A. P. Dove, H. Li, R. C. Pratt, B. G. G. Lohmeijer, D. A. Culkin, R. M. Waymouth, J. L. Hedrick. Stereoselective polymerization of *rac-* and *meso-*lactide catalyzed by sterically encumbered *N*-heterocyclic carbenes. *Chem. Commun.* **2006,** (27), 2881-2883.

[**19**] B. Guillerm, V. Lemaur, B. Ernould, J. Cornil, R. Lazzaroni, J.-F. Gohy, P. Dubois, O. Coulembier. A one-pot two-step efficient metal-free process for the generation of PEO-b-PCL-b-PLA amphiphilic triblock copolymers. *RSC Adv.* **2014,** *4* (20), 10028.

[**20**] H. Jung, N. t. Brummelhuis, S. K. Yang, M. Weck. One-pot synthesis of poly(norbornene)-block-poly(lactide) copolymers using a bifunctional initiator. *Polym. Chem.* **2013,** *4* (9), 2837.

[**21**] I. A. Barker, D. J. Hall, C. F. Hansell, F. E. Du Prez, R. K. O'Reilly, A. P. Dove. Tetrazine-norbornene click reactions to functionalize degradable polymers derived from lactide. *Macromol. Rapid Commun.* **2011,** *32* (17), 1362-1366.

[**22**] F. A. Leibfarth, N. Moreno, A. P. Hawker, J. D. Shand. Transforming polylactide into value-added materials. *J. Polym. Sci., Part A: Polym. Chem.* **2012,** *50* (23), 4814-4822.

[**23**] J. Garcia Hartjes, S. Bernardi, C. A. G. M. Weijers, T. Wennekes, M. Gilbert, F. Sansone, A. Casnati, H. Zuilhof. Picomolar inhibition of cholera toxin by a pentavalent ganglioside GM1os-calix[5]arene. *Org. Biomol. Chem.* **2013,** *11* (26), 4340-4349.

[**24**] W. W. Kallemeijn, M. D. Witte, T. Wennekes, J. M. F. G. Aerts, H. Derek, Chapter 4 - Mechanism-Based Inhibitors of Glycosidases: Design and Applications. In *Adv. Carbohydr. Chem. Biochem.*, Academic Press: 2014; Vol. Volume 71, pp 297-338.

[**25**] F. Duval, T. A. van Beek, H. Zuilhof. Key steps towards the oriented immobilization of antibodies using boronic acids. *Analyst* **2015,** *140* (19), 6467-6472.

[**26**] T. Verrecchia, G. Spenlehauer, D. V. Bazile, A. Murry-Brelier, Y. Archimbaud, M. Veillard. Non-stealth (poly(lactic acid/albumin)) and stealth (poly(lactic acid-polyethylene glycol)) nanoparticles as injectable drug carriers. *J. Controlled Release* **1995,** *36*, 49-61.

[**27**] J. F. Lutz. 1,3-dipolar cycloadditions of azides and alkynes: a universal ligation tool in polymer and materials science. *Angew. Chem. Int. Ed.* **2007,** *46* (7), 1018-1025.

[**28**] J. Dommerholt, S. Schmidt, R. Temming, L. J. Hendriks, F. P. Rutjes, J. C. van Hest, D. J. Lefeber, P. Friedl, F. L. van Delft. Readily accessible bicyclononynes for bioorthogonal labeling and three-dimensional imaging of living cells. *Angew. Chem. Int. Ed.* **2010,** *49* (49), 9422-9425.

[**29**] J. Guo, G. Chen, X. Ning, M. A. Wolfert, X. Li, B. Xu, G. J. Boons. Surface modification of polymeric micelles by strain-promoted alkyne-azide cycloadditions. *Chemistry* **2010,** *16* (45), 13360-13366.

[**30**] J. Zheng, K. Liu, D. H. Reneker, M. L. Becker. Post-assembly derivatization of electrospun nanofibers via strain-promoted azide alkyne cycloaddition. *J. Am. Chem. Soc.* **2012,** *134* (41), 17274-17277.

[**31**] P. A. Ledin, N. Kolishetti, M. S. Hudlikar, G. J. Boons. Exploring strain-promoted 1,3-dipolar cycloadditions of end functionalized polymers. *Chem. Eur. J.* **2014,** *20* (28), 8753-8760.

[**32**] S. Wang, X. Yang, W. Zhu, L. Zou, K. Zhang, Y. Chen, F. Xi. Strain-promoted azide-alkyne cycloaddition "click" as a conjugation tool for building topological polymers. *Polymer* **2014,** *55* (19), 4812-4819.

[**33**] C. F. Hansell, P. Espeel, M. M. Stamenovic, I. A. Barker, A. P. Dove, F. E. Du Prez, R. K. O'Reilly. Additive-free clicking for polymer functionalization and coupling by tetrazine-norbornene chemistry. *J. Am. Chem. Soc.* **2011,** *133* (35), 13828-13831.

[**34**] A.-C. Knall, C. Slugovc. Inverse electron demand Diels-Alder (iEDDA)-initiated conjugation: a (high) potential click chemistry scheme. *Chem. Soc. Rev.* **2013,** *42* (12), 5131-5142.

[**35**] N. K. Devaraj, R. Weissleder. Biomedical Applications of Tetrazine Cycloadditions. *Acc. Chem. Res.* **2011,** *44* (9), 816-827.

[**36**] A. Duda, A. Kowalski, J. Libiszowski, S. Penczek. Thermodynamic and Kinetic Polymerizability of Cyclic Esters. *Macromol. Symp.* **2005,** *224* (1), 71-84.

[**37**] D. R. Witzke, R. Narayan, J. J. Kolstad. Reversible Kinetics and Thermodynamics of the Homopolymerization of l-Lactide with 2-Ethylhexanoic Acid Tin(II) Salt. *Macromolecules* **1997,** *30* (23), 7075-7085.

[**38**] B. G. G. Lohmeijer, R. C. Pratt, F. Leibfarth, J. W. Logan, D. A. Long, A. P. Dove, F. Nederberg, J. Choi, C. Wade, R. M. Waymouth, J. L. Hedrick. Guanidine and Amidine Organocatalysts for Ring-Opening Polymerization of Cyclic Esters. *Macromolecules* **2006,** *39* (25), 8574-8583.

[**39**] N. Micic, A. Young, J. Rosselgong, C. Hornung. Scale-up of the Reversible Addition-Fragmentation Chain Transfer (RAFT) Polymerization Using Continuous Flow Processing. *Processes* **2014,** *2* (1), 58-70.

[**40**] M. T. Martello, A. Burns, M. Hillmyer. Bulk Ring-Opening Transesterification Polymerization of the Renewable δ-Decalactone Using an Organocatalyst. *ACS Macro Lett.* **2012,** *1* (1), 131-135.

[**41**] M. R. Karver, R. Weissleder, S. A. Hilderbrand. Synthesis and Evaluation of a Series of 1,2,4,5-Tetrazines for Bioorthogonal Conjugation. *Bioconjugate Chem.* **2011,** *22* (11), 2263-2270.

[**42**] O. Tosic, J. Mattay. New Photochromic Dithienylethenes through a Click Chemistry Approach. *Eur. J. Org. Chem.* **2011,** *2011* (2), 371-376.

[**43**] J. Yang, M. R. Karver, W. Li, S. Sahu, N. K. Devaraj. Metal-catalyzed one-pot synthesis of tetrazines directly from aliphatic nitriles and hydrazine. *Angew. Chem. Int. Ed.* **2012,** *51* (21), 5222-5225.

[**44**] S. Mandal, N. Sharma, B. Mukhopadhyay. H2SO4-Silica Promoted Direct Formation of β-Glycosides of N-Acetyl Glycosylamines under Microwave Conditions. *Synlett* **2009,** *2009* (19), 3111-3114.

Chapter 6

General Discussion

This thesis focuses on applying (organo)catalysis in continuous flow for synthesis of chemicals and polymers. The aims of the research described in it were to develop new surface functionalization techniques for silicon-based materials (silica, silicon carbide) and to study the application of solid-supported organocatalysis in continuous flow using (mesoporous) silica as a solid support.

Chapter 2 describes the covalent modification of silicon carbide (SiC) using 1-alkenes and microwave irradiation. The use of microwave assistance greatly speeds up the formation of organic monolayers on SiC, allowing the modification time to be shortened by more than an order of magnitude. This approach was extended to SiC particles (spheres and grits), although these required longer modification time. This is most likely caused by the higher porosity of the surface of these particles. The use of $1,\omega$-alkenes such as 1,12-dodecene led to alkene-terminated surfaces amenable to mild thiol-ene click chemistry. SiC is an extremely tough and chemically inert material. This makes it suitable as material for (micro-)flow reactors. Organic monolayers on SiC are among the most robust monolayers known and are therefore interesting as tether for high-performance catalysts, to passivate SiC flow reactors, and to attach other functionalities to the inside walls of SiC-based flow reactors.

Nevertheless, the research faced several issues, one of which was reproducibility of the covalent modification using ω-functional alkenes. Some substrates gave very good, densely packed monolayers, where others hardly showed any covalently-bound carbon in XPS. This can be partly attributed to the differences in SiC wafers. SiC wafers tend to have differences from batch to batch and the way SiC is produced apparently had a huge impact on the ability to modify SiC with organic monolayers. SiC can have very different structures, classified into polytypes, of

which more than 250 are known. The major polytypes are (ß)3C-SiC, 4H-SiC and (α)6H-SiC, of which 6H is easiest to produce, yet all have different electronic properties, for instance the bandgap. Furthermore, SiC can have dopants such as nitrogen which influence its properties. A systematic approach investigating parameters of the SiC production process (type of SiC polymorph, dopant species, dopant level, annealing process) might shed light on the issues faced during this project. Experimental setups that can monitor the inside of the microwave vessel are also interesting, as this would allow more precise monitoring of the reaction temperature.

To generate azide-bearing monolayers the surface modification was attempted with epoxy-, bromo- and chloro-alkenes. However, this gave poor monolayers with low surface coverage, most likely due to substantial upside-down attachment. Attempts to substitute the halogen for azide and subsequent CuAAC with a fluoroalkyne resulted in low conversions as measured by X-ray Photoelectron Spectroscopy (XPS). The covalent attachment of 1-alkynes on SiC has been reported in literature.[1] Modification of SiC with a 1,ω-dialkyne may enable the use of CuAAC with azide-bearing solution-phase molecules.

Full characterization of the SiC substrate may lead to greater reproducibility of the covalent modification. Due to the superior properties of SiC-bound monolayers, this material can be interesting for use in packed-bed microreactors. Similar materials, such as mesoporous silica, have already proven to be useful solid supports in continuous flow packed-bed reactors.

The novel covalent modification of MCM-41, a mesoporous silica, described in **chapter 3** is an excellent way to produce alkene-terminated silica, typically giving 2 mmol alkene/g silica (as determined by thermogravimetric analysis). These alkenes are then available for follow-up thiol-ene click chemistry. Quinine, a complex organocatalyst, could be attached by employing a two-step procedure (see Chapter 3, Figure 1). The resulting material was tested in flow and gave excellent

conversion of 3-methoxythiophenol and 2-cyclohexen-1-one to the thio-Micheal adduct at low flow rate.

The exact mechanism by which the alkene reacts with the surface is not fully understood. Evidence from infrared spectroscopy suggests at least a large portion of the alkenes react following Markovnikov's Rule due to the occurrence of methyl peaks in the IR spectrum that the parent molecule 1,7-octadiene does not show. A mixture of Markovnikov and anti-Markovnikov products cannot be ruled out by infrared spectroscopy. An interesting avenue for fundamental future experiments would be to synthesize a labeled octene molecule. Solid-state ^{13}C NMR can then be used to unambiguously assign the reaction product. If two peaks appear, then there must be a mixture of reaction products and multiple reaction pathways are at work (see Figure 1).
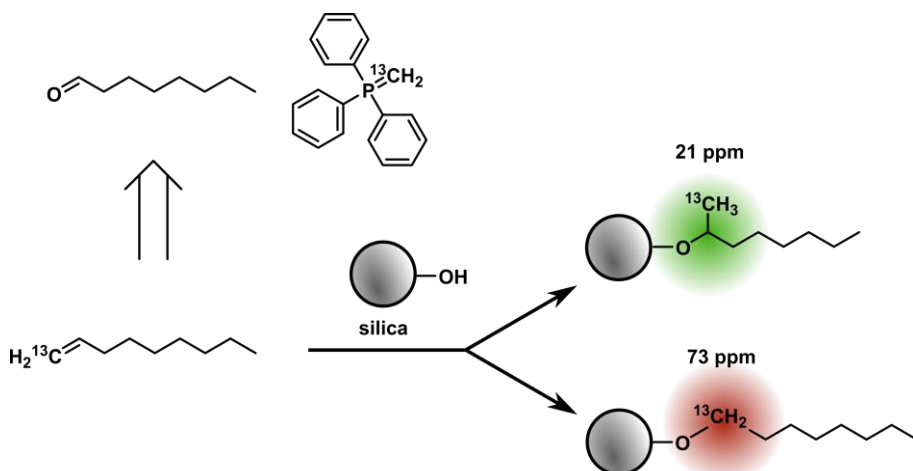
Figure 1. Synthesis of ^{13}C-labeled 1-octene via a Wittig reaction and subsequent reaction with silica will lead to unambiguous identification of reaction products by solid-state NMR.

The modification of mesoporous silica described in **chapter 3** was conducted on MCM-41 with a pore diameter of roughly 3 nm. This small pore diameter could make further follow-up reactions more difficult to perform due to steric hindrance. Indeed, conversions calculated from thermogravimetric analysis were low (typically 30% or less), suggesting inefficient pore functionalization. Future work could focus

on modification of other mesoporous silica materials with larger pores. The large pore size of SBA-15 (typically around 10 nm) should allow attachment of more complex and larger organocatalysts. This modification was attempted, yet seemed to produce less-densely packed monolayers as compared to MCM-41 (as observed with FTIR – lower and broader signals). This could be due to the material properties: MCM-41 is produced under basic conditions, whereas SBA-15 is produced under acidic conditions. This could lower the amount of surface silanols resulting in a less-densely packed monolayer. Future research into SBA-15 should include analysis with thermogravimetric analysis to estimate the amount of covalently-bound alkenes.

The scale-up of this reaction is necessary to produce enough material for use in the larger packed-bed microreactor used in **chapter 4**. Batches up to 300 mg calcined MCM-41 silica have been modified. However, for use in the packed-bed microreactor the material needs to be sieved to the correct size range and this requires several grams of fully modified silica (i.e. with catalyst attached) material. The material produced by our syntheses was SBA-15, yet consisted of irregular shapes with a large dispersity in size. Packing a reactor is made more difficult by the irregularity and large size distribution of the silica, although sieving the material helps. Spherical SBA-15 particles would be even better for packing into the packed-bed reactor. Although there are reports in literature that describe the synthesis of spherical particles,[2] the size is limited to a few microns, which is not large enough for use in the packed-bed reactor applied in this thesis.

The attachment strategy for quinine is not readily scaled up, partly due to the use of photo-initiated thiol-ene click chemistry with 1,2-ethanedithiol. It is known that UV light does not penetrate deeply into large reaction vessels, slowing down the reaction and potentially generating byproducts. This problem might be overcome by evaluating radical initiators such as azobisisobutyronitrile (AIBN) instead of photo-initiators in future experiments. Finally, 1,2-ethanedithiol is not only very smelly but also quite toxic, which makes large-scale reactions at the very least unpleasant.

Alternatives to this dithiol need to be small to avoid steric hindrance and non-volatile, e.g. 1,4-dithiobenzene or 1,4-benzenedimethanethiol.
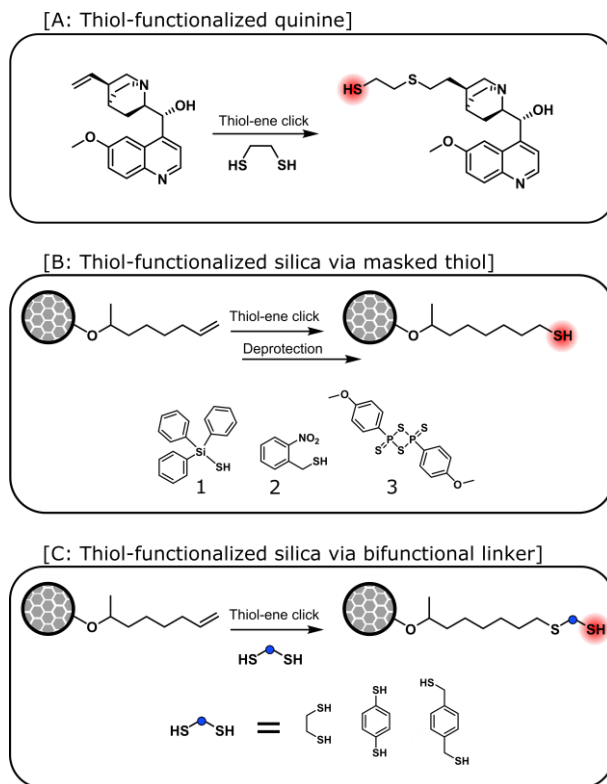
Figure 2. A: Synthesis of a thiol-functionalized quinine *via* thiol-ene click chemistry. **B:** Strategies towards thiol-functionalized silica from alkene-terminated or hydroxy-terminated silica *via* masked thiols (triphenylsilanethiol **1** and (2-nitrophenyl)-methanethiol **2**) and Lawesson's reagent (**3**). **C:** Functionalization of alkene-terminated silica surface using thiol-ene click chemistry and bifunctional thiol linkers.

The final quinine-functionalized silica in **Chapter 3** only had 0.1 mmol quinine/g silica. In the two-step procedure, the thiol-ene click reaction with 1,2-ethanedithiol yields a material with only 0.1–0.2 mmol thiol/g silica as determined by a modified Ellman's test. This test gives the number of *chemically accessible thiols.* A plausible explanation for the low number of thiols compared to the initial monolayer

(2.7 mmol/g according to TGA) is that the Ellman's reagent simply cannot react with all the surface-bound thiols due to steric hindrance. Secondly, a low thiol content could be due to a crosslinking reaction where one molecule of 1,2-ethanedithiol attaches to two surface bound alkenes, leaving no free thiol. To increase the loading of quinine we envisaged cutting down this two-step procedure to just one step. We explored this in several ways via some preliminary experiments: synthesizing a quinine with a thiol group, use of a stiffer linker (1,4-dithiobenzene), and use of masked thiols to convert the surface-bound alkenes to thiols (see Figure 2).

Initial attempts to synthesize a thiol-containing derivative of quinine proved challenging. Reaction of quinine with 1,2-ethanedithiol under thiol-ene click conditions led to incomplete conversion and dimerization of quinine. The use of triphenylsilanethiol (Ph_3SiSH) and (2-nitrophenyl)methanethiol as masked thiols was explored.[3, 4] Ph_3SiSH can be installed *via* thiol-ene click chemistry using AIBN and subsequent deprotection with trifluoroacetic acid yields the free thiol. This was attempted for quinine but again, incomplete conversion and difficult separation prevented this route from being useful.

A different strategy focused on introducing thiols on the surface of the alkene-terminated silica. In a proof-of-concept experiment (2-nitrophenyl)methanethiol could be installed with thiol-ene click chemistry on 1-octene and deprotection with 365 nm UV light led to 1-thiooctane (observed with GC-MS). However, attempts to transform the alkene-terminated silica into thiol-terminated silica via this reaction were met with failure. Full conversion of the surface alkenes could not be obtained (even with AIBN), most likely due to steric hindrance. Deprotection to the thiol using UV light did not yield a material with more than 0.2 mmol thiol/g silica as determined by Ellman's test.

Another as of yet unexplored option is the conversion of alcohols to thiols using Lawesson's reagent. This would require the initial monolayer to be generated from 11-undecenol (commercially available) with subsequent refluxing in toluene

containing Lawesson's reagent. The anticipated problems are the lower reactivity of 11-undecenol (which would give less densely packed monolayers) and the bulkiness of Lawesson's reagent. Byproducts from Lawesson's reagent could most likely be washed away using methanol. The steric hindrance experienced by the reagent in the pores might prevent full conversion of alcohols to thiols, which again points towards the need for mesoporous silica with pores larger than 3 nm in diameter.

Initial attempts to use 1,4-dithiobenzene as a stiffer linker to prevent cross-linking of surface alkenes were unsuccessful, mostly because of the very low solubility of this compound in organic solvents. An alternative might be 1,4-benzenedimethanethiol, which is possibly more soluble in typical organic solvents for thiol-ene click chemistry.
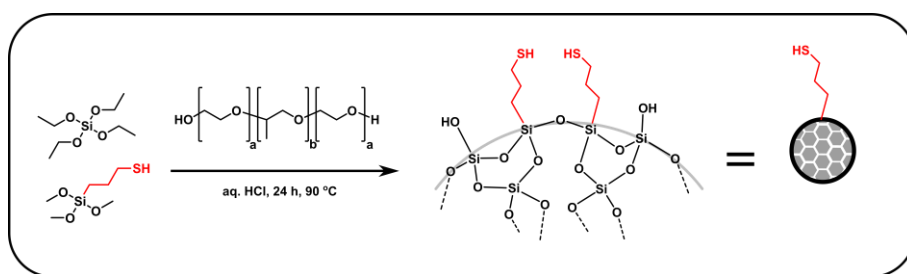
Figure 3. Sol-gel synthesis of thiol-functionalized SBA-15 mesoporous silica. Tetraethyl orhosilicate and (3-mercaptopropyl)trimethoxysilane are hydrolyzed in the presence of a templating agent (Pluronic P123, a triblock copolymer of ethylene oxide and propylene glycol. $a = 20$, $b = 70$ MW 5,800 Da) to yield hexagonally ordered silica after extraction.

A different strategy towards quinine-functionalized mesoporous silica was explored for SBA-15-based materials. These could be produced with surface-bound thiol groups *via* co-condensation with (3-mercaptopropyl)trimethoxysilane, as described in **chapter 4** (see Figure 3). This allows the one-step attachment of quinine *via* its double bond. The Ellman test was used successfully to determine the thiol loading, which was in the range of 0.15 to 0.45 mmol/g silica (as set by the stoichiometry of (3-mercaptopropyl)trimethoxysilane in the initial sol-gel). Higher loadings resulted in less ordered silica, most likely due to disturbance of the pore wall caused by the

bulky thiol. After performing the thiol-ene reaction to install quinine the resulting material proved to be less active than its MCM-41 counterpart in the quinine-catalyzed thio-Michael reaction described in **chapter 3**, even though the loading of quinine was higher. The reason for this might be the presence of acidic surface silanols, which complex with the tertiary amine of quinine. This amine is necessary for catalysis and the complexation to acidic silanols would deactivate the catalyst. A way to test for this in future experiments would be to inactivate the surface silanols with a capping agent such as trimethoxymethylsilane and then running the quinine-catalyzed reaction described in **chapter 3**. If the catalytic performance increases then there are indeed strong hints that the surface silanols are responsible for inactivation of the catalyst.

Thiol-functionalized mesoporous SBA-15 is a versatile material, besides its being useful in thiol-ene click reactions. **Chapter 4** deals with the application of the aforementioned SBA-15-SH material as a solid support for catalysts. Initially we wanted to explore its use as a solid support for palladium in the packed-bed microreactor, as this was reported in literature for microwave-assisted batch reactions by Crudden and co-workers.[5] This thiol-SBA-15 was loaded with palladium and packed into the continuous flow reactor. As a benchmark we chose a Pd-catalyzed Heck reaction. When running the reaction at 120–160 °C a black deposit on the inside of the microchannels formed, hinting at palladium leaching from the solid support. Furthermore, the reaction gave a higher conversion at shorter residence times after this black deposit formed. We could clearly attribute these observations to rapid leaching of the Pd catalyst from the solid support. We tentatively attribute this leaching to the different reaction conditions in flow *vs.* batch: In batch, the reaction is cooled down after completion which might allow the thiol-containing solid support to re-capture the palladium, whereas in flow the solid support is continuously rinsed at high temperatures, allowing no re-capture of the palladium. Furthemore, control experiments in batch showed coloring of the solution, indicative of Pd leaching. This is clearly not desirable for a solid-supported

catalyst. Not only does the palladium content diminish over time, the product also gets contaminated with palladium.

Again, the versatility of the thiol-functionalized SBA-15 material came to light. We could easily oxidize the surface thiols to sulfonic acids. This resulted in a solid-supported sulfonic acid catalyst which we wanted to investigate further. Using this catalyst we were able to conduct three different alcohol protection and deprotection reaction under continuous flow conditions at high (1.0 M) reagent concentration. Alcohols could be efficiently protected as their tetrahydropyranyl derivatives using 3,4-dihydro-*2H*-pyran. Compared to other flow-based approaches our packed-bed reactor produced more than an order of magnitude more material per hour.[6] Installation of trimethyl- and dimethylphenylsilyl groups on primary, secondary, benzylic, and phenolic alcohols could be performed using hexamethyldisilazane (HMDS) and dimethylphenylsilizane (DMPS) at elevated temperatures. Preliminary experiments were performed to generate trimethylsilyl-protected carbohydrates as they are excellent precursors to a wide variety of regioselectively protected carbohydrates.[7] Although initial experiments showed incomplete conversion of the carbohydrate hydroxyls, production of the trimethylsilylated carbohydrate precursor in a continuous flow setup would be of great synthetic value, even more so if subsequent reactions could be performed *on-line*. In **chapter 4** a distinct advantage of the microreactor is highlighted: the use of a back-pressure regulator allowed the use of reaction temperatures well above the boiling point of DCM and MeCN. The scale out of these reactions gave access to tens to hundreds of milligrams of material in short time. Workup was considerably simplified and typically consisted of evaporation of the solvent.

This work focused on commercially available disilazanes. The bulky diphenylmethylsilazane (DPMS) could only be installed at high temperatures. However, there seems to be room for improvement towards protecting groups that are more often used, such as the synthetically interesting *tert*-butyldimethylsilyl group (TBDMS). The corresponding silazane was not widely commercially available at that time. Future work could investigate a cascade of reactions, such as

selective installation of a protecting group onto an alcohol, a transformation of the molecule under which conditions the unprotected alcohol is not stable and final removal of the protecting group. Such a cascade would be akin to a "molecular assembly line" and is a very interesting direction of chemistry.

The biggest drawback currently is the silica itself. Although it is carefully sieved to the appropriate size (45–70 micron), small pieces still manage to dislodge and clog the channel downstream, leading to cataclysmic reactor failure. Upon inspection with a SEM, the silica appears to be consisting of clusters of silica particles. It would be better if the mesoporous silica would consists of hard spheres of the right diameter. While there has been work done in this area,[2, 8] the synthesis of large (50 micron), well-defined mesoporous silica spheres is an art on itself.

In the final research chapter of this thesis we moved away from solid-supported catalysis and ventured into the homogeneous catalysis in flow. As can be seen from **chapter 5**, microreactor technology and polymer chemistry are a good match. The exothermic nature of polymerizations requires excellent heat transfer capabilities, which microreactors can provide. Furthermore, rapid mixing ensures that all polymer chains start growing at the same time, leading to low polydispersity. The work in that chapter demonstrates that we are able to conduct the rapid polymerization of L-lactide in continuous flow with good (> 95%) conversion and do not need to perform the polymerization in a glovebox. The use of the microreactor enables quick screening of reaction parameters and fast identification of optimal reaction conditions. Furthermore, the short contact time (typically 2–5 s) between the highly basic TBD organocatalyst and the rest of the reagents enables the use of a strained cyclooctyne derivative and a base-labile tetrazine derivative (see Figure 4) without significant degradation of either initiator. This metal-free, organocatalytic synthesis opens the way for PLA-based materials for use in biomedical and other applications.

Nevertheless, the polydispersities attained in chapter 5 are either on par (typically 1.2 for degree of polymerization of 80) or higher than those found in batch.[9] Only a

handful of conditions led to PDIs < 1.2. Targeting a polymer with a large degree of polymerization (i.e. DP = 240) with incomplete conversion yields polymers of DP 160–200 with PDI of around 1.16-1.18. From all the data combined, it would seem that a PDI of 1.2 is a plateau value. When using DBU, a related amidine base, the polymerization is an order of magnitude slower and application in flow might lead to lower PDI values, as suggested by the results of Pratt et al.[9] In the work described in chapter 5, relatively high catalyst loadings are used (0.25-1.0 mol% vs 0.1 mol% in batch) which might play a role. Another potential source of the broader molecular weight distribution are the syringe pumps used. If the flow rate is low then the pumping may become pulsating, leading to a broadened residence time distribution. However, this should only become a problem at really low flow rates (less than 1 µL/min). The use of alternate pumps, such as HPLC pumps, may alleviate this potential problem. A last source of broad residence time distribution may arise from the fact that the flow profile inside the microchannel is parabolic: flow is faster in the center of the channel and slower on the edges, leading to differences in residence times.[10] This parabolic profile is not present when using electroosmotic flow (EOF). However, EOF is not compatible with dichloromethane. Nevertheless, a control experiment with EOF in combination with another reaction solvent may rule out the influence of the parabolic flow profile.
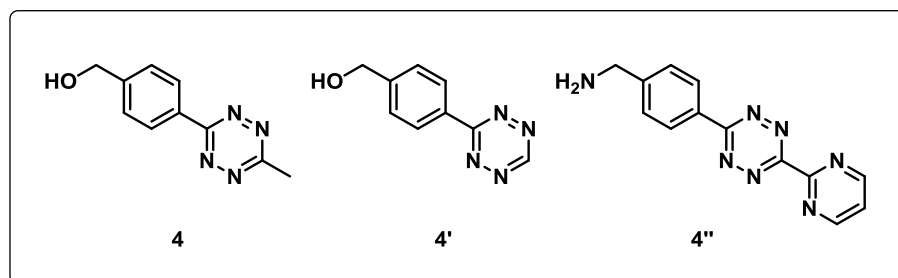
Figure 4: Tetrazine derivative **4** was used in chapter 5 yet proved to be slow in the [4+2] cycloaddition. Literature suggests that **4'** and **4''** react faster.

With regards to the click chemistry employed, the tetrazine-norbornene combination can be further optimized. The tetrazine was chosen for its similarity to the 4-*tert*-

butylbenzyl alcohol initiator, its relative stability, and readily available starting materials combined with previous experience in our laboratory. Although the yield of the tetrazine synthesis was sufficient for use in the polymerization studies, it was rather low compared to literature. Yang et al. report 66% yield, yet Hansell et al. report 13% yield for the same methyl-substituted tetrazine derivative.[11, 12] The synthesis performed by us yielded 11% of the desired tetrazine after recrystallization and was pure by TLC and ^{1}H NMR. The low yield may be due to the use of hydrazine monohydrate instead of anhydrous hydrazine as reported by Yang et al. Furthermore, a large amount of 1,4-dimethyl-1,2,4,5-tetrazine is generated as byproduct. Lastly, the low yield could be due to the solubility of the tetrazine or the unoxidized precursor (1,4-dihydro-1,2,4,5-tetrazine) in water. The use of anhydrous hydrazine is thus recommended for future syntheses via this route.

After performing the polymerization and confirming the survival of the tetrazine, the click reaction with a norbornene derivative proved quite slow. The methyl substituent of the 1,2,4,5-tetrazine is electron donating, which decreases the reactivity of the tetrazine about twenty times compared to the hydrogen analogue.[13] Future work could focus on tetrazines with electron-withdrawing substituents or no substitution on the 3-position at all (see Figure 4). In terms of stability, the short contact time between TBD and the tetrazine will most likely not lead to significant degradation. Furthermore, the tetrazine-norbornene click product consists of a mixture of isomers, complicating analysis. The reaction between a tetrazine and cyclooctyne-derived BCN is not only faster, but also yields only one product, simplifying analysis.

There are several ways one can expand on the extremely fast organocatalytic L-lactide polymerization in flow presented in chapter 5. Currently, only the polymerization of L-lactide has been investigated. Other cyclic esters are amenable to TBD-catalyzed polymerization, such as δ-valerolactone and ε-caprolactone.[9] A drawback is that these monomers polymerize two orders of magnitude slower, which means that either the residence time needs to increase to several minutes (which is

still possible within the Chemtrix setup) or the catalyst concentration must be increased.

L-Lactide containing block copolymers were made from a PEG macroinitiator or by offline click chemistry. Ideally, the blocks would both be introduced from the respective monomers, as this gives greater control over the composition of the resulting block copolymer. Junkers and co-workers have reported a continuous flow system for the synthesis of di- and triblock copolymers of 2-oxazoline derivatives.[14] A similar setup should make it possible to create block copolymers of L-lactide, δ-valerolactone, and ε-caprolactone with tailored properties in a continuous fashion.[9] This paves the way for systems that can create diverse polymeric architectures on demand.

Finally, the catalyst system used in **chapter 5** is homogeneous and it would be advantageous to use a solid-supported catalyst system. This would no longer require the deactivation of the catalyst by an excess of benzoic acid and thereby greatly simplify the workup of the resulting PLA. Previous work by others on continuous flow ATRP polymerization with solid-supported catalysts suggests that an increase in PDI may arise due to the solid support.[15] This was attributed to the increase in viscosity of the reaction medium, which hindered active polymer chains from entering the catalytic sites. The active polymer chains were not deactivated fast enough, resulting in uncontrolled growth and concomitant high PDI. In the ring-opening polymerization of **chapter 5** the polymer chain will not elongate without the catalyst. This may result in slower polymer growth and possibly a *decrease* in PDI. Therefore, solid-supported guanidine bases are very interesting catalysts for ring-opening polymerization of cyclic lactones in continuous flow.

Preliminary results for the Van Leusen oxazole synthesis in flow were obtained. Oxazoles can be obtained from aldehydes and toluenesulfonylmethyl isocyanide (TosMIC; see Figure 5).
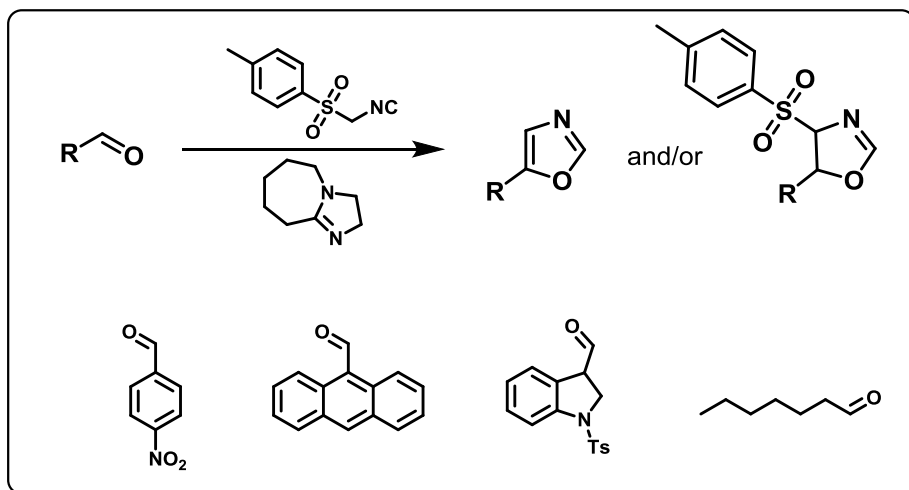
Figure 5. Van Leusen oxazole synthesis in flow using TosMIC tried on four different aldehydes.

The reaction was performed in dichloromethane under pressure to allow reaction temperatures above the boiling point of the solvent. Initial experiments conducted in flow at resulted in full conversion of aldehyde at 70 °C and 15–30 s residence time. The reaction could be run at 0.25 M aldehyde concentration with 1.1 equivalents of TosMIC and 1.2 equivalents of base (DBU). However, in addition to the intended oxazole, the non-eliminated 4,5-dihydrooxazole product (see Figure 5) was still present. The elimination occurs at elevated temperatures, so extended residence times may improve the oxazole yield. Further optimization of this reaction may lead to a flow-based protocol towards oxazoles from aldehydes. Particularly useful would be the inline extraction of the basic DBU and tosic acid side products, which would result in cleaner output. Inline extraction has already been successfully applied in a number of cases and often resulted in easier workup.[16]

Personal Reflection

Upon starting this PhD thesis the flow chemistry setup was introduced as a "plug & play" system, but this is oversimplified. Transitioning from batch to flow chemistry is not done overnight. Instead, it is trial and error and takes a lot of practice. Not only does the chemistry have to fit continuous flow (clogging is always a potential problem), practical problems also emerged in the early phase of the project. It took a lot of trial and error to finally get the microreactor working properly. Leaking syringes, damaged O-rings, the way the tubing is cut, everything has to be dealt with accordingly and this can only be learned after encountering failures. Clogging of microchannels by precipitates is an issue that is hard to solve. Careful selection and batch evaluation of reaction conditions is necessary *before* attempting reactions in flow. Starting the microflow reaction at low concentrations (0.05 M) is desirable as this can help to avoid serious damage by blocking of microchannels. If relevant amounts of material are desired then the concentration needs to increase to the range of 0.1–1.0 M. When running reactions with the packed-bed chip, little pieces of sieved mesoporous silica can still break off and cause clogging. More well-defined solid supports, such as SiC microspheres, may be the way forward. Lightly crosslinked polymers should never be used in this chip as they might swell too much and cause reactor failure.

The way the syringe pumps behave can be a tell-tale sign when a blocking event is eminent, which was learned the hard way. Glass microreactors are able to withstand 20–25 bar of pressure, but will break above a critical pressure. Syringe pumps that could detect the resistance to pumping and switch off in case of a blocked microchannel would be a great addition to the setup. It might save a microchip or two.

On the other hand, after these practical problems are solved and become manageable, the microreactor setup is great for rapidly screening reaction conditions and producing large amounts of data. The optimization of the polymerization of chapter 5 would have taken much longer in batch than in flow. In flow we could

rapidly test the entire range of temperatures and residence times in a single day using very little monomer and catalyst. Once optimal conditions were identified, the same setup could directly be used for producing larger amounts of material.

The current setup is reasonably flexible and has a good range of reliable reaction temperatures (–10 to 180 °C). Reactions at high temperatures have to be equilibrated at intermediate temperatures to avoid thermal shock to the glass microreactor. The residence time depends on the microreactor chip and can be anywhere from 2 s to 5 min. Longer residence times are sometimes desirable and if extremely high temperatures are not necessary, coil reactors may be a flexible alternative.

In this thesis samples are collected and analyzed offline, by ^{1}H NMR, GC-MS or GPC. Online reaction monitoring *via* e.g. IR or UV spectroscopy would enable even faster reaction optimization. Equilibration between samples often equates to 5 to 10 min of waiting time. When online techniques are integrated a microreactor system can be automated, which allows the operator to program a certain set of experiments. The system then executes the reactions, analyzes them, and reports back to the operator, which could be a huge time-saver. As can be seen in for instance chapter 5, reaction screening was performed using a full-factorial approach, yet there are experimental designs that can be used to minimize the amount of experiments necessary for optimization.

Overall, continuous flow chemistry will not replace batch chemistry, but will likely grow significantly in the decades to come and certainly complement batch chemistry. Continuous flow chemistry is becoming part of the toolset readily available to chemists. It will hopefully play an important part in the future of chemistry in the Digital Age. The combination of high-throughput flow chemistry and computers could prove to be invaluable for automated reaction optimization, as demonstrated by Jensen and co-workers.[17-19] Continuous flow reactions, combined with online monitoring and semi-intelligent computer algorithms, may one day be designed, optimized, and scaled out automatically, leaving skilled chemists free to be creative in designing new molecules!

References

[**1**] S. P. Pujari, L. Scheres, T. Weidner, J. E. Baio, M. A. Stuart, C. J. van Rijn, H. Zuilhof. Covalently Attached Organic Monolayers onto Silicon Carbide From 1-Alkynes: Molecular Structure and Tribological Properties. *Langmuir* **2013,** *29* (12), 4019-4031.

[**2**] D. Zhao, J. Sun, Q. Li, G. D. Stucky. Morphological Control of Highly Ordered Mesoporous Silica SBA-15. *Chem. Mater.* **2000,** *12* (2), 275-279.

[**3**] B. Haché, Y. Gareau. Free-radical addition to olefins of an H2S equivalent: Triphenylsilanethiol. *Tetrahedron Lett.* **1994,** *35* (12), 1837-1840.

[**4**] T. Pauloehrl, G. Delaittre, M. Bastmeyer, C. Barner-Kowollik. Ambient temperature polymer modification by in situ phototriggered deprotection and thiol-ene chemistry. *Polym. Chem.* **2012,** *3* (7), 1740-1749.

[**5**] C. M. Crudden, M. Sateesh, R. Lewis. Mercaptopropyl-Modified Mesoporous Silica: A Remarkable Support for the Preparation of a Reusable, Heterogeneous Palladium Catalyst for Coupling Reactions. *J. Am. Chem. Soc.* **2005,** *127* (28), 10045-10050.

[**6**] C. Wiles, P. Watts. Parallel synthesis in an EOF-based micro reactor. *Chem. Commun.* **2007,** (46), 4928-4930.

[**7**] C.-C. Wang, J.-C. Lee, S.-Y. Luo, S. S. Kulkarni, Y.-W. Huang, C.-C. Lee, K.-L. Chang, S.-C. Hung. Regioselective one-pot protection of carbohydrates. **2007,** *446* (7138), 896-899.

[**8**] A. Katiyar, S. Yadav, P. G. Smirniotis, N. G. Pinto. Synthesis of ordered large pore SBA-15 spherical particles for adsorption of biomolecules. *J. Chromatogr. A* **2006,** *1122* (1-2), 13-20.

[**9**] R. C. Pratt, B. G. G. Lohmeijer, D. A. Long, R. M. Waymouth, J. L. Hedrick. Triazabicyclodecene: A Simple Bifunctional Organocatalyst for Acyl Transfer and Ring-Opening Polymerization of Cyclic Esters. *J. Am. Chem. Soc.* **2006,** *128* (14), 4556-4557.

[**10**] B. P. Mason, K. E. Price, J. L. Steinbacher, A. R. Bogdan, D. T. McQuade. Greener Approaches to Organic Synthesis Using Microreactor Technology. *Chem. Rev.* **2007,** *107* (6), 2300-2318.

[**11**] J. Yang, M. R. Karver, W. Li, S. Sahu, N. K. Devaraj. Metal-catalyzed one-pot synthesis of tetrazines directly from aliphatic nitriles and hydrazine. *Angew. Chem. Int. Ed.* **2012,** *51* (21), 5222-5225.

[**12**] C. F. Hansell, A. Lu, J. P. Patterson, R. K. O'Reilly. Exploiting the tetrazine-norbornene reaction for single polymer chain collapse. *Nanoscale* **2014,** *6* (8), 4102-4107.

[**13**] M. R. Karver, R. Weissleder, S. A. Hilderbrand. Synthesis and Evaluation of a Series of 1,2,4,5-Tetrazines for Bioorthogonal Conjugation. *Bioconjugate Chem.* **2011,** *22* (11), 2263-2270.

[**14**] E. Baeten, B. Verbraeken, R. Hoogenboom, T. Junkers. Continuous poly(2-oxazoline) triblock copolymer synthesis in a microfluidic reactor cascade. *Chem. Commun.* **2015,** *51* (58), 11701-11704.

[**15**] Y. Shen, S. Zhu. Continuous atom transfer radical block copolymerization of methacrylates. *AIChE J.* **2002,** *48* (11), 2609-2619.

[**16**] F. A. Leibfarth, J. A. Johnson, T. F. Jamison. Scalable synthesis of sequence-defined, unimolecular macromolecules by Flow-IEG. *Proc. Natl. Acad. Sci. U. S. A.* **2015,** *112* (34), 10617-10622.

[**17**] J. P. McMullen, M. T. Stone, S. L. Buchwald, K. F. Jensen. An Integrated Microreactor System for Self-Optimization of a Heck Reaction: From Micro- to Mesoscale Flow Systems. *Angew. Chem., Int. Ed.* **2010,** *49* (39), 7076-7080.

[**18**] J. P. McMullen, K. F. Jensen. Integrated microreactors for reaction automation: new approaches to reaction development. *Annu. Rev. Anal. Chem.* **2010,** *3*, 19-42.

[**19**] J. P. McMullen, K. F. Jensen. Rapid Determination of Reaction Kinetics with an Automated Microfluidic System. *Org. Process Res. Dev.* **2011,** *15* (2), 398-407.

Appendix 1

Supporting Information for Chapter 2

Microwave-Assisted Formation of Organic Monolayers from 1-Alkenes on Silicon Carbide
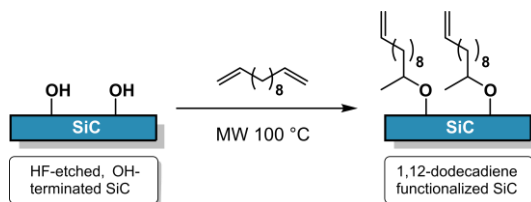
Scheme S1. Reaction of hydroxyl-terminated SiC surfaces with 1,11-dodecadiene yields alkene terminated surfaces, likely with multilayer formation (not shown).
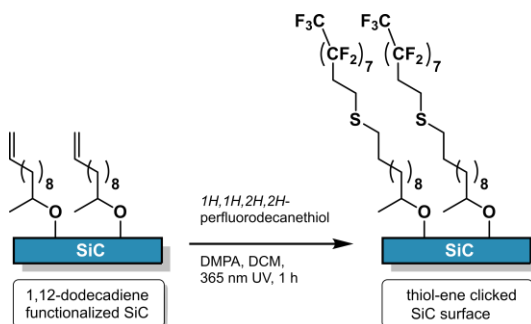
Scheme S2. Reaction of 1,11-dodecadiene functionalized SiC surfaces with *1H,1H,2H,2H-perfluorodecanethiol* under thiol-ene conditions yields fluorinated surfaces with high contact angles.
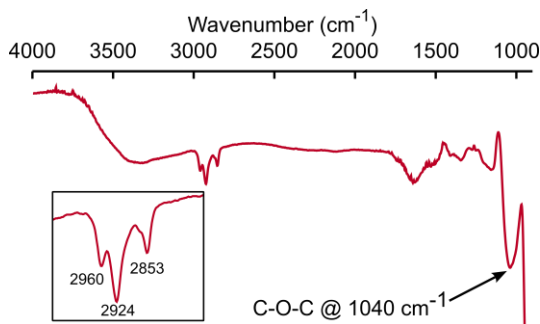
Figure S1. IRRAS spectrum of 1-hexadecene-modified SiC surface obtained upon microwave irradiation at 100 °C for 60 min, showing an absorption at 1040 cm^{-1} which is tentatively ascribed to the presence of C-O-C bonds. Inset: zoom of C-H region; the wavenumbers indicate the presence of disordered monolayers.[1, 2]
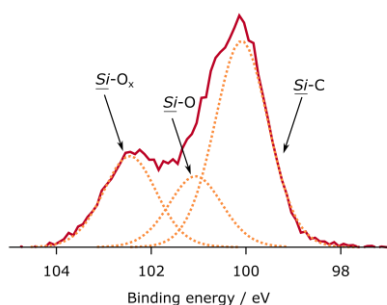
Figure S2: XPS Si2p narrow scan of a plasma-oxidized SiC surface showing the presence of $\underline{Si}$-O$_x$ at 103-104 eV.
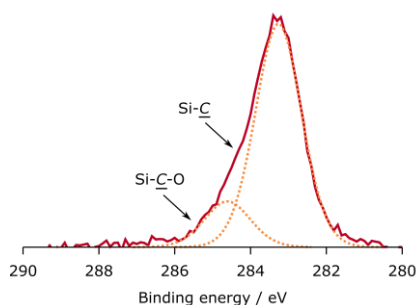
Figure S3. XPS C1s narrow scan of a freshly HF-etched, bare SiC surface showing the presence of oxycarbide (Si-$\underline{C}$-O$_x$) species at ~ 285 eV.
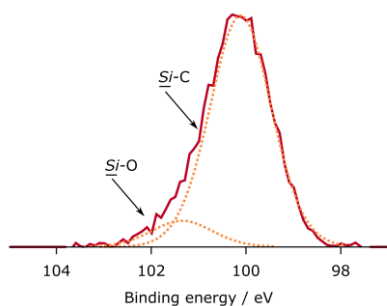
Figure S4: XPS Si2p narrow scan of a freshly HF-etched, bare SiC surface showing the presence of silicon singly bound to oxygen ($\underline{Si}$-O) at ~101.5 eV.
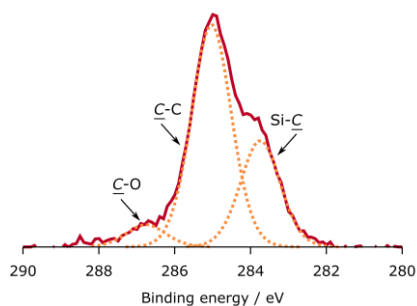
Figure S5. XPS C1s narrow scan of 1,11-dodecadiene monolayer on SiC shows high contribution of $\underline{C}$-C, indicating multilayer formation.
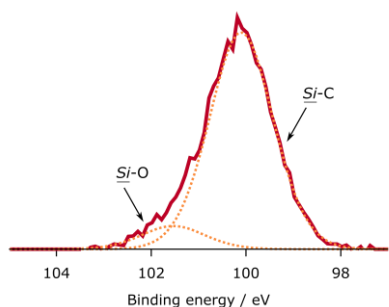
Figure S6: XPS Si2p narrow scan of a 1-hexadecene functionalized SiC surface showing the presence of silicon singly bound to oxygen (*Si*-O) at ~101.5 eV.
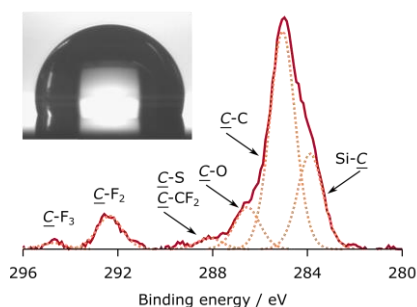
Figure S7. XPS C1s narrow scan of 1,11-dodecadiene monolayer after thiol-ene click reaction with *1H,1H,2H,2H*-perfluorodecanethiol. The inset shows the contact angle (107°) of a drop of water on the clicked surface.
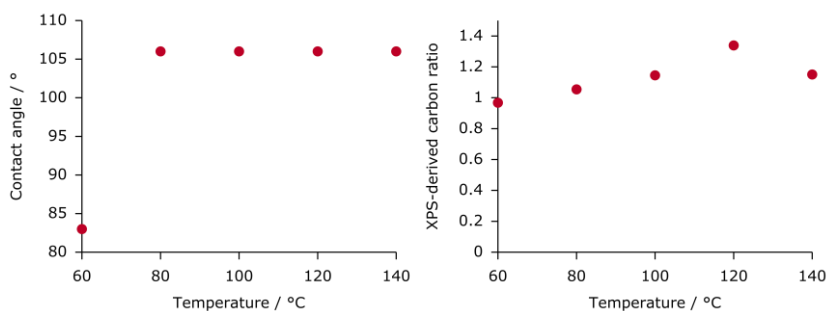
Figure S8. Influence of reaction temperature on the microwave-assisted attachment of monolayers on SiC surfaces. **Left:** Development of the static water contact angle (±1°). **Right:** XPS-derived (*C*-C +*C*-O)/Si-*C* ratio versus reaction time (min). *NB*: these reactions were carried out on a different batch of SiC, which explains the difference in XPS-derived (*C*-C +*C*-O)/Si-*C* ratio.
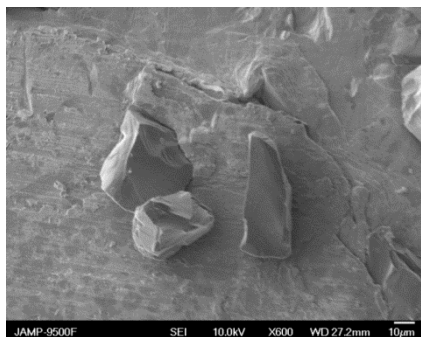
Figure S9. SEM image of freshly etched SiC microgrits.
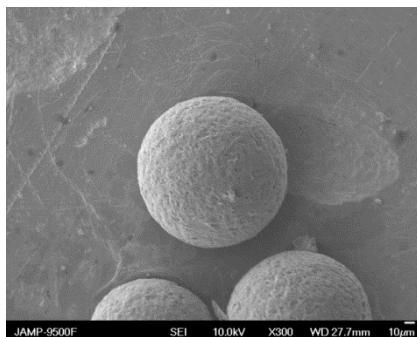
Figure S10. SEM image of freshly etched SiC microspheres.
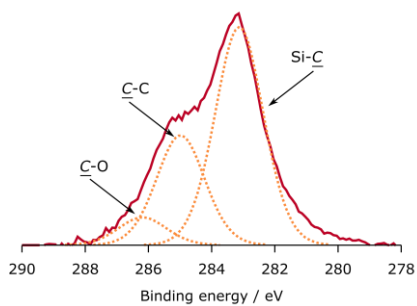
Figure S11. XPS C1s spectrum for 1,11-dodecadiene-modified SiC microspheres. Due to the use of the twin-beam (non-monochrome) X-ray source, some peak broadening occurs.
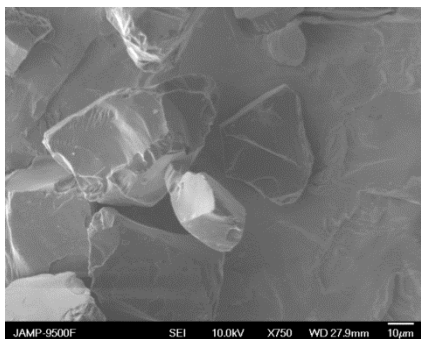
Figure S12. SEM image of microgrits functionalized with 1,11-dodecadiene after thiol-ene coupling of *1H,1H,2H,2H*-perfluorodecanethiol.
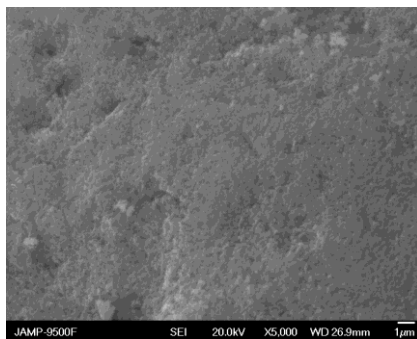
Figure S13. SEM image of microparticles at 5000x magnification.
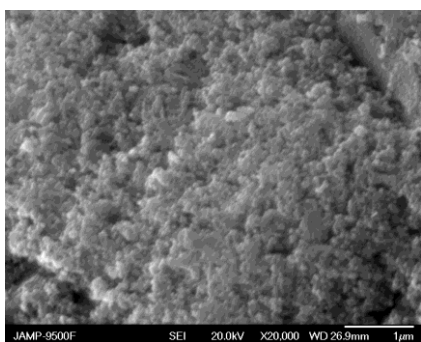
Figure S14. SEM image of microparticles at 20000x magnification, showing the surface porosity and morphology.
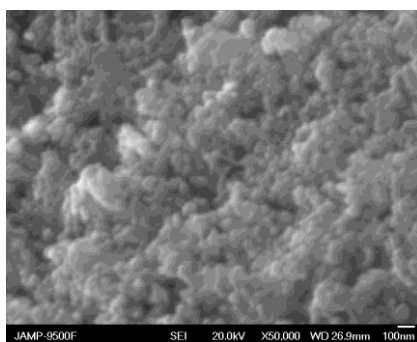
Figure S15. SEM image of microparticles at 50000x magnification, showing the surface porosity and morphology in detail.

Figure S16. Left: Microwave reactor employed in this work (CEM Discover, CEM Corporation, Charlotte, NC, USA). **Right:** Standard 10 mL Pyrex microwave vial, containing neat 1-hexadecene and a SiC surface, sealed with a crimp cap

Table S1. Irradiation parameters and XPS-derived elemental composition after microwave assisted surface modification of SiC microparticles with ω-vinyl 1-alkenes

Substrate	ω-Vinyl 1-alkene	Power (W)/T (°C)/t (h)	C_{1s} %	Si_{2p} %	O_{1s} %	F_{1s} %
HF treated microgrit			44.4	43.6	10.7	1.3
HF treated microgrit	1,7-octadiene	80/120/8	50.2	39.5	9.0	1.3
HF treated microgrit	1,11-dodecadiene	150/85/8	48.3	39.6	10.5	1.6
HF treated microspheres			40.2	49.2	9.8	0.8
HF treated microspheres	1,11-dodecadiene	150/100/3	51.3	40.3	8.4	

Table S2. XPS C 1s binding energies, curve fittings in %, and calculated thickness of 1,7-octadiene and 1,11-dodecadiene derived monolayers.

Species [binding energy, eV]	Microgrits-1,7-octadiene	Microgrits-1,11-dodecadiene	Microspheres-1,11-dodecadiene
Si–C [≈ 283 eV]	57.8	63.3	67.7
C–C + C=C [≈ 285 eV]	36.0	31.6	28.0
C–O [≈ 287 eV]	6.2	5.1	4.3
Thickness (nm)	1.8	1.5	1.3

Table S3. XPS-Derived elemental composition and atomic ratios after thiol-ene click reaction on ω-vinyl-functionalized SiC particles.

Particle	Si_{2p} %	C_{1s} %	O_{1s} %	F_{1s} %	C/Si	O/Si	F/Si	F/C
MG-OCT-Rf[a]	35.5	42.7	10.7	11.1	1.20	0.30	0.31	0.26
MG-DOD-Rf[b]	37.9	42.9	10.5	8.7	1.13	0.28	0.23	0.20
MS-DOD-Rf[c]	32.3	44.3	6.8	16.6	1.37	0.21	0.51	0.37

[a]MG-OCT-Rf: fluorothiol-terminated octadiene-functionalized microgrits. [b]MG-DOD-Rf: fluorothiol-terminated dodecadiene-functionalized microgrits. [c]MS-DOD-Rf: fluorothiol-terminated dodecadiene-functionalized microspheres.

Table S4. XPS C 1s binding energies, curve fittings in %, and calculated thickness of organic layer after thiol-ene click functionalization of microparticles.

Species [binding energy, eV]	ω-vinyl functionalized particle		
	Microgrits-1,7-octadiene	Microgrits-1,11-dodecadiene	Microspheres-1,11-dodecadiene
Si–C [≈ 283 eV]	59.3	62.9	58.7
C–C [≈ 285 eV]	30.1	29.3	30.3
C–O, C–S, C–CF_2 [≈ 287 eV]	7.1	5.2	3.3
C–F_2 [≈ 292 eV]	3.5	2.6	6.6
C–F_3 [≈ 294 eV]			1.1
Thickness (nm)	1.7	1.5	1.8

Table S5. XPS-derived elemental composition and atomic ratios after stability test of MS-DOD-Rf particles.

	Si_{2p} %	C_{1s} %	O_{1s} %	F_{1s} %	C/Si	O/Si	F/Si	F/C
PBS (pH 7.4)	30.6	44.6	9.8	12.9	1.45	0.32	0.42	0.29
CF3CH2OH (pH 2)	35.0	43.4	7.6	14.0	1.24	0.22	0.40	0.32

References

[**1**] M. Rosso, A. Arafat, K. Schroën, M. Giesbers, C. S. Roper, R. Maboudian, H. Zuilhof. Covalent Attachment of Organic Monolayers to Silicon Carbide Surfaces. *Langmuir* **2008,** *24* (8), 4007-4012.

[**2**] M. Rosso, M. Giesbers, A. Arafat, K. Schroën, H. Zuilhof. Covalently Attached Organic Monolayers on SiC and Si_xN_4 Surfaces: Formation Using UV Light at Room Temperature. *Langmuir* **2009,** *25* (4), 2172-2180.

Appendix 2

Supporting Information for Chapter 3

Clickable Mesoporous Silica via Functionalization with 1,ω-Alkenes
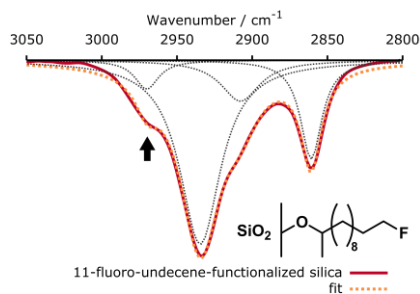
Figure S1. FTIR of 11-fluoro-undecene functionalized silica with structure as inset. This spectrum was deconvoluted into four contributions, at 2860, 2908, 2934 and 2970 cm^{-1}. The peak at 2970 cm^{-1} is attributed to a methyl C-H stretching vibration.
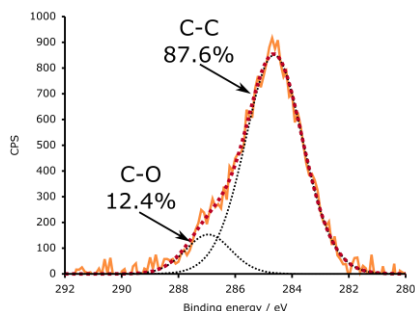
Figure S2. XPS narrow scan of C1s region. Deconvolution of the main peak into two contributions yields peak at 285.0 eV, belonging to C-C bonds and at 287.5 eV, belonging to C-O bonds. The ratio of these two peaks is 7 : 1, which indicates monolayer formation according to a Markovnikov-type addition.

Table S1. Atomic percentages obtained from wide-scan XPS spectra of thiol-ene clicked samples with corresponding structure.

Structure	Entry	%C	%S	%F	%N	Conversion[a]
	1	25.3				
	2	28.9	1.5	24.5		60%
	3	83.7	9.4	6.9		60% (49%)[b]
	4	89.9	6.6		3.5	55% (53%)[b]

[a] Conversion calculated from XPS data*; [b] Conversion of second thiol-ene click reaction in brackets.

* These values were derived from the XPS data using a custom-made Python script (see Appendix 3). Each thiol-ene click step adds carbon. In case of incomplete

conversion, the ratio of carbon to reporter elements such as fluorine cannot be used directly, because two contributing types of alkyl chains contribute different amounts of carbon to the surface. Instead, the relative amount of carbon contributed by each alkyl chain (one reacted, one unreacted) must be taken into account (see Figure S3). The Python script calculates for each possible conversion, the resulting atomic ratios that would be obtained from the XPS spectra and reports the best fit.
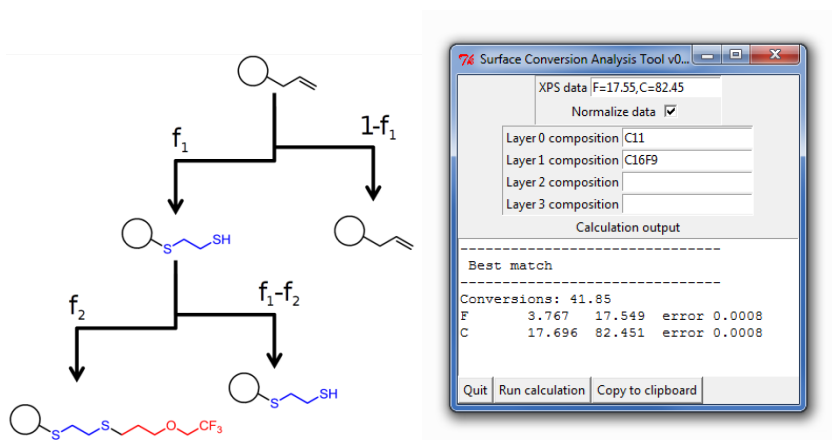
Figure S3. Left: Schematic representation of structures on the surface with incomplete conversion. **Right:** Example output of a custom-made Python script which calculates all possible conversions f_1 and f_2 and predicts the XPS atomic ratios, allowing one to estimate the surface conversion.

Mic	HV	HFW	Mag	Date	Sample	
1010	70 kV	536,2 nm	250000 x	08.09.13, 19:05	-	——100 nm——
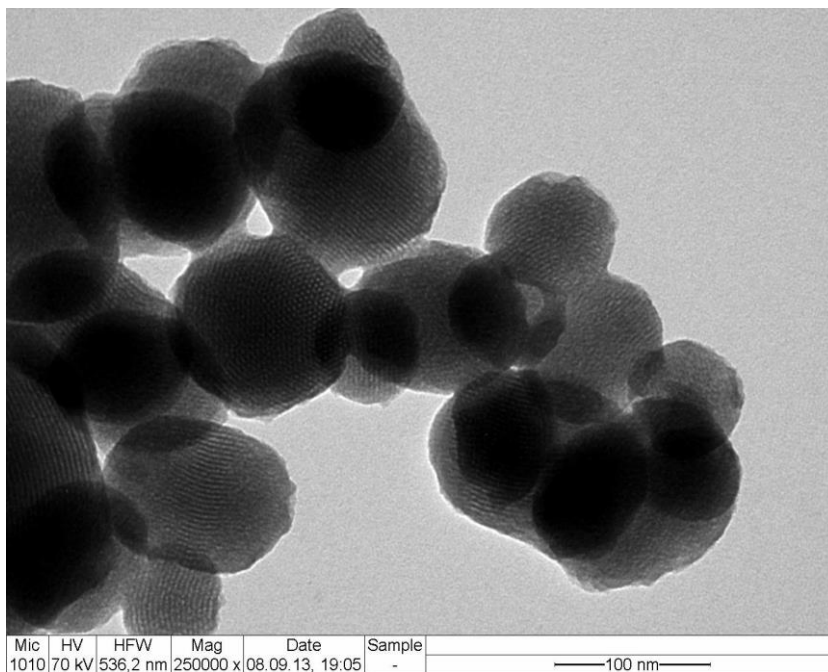
Figure S4. TEM image of quinine-functionalized mesoporous silica, which shows intact pores.

Appendix 3

Source code of surface composition determination script

This source code can also be found online at:

https://gist.github.com/barrebas/705fdecd6c7e600cc945.

```python
#!/usr/bin/python

import re, math
from Tkinter import *

class Element():
        """Element class"""

        def __init__(self, label=None, stoichiometry=None, percentage=None, amount=None):
                self.label = label
                self.stoichiometry = stoichiometry
                self.percentage = percentage
                self.amount = amount
                self.error = 0

        def setPercentage(self, percentage):
                self.percentage = percentage

        def getPercentage(self):
                return self.percentage

class Layer():
        """Layers contain Elements"""

        def addElement(self, label=None, stoichiometry=None, percentage=None):
                self.elements.append(Element(label, stoichiometry, percentage))

        def getElement(self, label):
                for e in self.elements:
                        if e.label == label:
                                return e
                return Element("", 0, 0, 0)

        def getStoichiometry(self, label):
                return self.getElement(label).stoichiometry

        def __init__(self, data):
```

```
                self.elements = []

                matches = re.findall('([A-Z])(\d+)', data)
                if (matches):
                        for (label, stoichiometry) in matches:
                                self.addElement(label, int(stoichiometry))

class XPSData():
        """Contains XPS element percentages"""

        def __init__(self):
                self.elements = []

        def addElement(self, label, stoichiometry, percentage):
                self.elements.append(Element(label, stoichiometry, percentage))

        def getElement(self, label):
                for e in self.elements:
                        if e.label == label:
                                return e

        def fixXPSData(self):
                total = 0.0
                for e in self.elements:
                        total += e.percentage
                for e in self.elements:
                        e.percentage = e.percentage / total * 100

        def checkXPSData(self):
                total = 0.0
                for e in self.elements:
                        total += e.percentage
                # cannot directly compare floats, so check the relative error instead
                if (abs(total - 100.0) > 0.01):
                        return (False, total)
                else:
                        return (True, total)
```

```
class Surface():
        """Surface contains Layers and XPS data"""

        def addLayer(self, data):
                self.layers.append(Layer(data))

        def addXPSData(self, data):
                matches = re.findall('([A-Z])\W*=\W*(\d+\.\d+)\W*', data)
                if (matches):
                        for (label, percentage) in matches:
                                percentage = float(percentage)
                                self.xps.addElement(label, 0, percentage)

        def getElement(self, label):
                for e in self.elements:
                        if e.label == label:
                                return e

        def fixXPSData(self):
                self.xps.fixXPSData()

        def checkXPSData(self):
                return self.xps.checkXPSData()

        # recursive function -- here be dragons
        def r(self, i):
                if (i == len(self.conversion)):
                        # test holds the calculated elements
                        self.test = []
                        # total holds the contribution of all elements
                        self.total = 0
                        for e in self.xps.elements:
                                amount = 0
                                factor = 1
                                # for each layer, the added amount is proportional to the conversion
                                # each layer therefore contains the relative amount of element that is added
```

146

```
                         # calculate total contribution of element in each layer
                         correctedAmount = 0

                         for x in range(len(self.layers)):
                                 amount += factor * self.layers[x].getElement(e.label).stoichiometry

                                 if (x < len(self.layers)-1):
                                         factor *= self.conversion[x]

                         self.test.append(Element(e.label, 0, 0, amount))

                         # we need the total amount to calculate the percentage
                         self.total += amount

                 # check if calculations match experimental values
                 self.flag = 1
                 for e in self.test:
                         e.percentage = e.amount / self.total * 100
                         error = abs(e.percentage - self.xps.getElement(e.label).percentage)
                         e.error = error
                         if (error > self.maxError):
                                 self.flag = 0
                 if (self.flag == 1):
                         # save for later, by making copies using list()
                         self.matchingConversions.append((list(self.conversion),list(self.test)))

         else:
                 self.conversion[i] = 0.01
                 while (self.conversion[i] < 1):
                         self.r(i+1)
                         self.conversion[i] += self.delta

 def calculateConversions(self):
         self.conversion = []

         for i in range(len(self.layers)-1):
```

```
                    self.conversion.append(0.0)

            self.r(0) # start recursing

     def getConversions(self):
            return self.matchingConversions

     def setDelta(self, delta):
            self.delta = delta

     def maxError(self, maxError):
            self.maxError = maxError

     def __init__(self):
            self.elements = []
            self.layers = []
            self.matchingConversions = []
            self.xps = XPSData()
            self.delta = 0.0005
            self.maxError = 0.05

class Driver:
     def runCalculations(self):
            self.outputText.delete(1.0, END)
            surface = Surface()
            data = self.elementList.get()
            if data == "":
                    self.outputText.insert(INSERT, "No XPS data given -- aborting calculation...\n")
                    return -1

            surface.addXPSData(data)

            # extract layer data
            for x in range(4):
                    layerData = self.layerEntries[x].get()
                    if layerData != "":
                            surface.addLayer(layerData)
```

```
                (flag, total) = surface.checkXPSData()
                if (flag == False):
                        self.outputText.insert(INSERT, "WARNING: XPS atom percentages do not add up to 100% - is
now " + str(total) + "\n")
                        if self.fix.get() == 1:
                                surface.fixXPSData()

                surface.calculateConversions()

                # get best match with lowest error in percentages
                v = surface.getConversions()
                lowestError = 10000000

                bestConversions = []
                bestElements = []

                for (conversions, elements) in v:
                        totalError = 0
                        for e in elements:
                                totalError += e.error
                        if (lowestError > totalError):
                                bestConversions = conversions
                                bestElements = elements
                                lowestError = totalError

                output = ""
                output += "-----------------------------\n Best match\n-----------------------------\n"
                output += "Conversions: "
                for b in bestConversions:
                        output += str(round(b*100, 5)) + " "
                output += "\n"
                for e in bestElements:
                        output += e.label + "\t"
                        output += str(round(e.amount, 3)) + "\t"
                        output += str(round(e.percentage, 3)) + "\t"
                        output += "error "
```

149

```
                    output += str(round(e.error, 4)) + "\t"
                    output += "\n"
            self.outputText.insert(INSERT, output)
            print output

    def ctrlV(self):
            r = Tk()
            r.withdraw()
            r.clipboard_clear()
            r.clipboard_append(self.outputText.get(1.0, END))
            r.destroy()

    def __init__(self, master):
            self.frame = Frame(master)
            self.frame.pack()

            self.framex = Frame(self.frame, relief=GROOVE, bd=1)
            self.framex.pack(side=TOP)

            self.frame2 = Frame(self.framex)
            self.frame2.pack(side=TOP)

            self.elementListDesc = Label(self.frame2, text="XPS data")
            self.elementListDesc.pack(side=LEFT)
            self.elementList = Entry(self.frame2, text="")
            self.elementList.pack(side=RIGHT)

            self.frame2 = Frame(self.framex)
            self.frame2.pack(side=TOP)

            self.fix = IntVar()
            self.fixXPSData = Checkbutton(self.frame2, variable=self.fix)
            self.fixXPSDataDesc = Label(self.frame2, text="Normalize data")
            self.fixXPSData.pack(side=RIGHT)
            self.fixXPSDataDesc.pack(side=LEFT)
            self.fixXPSData.select()
```

```python
                self.frame3 = Frame(self.frame, relief=GROOVE, bd=1)
                self.frame3.pack(side=TOP)

                self.layerEntries = []
                self.layerEntriesDesc = []
                for x in range(4):
                        self.framex = Frame(self.frame3)
                        self.framex.pack(side=TOP)
                        self.layerEntriesDesc.append(Label(self.framex, text="Layer " + str(x) + " composition"))
                        self.layerEntriesDesc[x].pack(side=LEFT)
                        self.layerEntries.append(Entry(self.framex))
                        self.layerEntries[x].pack(side=RIGHT)

                self.elementList.insert(INSERT, "F=17.55,C=82.45")
                self.layerEntries[0].insert(INSERT, "C11")
                self.layerEntries[1].insert(INSERT, "C16F9")
                self.outputDesc = Label(self.frame, text="Calculation output")
                self.outputDesc.pack(side=TOP)
                self.outputText = Text(self.frame, height=8, width=40)
                self.outputText.pack(side=TOP)
                self.button = Button(self.frame, text="Quit", command=self.frame.quit)
                self.button.pack(side=LEFT)
                self.run_calc = Button(self.frame, text="Run calculation", command=self.runCalculations)
                self.run_calc.pack(side=LEFT)
                self.button = Button(self.frame, text="Copy to clipboard", command=self.ctrlV)
                self.button.pack(side=LEFT)

def main():
        # Tkinter GUI
        root = Tk()
        driver = Driver(root)
        root.wm_title("Surface Conversion Analysis Tool v004 (c) Bas 2013")
        root.mainloop()


if __name__ == "__main__":
        main()
```

Appendix 4

Supporting Information for Chapter 4

Continuous-Flow Alcohol Protection and Deprotection Reactions Catalyzed by Silica-Supported Sulfonic Acid
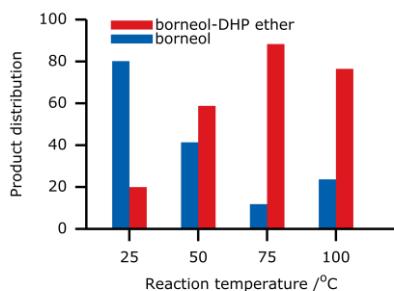
Figure S1: GC yield for the tetrahydropyranylation of *endo*-borneol at different temperatures. The bars denote the peak area relative to the peak area of internal standard (1-fluoronaphthalene).
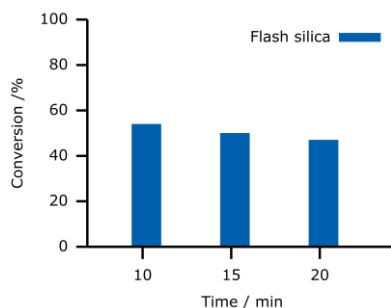
Figure S2: Conversion (GC-MS area) of 4-methoxyphenol trimethylsilyl ether using regular flash silica as catalyst. The conversion of 4-methoxyphenol is decreasing steadily.
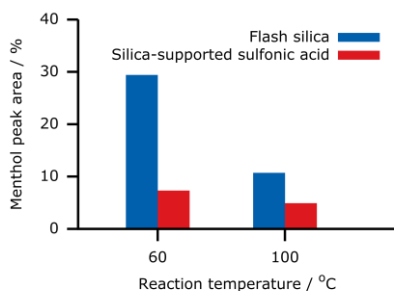
Figure S3: Comparison of catalytic performance of regular flash silica (blue bars) versus silica-supported sulfonic acid (red bars). The bars denote the relative amount of unreacted menthol as detected by GC-MS. The silica-supported sulfonic acid is much more active at lower temperatures.
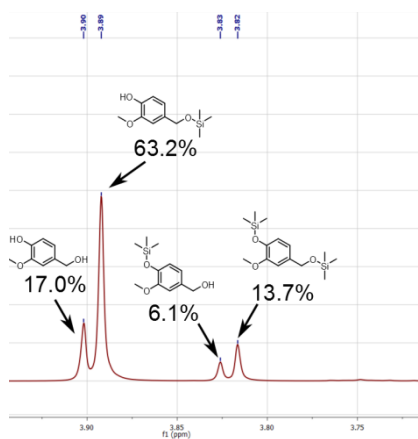
Figure S4: Selective protection of benzylic alcohol over phenolic alcohol in vanillyl alcohol. ^{1}H NMR spectrum zoom of methoxy region, showing four different peaks. The peaks were deconvoluted using MNOVA software version 9.0.0.
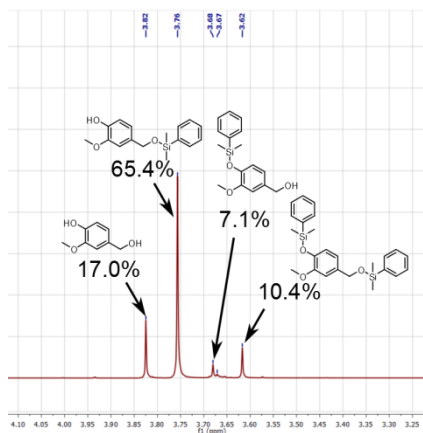
Figure S5: Selective protection of benzylic alcohol over phenolic alcohol in vanillyl alcohol. ^{1}H NMR spectrum zoom of methoxy region, showing four different peaks. The peaks were deconvoluted using MNOVA software version 9.0.0.
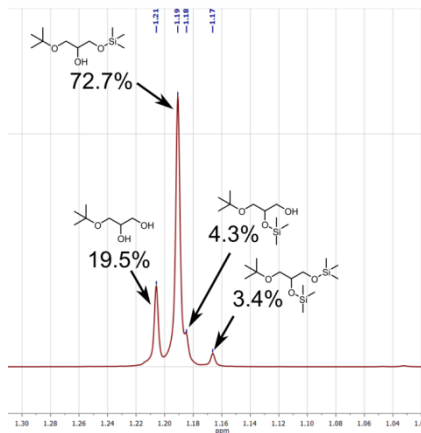
Figure S6: Selective protection of primary alcohol over secondary alcohol in 3-(tert-butoxy)propane-1,2-diol. ^{1}H NMR spectrum zoom of tert-butyl group region, showing four different peaks. The peaks were deconvoluted using MNOVA software version 9.0.0.
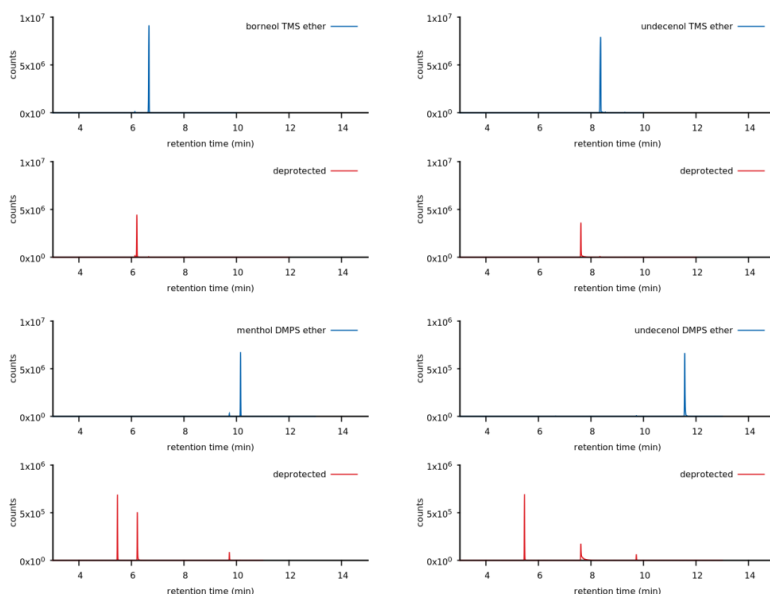
Figure S7: GC-MS measurements of aliquots taken from the deprotection reaction in methanol under continuous flow.
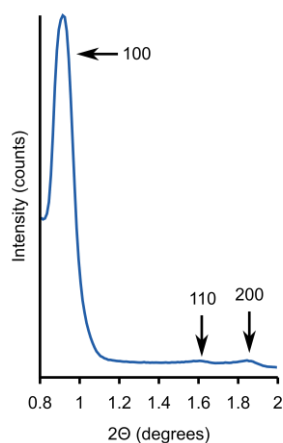
Figure S8: X-ray diffraction spectrum of as-synthesized (not extracted) SBA-SO₃H, showing peaks corresponding to a hexagonal phase.

Spectra of synthesized compounds

Trimethyl(undec-10-en-1-yloxy)silane **2b**

^{1}H NMR (400 MHz, CDCl₃) δ 5.81 (ddt, J = 16.9, 10.1, 6.7 Hz, 1H), 5.04 − 4.88 (m, 2H), 3.57 (t, J = 6.7 Hz, 2H), 2.04 (tdd, J = 6.6, 5.4, 1.4 Hz, 2H), 1.57 − 1.48 (m, 2H), 1.36 (dt, J = 14.4, 7.4 Hz, 3H), 1.29 (d, J = 4.3 Hz, 10H), 0.11 (s, 9H). MS (EI, m/z (%)): 228 (6), 227 (32), 103 (14), 95 (6), 89 (7), 81 (5), 76 (7), 75 (100), 73 (25), 67 (6), 55 (15).

Figure S9: ^{1}H NMR spectrum of trimethyl(undec-10-en-1-yloxy)silane **2b**.

Trimethyl((1,7,7-trimethylbicyclo[2.2.1]heptan-2-yl)oxy)silane **3b**

^{1}H NMR (400 MHz, CDCl$_3$) δ 3.89 (ddd, J = 9.6, 3.4, 2.0 Hz, 1H), 2.20 – 1.96 (m, 2H), 1.73 – 1.54 (m, 2H), 1.27 – 1.06 (m, 2H), 0.91 (dd, J = 13.0, 3.4 Hz, 1H), 0.84 (s, 6H), 0.76 (s, 3H), 0.07 (s, 9H). **^{13}C NMR** (400 MHz, CDCl$_3$) δ 76.9, 49.4, 47.1, 47.0, 45.2, 39.3, 28.2, 26.0, 20.1, 18.6, 13.3, 0.0. **MS** (EI, m/z (%)): 226 (32), 155 (16), 136 (28), 121 (41), 117 (22), 108 (51), 101 (19), 95 (100), 93 (35), 75 (42), 73 (55).
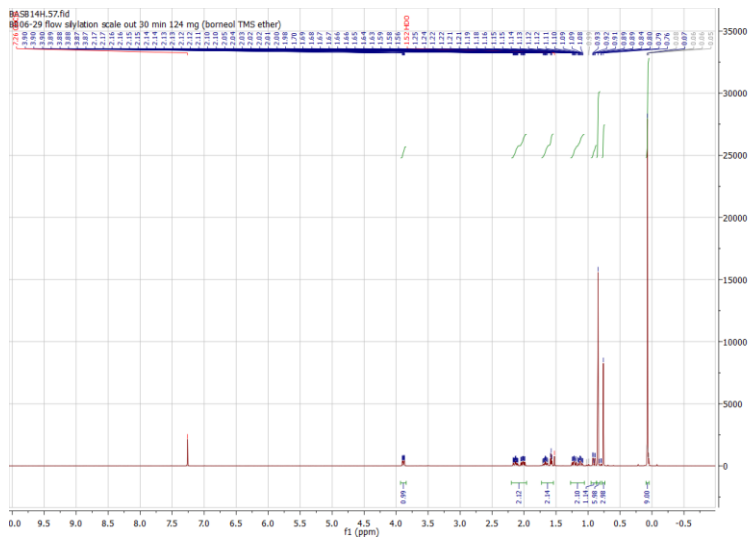
Figure S10: ¹H NMR spectrum of trimethyl((1,7,7-trimethylbicyclo[2.2.1]heptan-2-yl)oxy)silane **3b**.
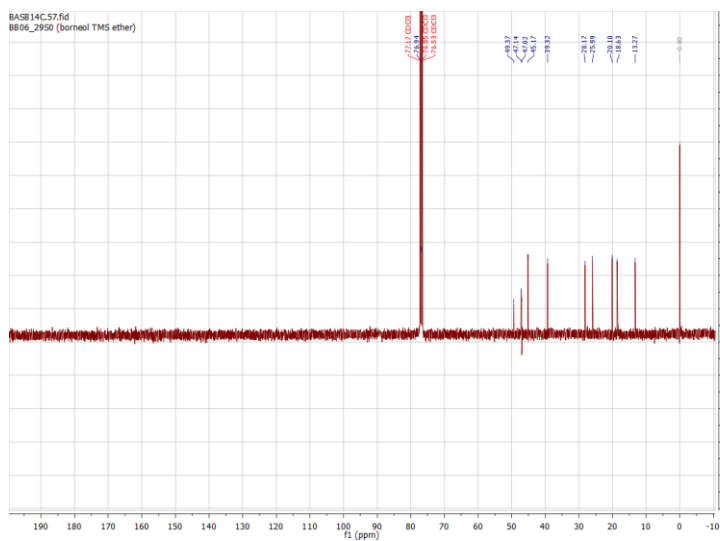
Figure S11: ¹³C NMR spectrum of trimethyl((1,7,7-trimethylbicyclo[2.2.1]heptan-2-yl)oxy)silane **3b**.

((2-isopropyl-5-methylcyclohexyl)oxy)trimethylsilane **4b**

^{1}H NMR (400 MHz, CDCl$_3$) δ 3.39 (td, J = 10.3, 4.4 Hz, 1H), 2.14 (pd, J = 7.0, 2.5 Hz, 1H), 1.89 – 1.79 (m, 1H), 1.60 (dddd, J = 18.3, 12.3, 5.8, 2.8 Hz, 2H), 1.37 (dddd, J = 15.0, 13.0, 6.5, 3.1 Hz, 1H), 1.19 – 1.07 (m, 1H), 1.07 – 0.77 (m, 9H), 0.73 (d, J = 7.0 Hz, 3H), 0.11 (s, 9H). **^{13}C NMR** (400 MHz, CDCl$_3$) δ 71.9, 49.5, 45.0, 34.0, 31.2, 24.7, 22.5, 21.7, 20.7, 15.4, 0.0. **MS** (EI, m/z (%)): 213 (10), 144 (12), 143 (100), 138 (13), 95 (11), 82 (5), 81 (16), 75 (39), 73 (31), 67 (5), 55 (7).
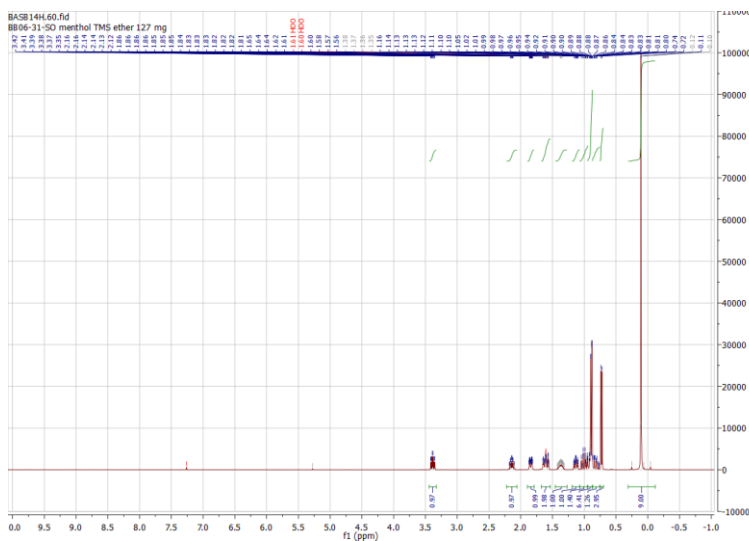
Figure S12: ^{1}H NMR spectrum of ((2-isopropyl-5-methylcyclohexyl)oxy)trimethylsilane **4b**.

Figure S13: [^13]C NMR spectrum of ((2-isopropyl-5-methylcyclohexyl)oxy)trimethylsilane **4b**.

Trimethyl((4-nitrobenzyl)oxy)silane **5b**

[^1]H NMR (400 MHz, CDCl$_3$) δ 8.24-8.15 (m, 2H), 7.49 (m, 2H), 4.79 (s, 2H), 0.18 (s, 9H). **[^13]C NMR** (400 MHz, CDCl$_3$) δ 149.3, 147.6, 127.1, 124.0, 64.1, 47.7, 0.0. **MS** (EI, m/z (%)): 195 (6), 194 (35), 181 (4), 180 (16), 179 (100), 163 (5), 91 (5), 82 (12), 77 (6), 75 (5), 73 (22).

Figure S14: ¹H NMR spectrum of trimethyl((4-nitrobenzyl)oxy)silane **5b**.

Figure S15: ¹³C NMR spectrum of trimethyl((4-nitrobenzyl)oxy)silane **5b**.
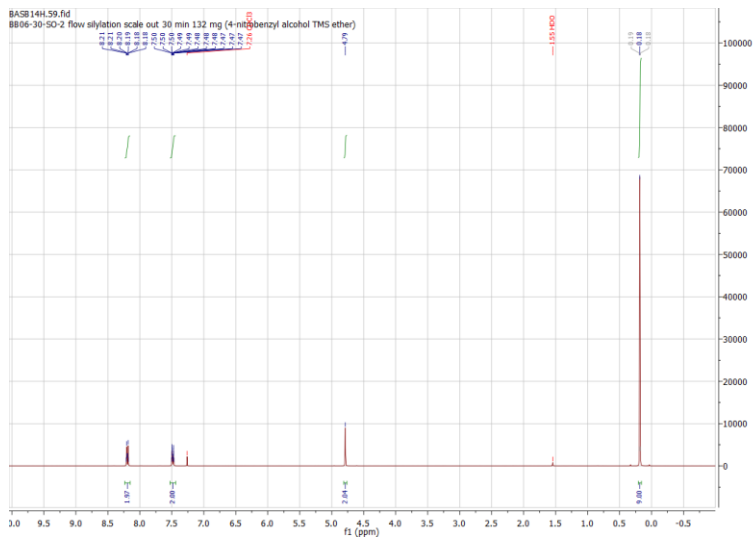
<ins>((3,4-dimethoxybenzyl)oxy)trimethylsilane **6b**</ins>

^{1}H NMR (400 MHz, CDCl$_3$) δ 6.92 – 6.41 (m, 3H), 4.48 (s, 2H), 3.73 (s, 3H), 3.71 (s, 3H), 0.0 (s, 9H). **^{13}C NMR** (400 MHz, CDCl$_3$) δ 149.2, 148.5, 133.8, 119.2, 111.2, 110.5, 65.0, 56.2, 56.1, 0.0. **MS** (EI, m/z (%)): 241 (6), 240 (36), 239 (10), 225 (10), 210 (6), 209 (22), 152 (10), 151 (100), 112 (3), 107 (6), 73 (17).
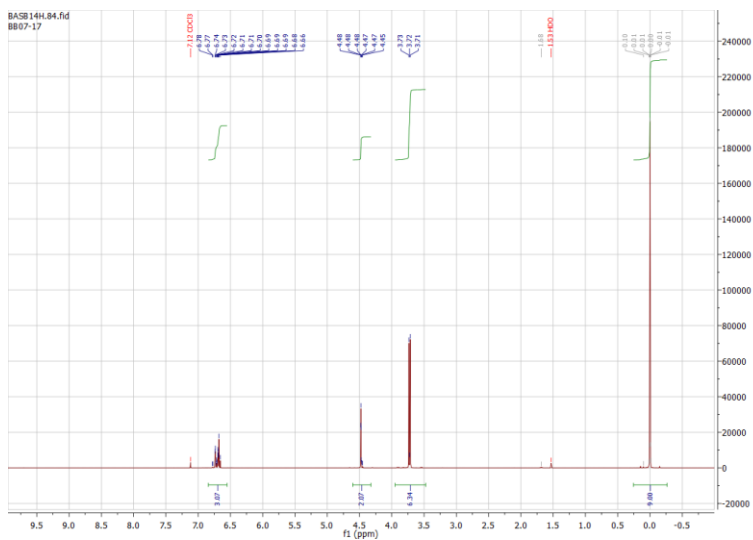
Figure S16: ^{1}H NMR spectrum of ((3,4-dimethoxybenzyl)oxy)trimethylsilane **6b**.
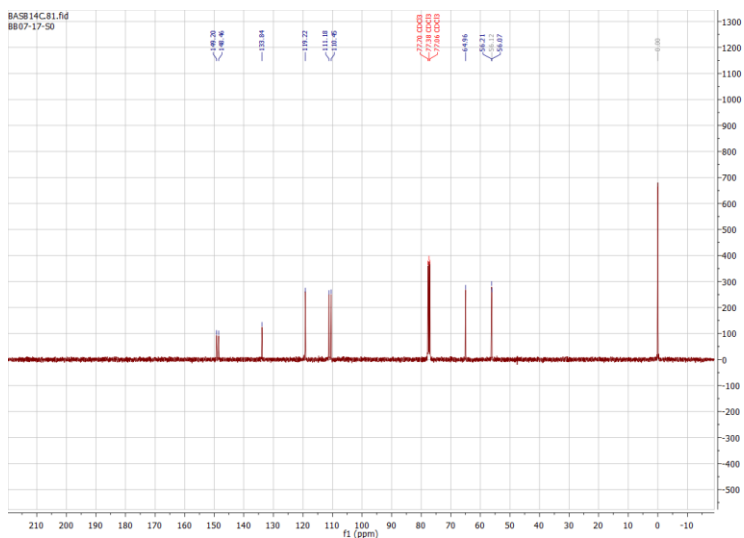
Figure S17: ^{13}C NMR spectrum of ((3,4-dimethoxybenzyl)oxy)trimethylsilane **6b**.

 (4-methoxyphenoxy)trimethylsilane **9b**

^{1}H NMR (400 MHz, CDCl$_3$) δ 6.79 (s, 4H), 3.77 (s, 3H), 0.26 (s, 9H). **^{13}C NMR** (400 MHz, CDCl$_3$) δ 154.1, 148.7, 120.5, 114.4, 55.4, 0.0. **MS** (EI, m/z (%)): 197 (10), 196 (67), 183 (4), 182 (15), 181 (100), 123 (5), 121 (4), 90 (6), 77 (4), 75 (6), 73 (36).
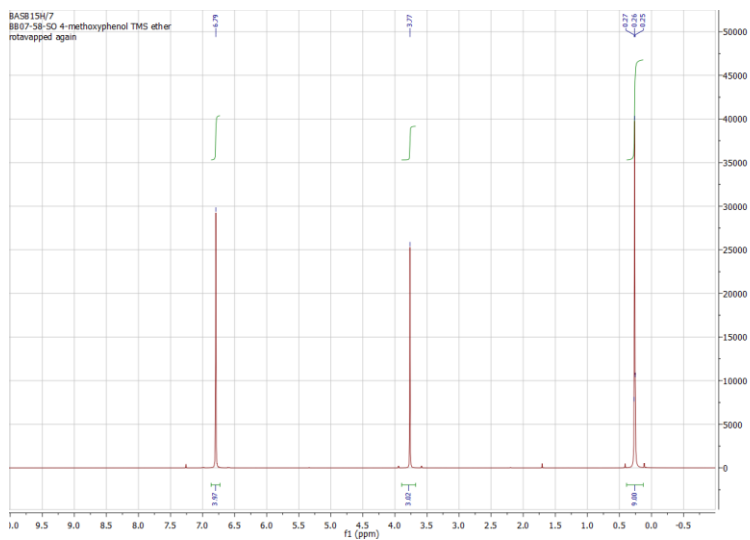
Figure S18: ^{1}H NMR spectrum of (4-methoxyphenoxy)trimethylsilane **9b**.
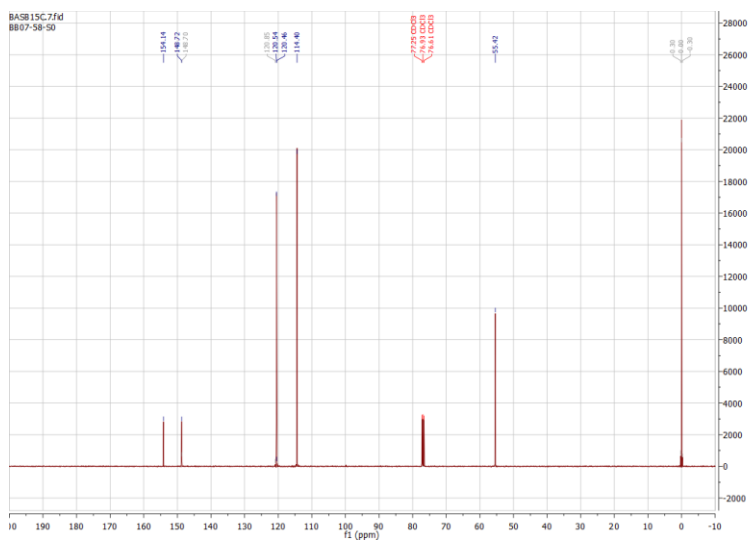
Figure S19: ^{13}C NMR spectrum of (4-methoxyphenoxy)trimethylsilane **9b**.

(4-ethylphenoxy)trimethylsilane **10b**

^{1}H NMR (400 MHz, CDCl$_3$) δ 7.19 – 7.05 (m, 2H), 6.93 – 6.75 (m, 2H), 2.65 (q, J = 7.6 Hz, 2H), 1.27 (t, J = 7.6 Hz, 3H), 0.32 (s, 9H). **^{13}C NMR** (400 MHz, CDCl$_3$) δ 152.8, 136.8, 128.4, 119.6, 27.8, 15.5, 0.0. **MS** (EI, m/z (%)): 195 (6), 194 (35), 181 (4), 180 (16), 179 (100), 163 (5), 91 (5), 82 (12), 77 (6), 75 (5), 73 (22).
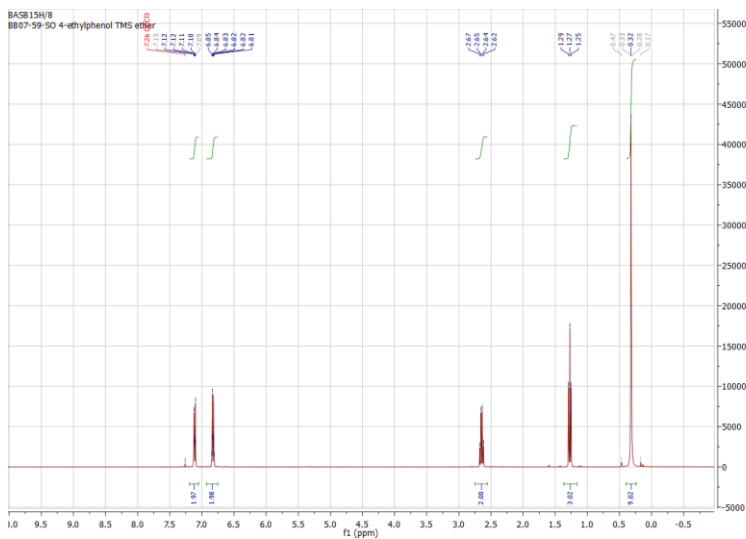
Figure S20: ^{1}H NMR spectrum of (4-ethylphenoxy)trimethylsilane **10b**.
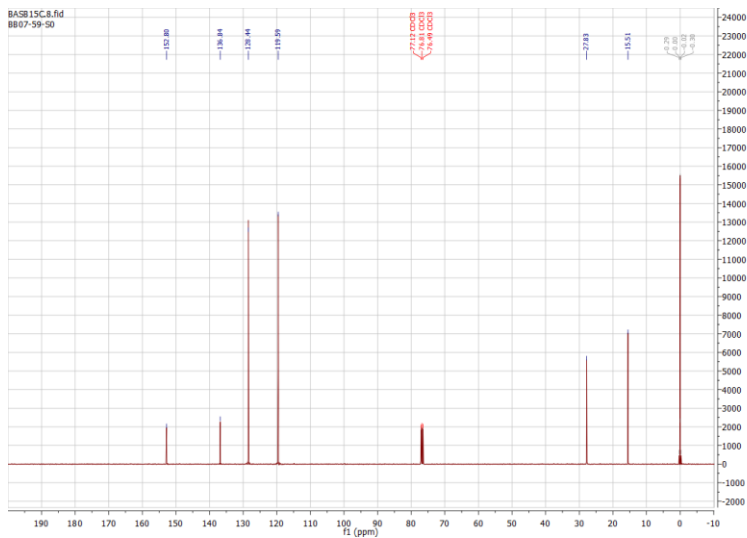
Figure S21: ^{13}C NMR spectrum of (4-ethylphenoxy)trimethylsilane **10b**.

((4-(tert-butyl)benzyl)oxy)trimethylsilane **11b**

^{1}**H NMR** (400 MHz, CDCl$_3$) δ 7.39 (d, J = 8.4 Hz, 2H), 7.29 (d, J = 8.1 Hz, 2H), 4.69 (s, 2H), 1.34 (s, 9H), 0.19 (d, J = 1.3 Hz, 9H). ^{13}**C NMR** (400 MHz, CDCl$_3$) δ 150.0, 137.9, 126.5, 125.2, 64.5, 34.5, 31.4, -0.3.
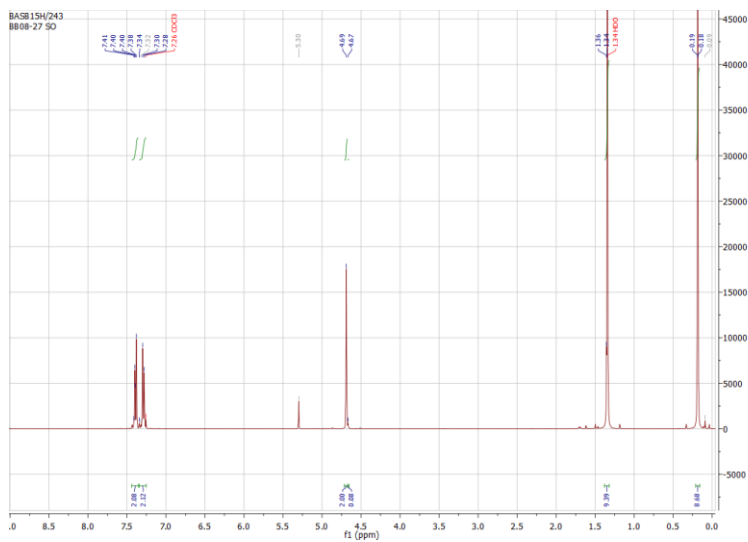
Figure S22: ^{1}H NMR spectrum of ((4-(tert-butyl)benzyl)oxy)trimethylsilane **11b.**
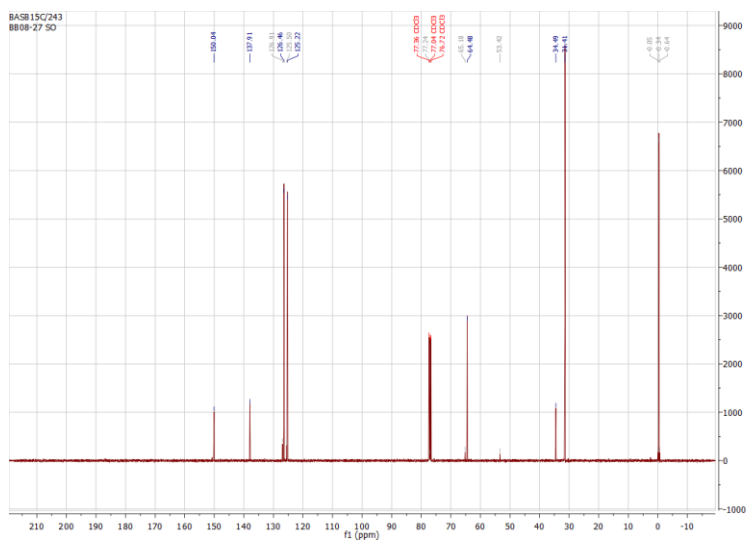
Figure S23: ^{13}C NMR spectrum of ((4-(tert-butyl)benzyl)oxy)trimethylsilane **11b.**

Trimethyl(o-tolyloxy)silane **12b**

^{1}**H NMR** (400 MHz, CDCl$_3$) δ 7.16 (dd, J = 7.5, 1.8 Hz, 1H), 7.09 (td, J = 7.7, 1.7 Hz, 1H), 6.90 (td, J = 7.4, 1.3 Hz, 1H), 6.80 (dd, J = 8.0, 1.3 Hz, 1H), 2.22 (s, 3H), 0.29 (d, J = 1.5 Hz, 9H). ^{13}**C NMR** (400 MHz, CDCl$_3$) δ 153.6, 130.9, 129.0, 126.6, 121.3, 119.0, 16.6, 0.5.
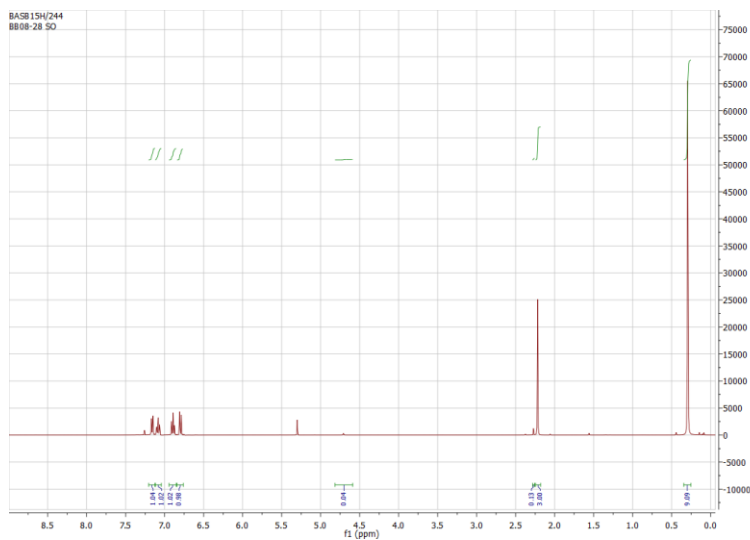
Figure S24: ^{1}H NMR spectrum of trimethyl(o-tolyloxy)silane **12b.**
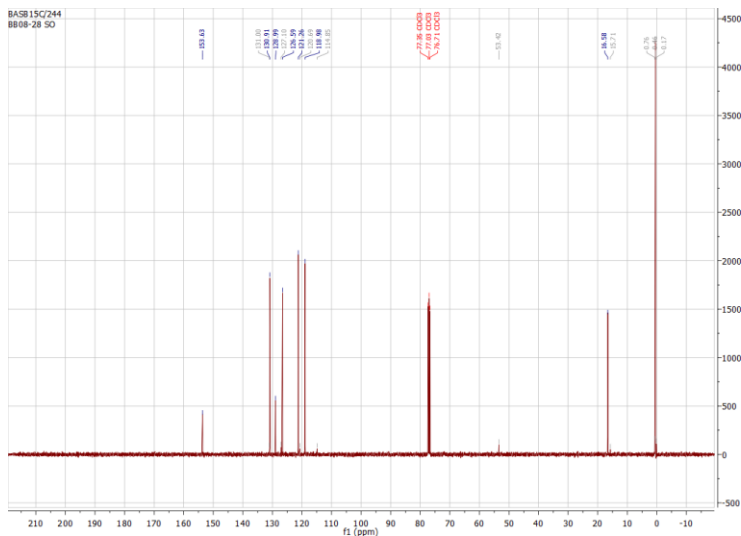
Figure S25:^{13}C NMR spectrum of trimethyl(o-tolyloxy)silane **12b.**

 (benzyloxy)dimethyl(phenyl)silane **1c**

^{1}H NMR (400 MHz, CDCl₃) δ 7.57 – 7.49 (m, 2H), 7.36 – 7.10 (m, 8H), 4.62 (s, 2H), 0.34 (s, 6H). **^{13}C NMR** (400 MHz, CDCl₃) δ 142.4, 139.3, 135.2, 131.3, 129.9, 129.6, 128.8, 128.2, 66.7, 0.3. **MS** (EI, m/z (%)): 227 (56), 198 (16), 197 (88), 167 (29), 165 (18), 164 (100), 149 (52), 135 (21), 121 (13), 91 (93), 65 (15)

Figure S26: ¹H NMR spectrum of (benzyloxy)dimethyl(phenyl)silane **1c**.

Figure S27: ¹³C NMR spectrum of (benzyloxy)dimethyl(phenyl)silane **1c**.
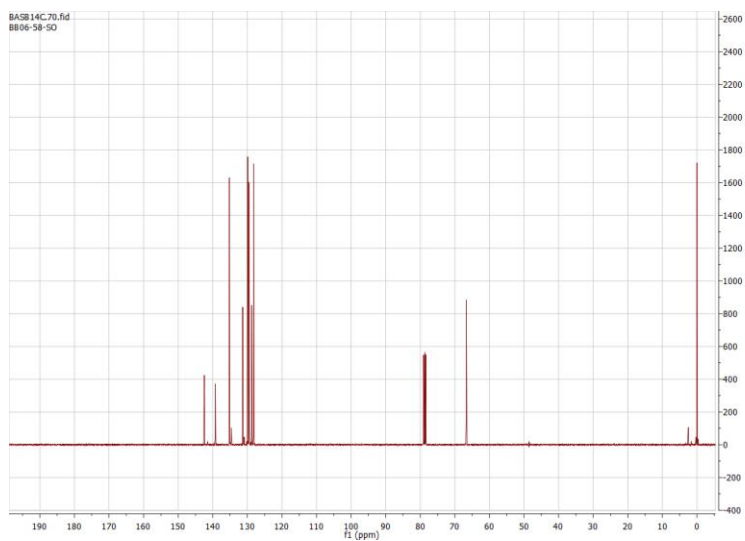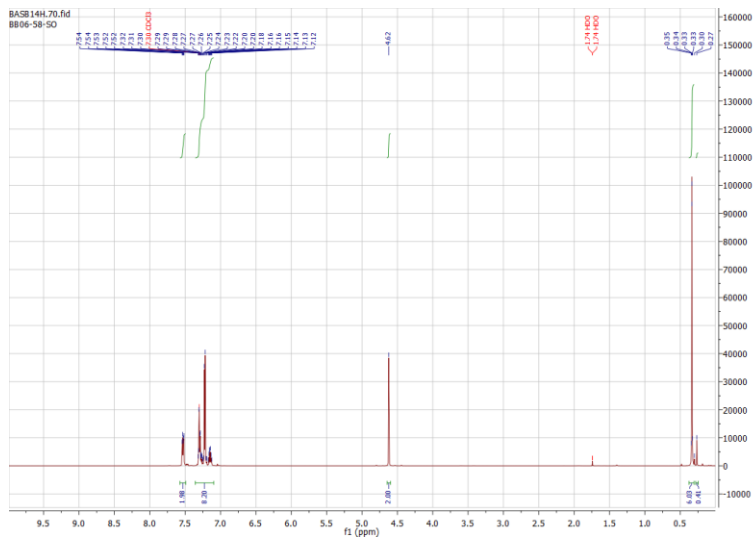
Dimethyl(phenyl)(undec-10-en-1-yloxy)silane 2c

^{1}H NMR (400 MHz, CDCl$_3$) δ 7.49 – 7.41 (m, 2H), 7.28 – 7.17 (m, 3H), 5.68 (ddt, J = 16.9, 10.2, 6.7 Hz, 1H), 4.92 – 4.76 (m, 2H), 3.46 (t, J = 6.7 Hz, 2H), 1.96 – 1.86 (m, 2H), 1.40 (dt, J = 7.9, 6.3 Hz, 2H), 1.24 – 1.14 (m, 7H), 1.14 (s, 3H), 0.25 (s, 6H). **^{13}C NMR** (400 MHz, CDCl$_3$) δ 140.8, 139.8, 135.2, 131.2, 129.5, 115.9, 64.9, 35.6, 34.4, 31.3, 31.2, 31.1, 30.9, 30.7, 27.6, 0.0. **MS** (EI, m/z (%)): 290 (5), 289 (20), 211 (10), 151 (5), 138 (12), 137 (100), 135 (26), 121 (10), 91 (5), 75 (6), 55 (5)

Figure S28: ^{1}H NMR spectrum of dimethyl(phenyl)(undec-10-en-1-yloxy)silane **2c**.
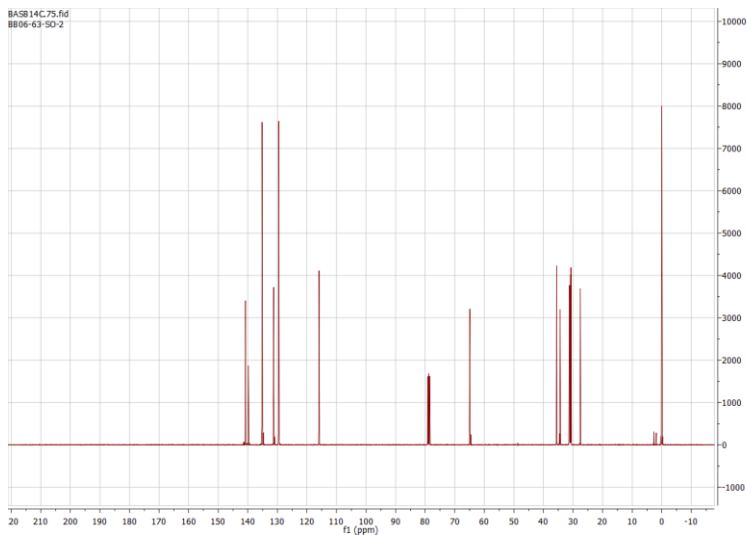
Figure S29: ^{13}C NMR spectrum of dimethyl(phenyl)(undec-10-en-1-yloxy)silane **2c**.

<u>Dimethyl((4-nitrobenzyl)oxy)(phenyl)silane **3c**</u>

^{1}H NMR (400 MHz, CDCl$_3$) δ 8.23 – 8.16 (m, 2H), 7.67 – 7.60 (m, 2H), 7.53 – 7.35 (m, 5H), 4.81 (s, 2H), 0.49 (s, 6H). **^{13}C NMR** (400 MHz, CDCl$_3$) δ 150.0, 148.6, 138.4, 135.0, 131.6, 129.6, 128.2, 125.1, 65.5, -0.3. **MS** (EI, m/z (%)): 273 (21), 272 (100), 242 (28), 212 (23), 210 (15), 209 (89), 194 (18), 135 (18), 121 (49), 89 (14), 78 (15).
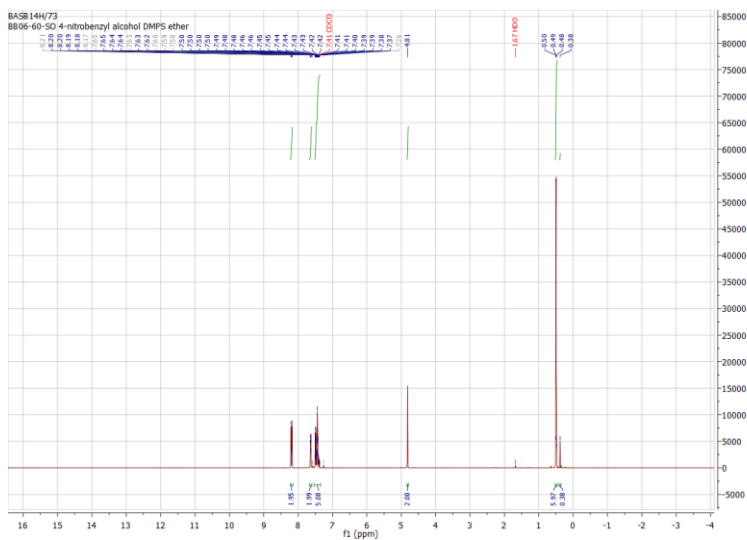
Figure S30: ^{1}H NMR spectrum of dimethyl((4-nitrobenzyl)oxy)(phenyl)silane **3c**.

Figure S31: ^{13}C NMR spectrum of dimethyl((4-nitrobenzyl)oxy)(phenyl)silane **3c**.
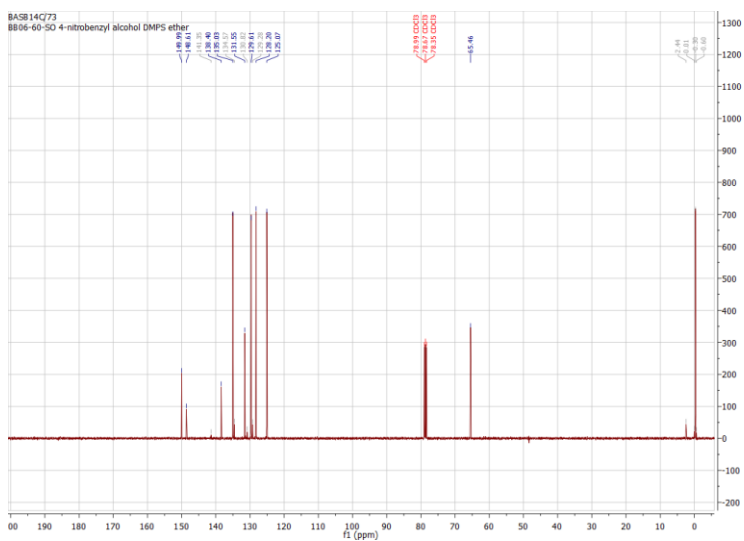
((2-isopropyl-5-methylcyclohexyl)oxy)dimethyl(phenyl)silane **4c**

¹H NMR (400 MHz, CDCl₃) δ 7.66 (m, 2H), 7.42 (m, 3H), 3.48 (td, *J* = 10.3, 4.4 Hz, 1H), 2.25 (m, 1H), 1.89 (m, 1H), 1.63 (dd, *J* = 13.0, 3.1 Hz, 2H), 1.30 – 1.18 (m, 1H), 1.09 (td, *J* = 12.2, 10.6 Hz, 1H), 1.00 – 0.79 (m, 8H), 0.68 (d, *J* = 6.9 Hz, 3H), 0.46 (d, *J* = 3.0 Hz, 6H). **¹³C NMR** (400 MHz, CDCl₃) δ 140.2, 135.1, 131.0, 129.3, 74.4, 51.7, 46.7, 36.1, 33.2, 26.8, 24.4, 23.9, 22.9, 17.3. **MS** (EI, m/z (%)): 275 (21), 212 (51), 206 (15), 205 (81), 138 (17), 137 (100), 136 (36), 135 (90), 95 (11), 81 (14), 75 (25).
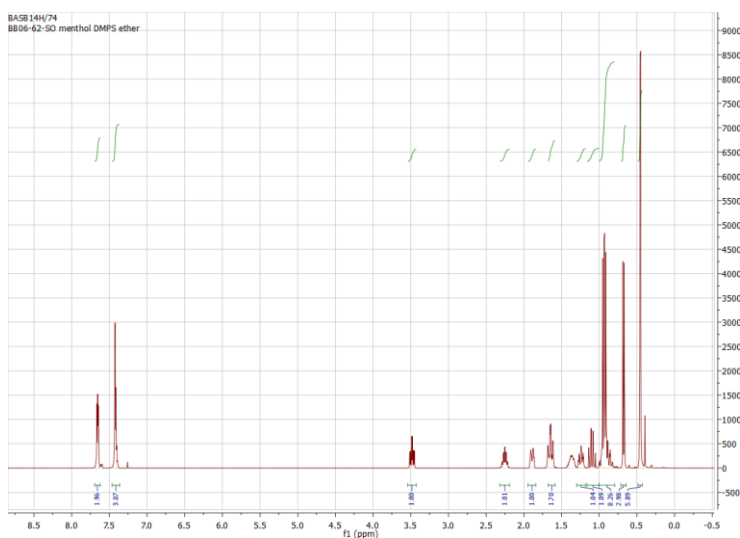
Figure S32: ¹H NMR spectrum of ((2-isopropyl-5-methylcyclohexyl)oxy)dimethyl(phenyl)silane **4c**.

Figure S33: ^{13}C NMR spectrum of ((2-isopropyl-5-methylcyclohexyl)oxy)dimethyl(phenyl)silane **4c**.

Figure S34: ^{1}H NMR spectrum of crude reaction mixture of trimethylsilylation of 4-cyanophenol to silyl ether **7b**. Conversion is approximately 90%, determined from the ratio of aromatic signals to the singlet at 2 ppm.
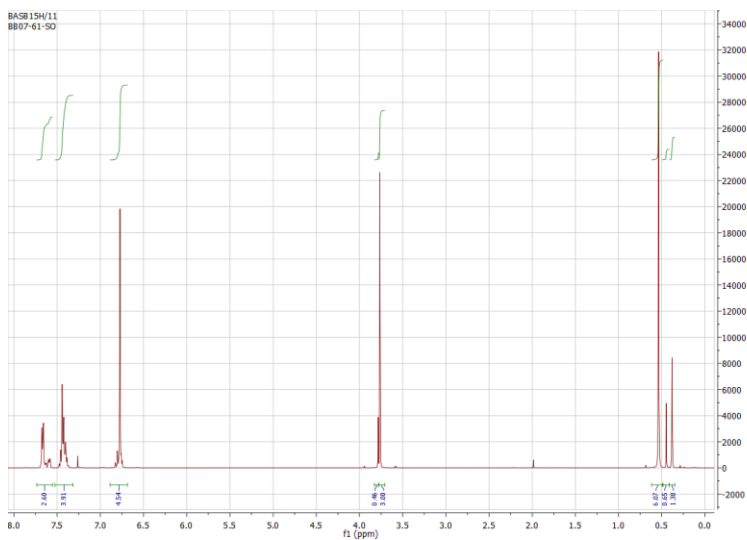
Figure S35: ^{1}H NMR spectrum of crude reaction mixture of dimethylphenylsilylation of 4-methoxyphenol to silyl ether **9c**. Conversion is approximately 86%, determined from the ratio of the peaks at 3.6 ppm.
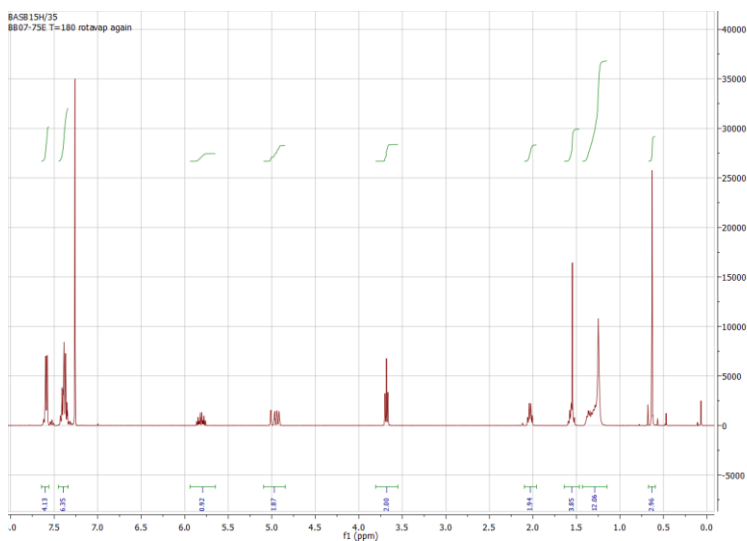
Figure S36: ^{1}H NMR spectrum of crude reaction mixture of diphenylmethylsilylation of 10-undecen-1-ol to silyl ether **2d**.

Approximation of relative rate constants

For the reactions
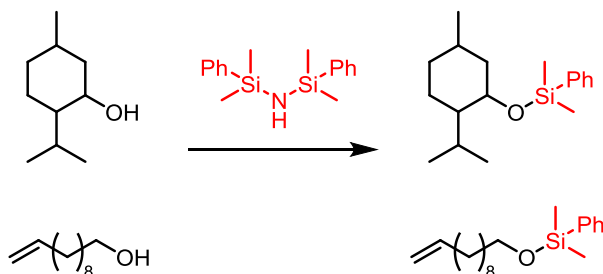
Scheme S1: Reactions used in the competition experiment for selective protection of alcohols.

the following equations can be set up:

undecenol + disilazane $\overset{k1}{\rightarrow}$ undecenol DMPS ether + monosilazane

menthol + disilazane $\overset{k2}{\rightarrow}$ menthol DMPS ether + monosilazane

undecenol + monosilazane $\overset{k3}{\rightarrow}$ undecenol DMPS ether

menthol + monosilazane $\overset{k4}{\rightarrow}$ menthol DMPS ether
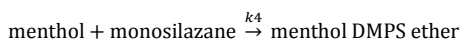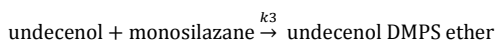
Simplify by making k_3 equal to k_1 and k_4 equal to k_2. The differential equations become:

$$\frac{\delta[\text{undecenol}]}{\delta t} = -k1 \cdot ([\text{disilazane}] \cdot [\text{undecenol}] + [\text{monosilazane}] \cdot [\text{undecenol}])$$

$$\frac{\delta[\text{menthol}]}{\delta t} = -k2 \cdot ([\text{disilazane}] \cdot [\text{menthol}] + [\text{monosilazane}] \cdot [\text{menthol}])$$

$$\frac{\delta[\text{undecenol DMPS ether}]}{\delta t} = k1 \cdot ([\text{disilazane}] \cdot [\text{undecenol}] + [\text{monosilizane}] \cdot [\text{undecenol}])$$

$$\frac{\delta[\text{menthol DMPS ether}]}{\delta t} = k2 \cdot ([\text{disilazane}] \cdot [\text{menthol}] + [\text{monosilazane}] \cdot [\text{menthol}])$$

$$\frac{\delta[\text{disilazane}]}{\delta t} = -k1 \cdot [\text{disilazane}] \cdot [\text{undecenol}] - k2 \cdot [\text{disilazane}] \cdot [\text{menthol}]$$

$$\frac{\delta[\text{monosilazane}]}{\delta t} = k1 \cdot [\text{undecenol}] \cdot ([\text{disilazane}] \cdot -[\text{monosilazane}]) + k2$$
$$\cdot [\text{menthol}]([\text{disilazane}] - [\text{monosilazane}])$$

These differential equations are numerically solved using an explicit Runge-Kutta fourth order algorithm, implemented in Python (see Appendix 5 for source code).

Sample output

```
Simulation results

k2: 0.061
k1/k2: 16.393
t: 61

Final concentrations:
 DS   | MENTHOL DMPS | UNDECENOL DMPS
-------+-------------+---------------
 0.000 | 0.060     | 0.439

percent: 12.05
```
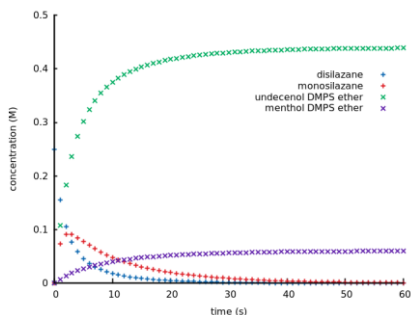
Figure S37: Plot of values returned from the simulation for k_2 = 0.061. Initial concentration of disilazane = 0.25 M, undecenol = 0.5 M, menthol = 0.5 M, monosilazane = 0.0 M, undecenol DMPS ether = 0.0 M, menthol DMPS ether = 0.0 M.
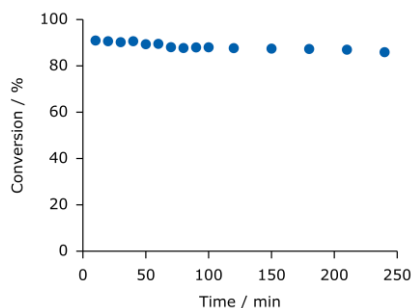
Figure S38: Graph of relative peak area of product as measured with GC-MS. The reaction was performed at 30 °C (normally performed at 60 °C) for four hours with a packed bed containing 4.3 mg SBA15-SO$_3$H, taking samples at regular intervals. The conversion drops slightly over time, indicating that the ammonia formed in the reaction slowly deactivates the sulfonic acid groups.
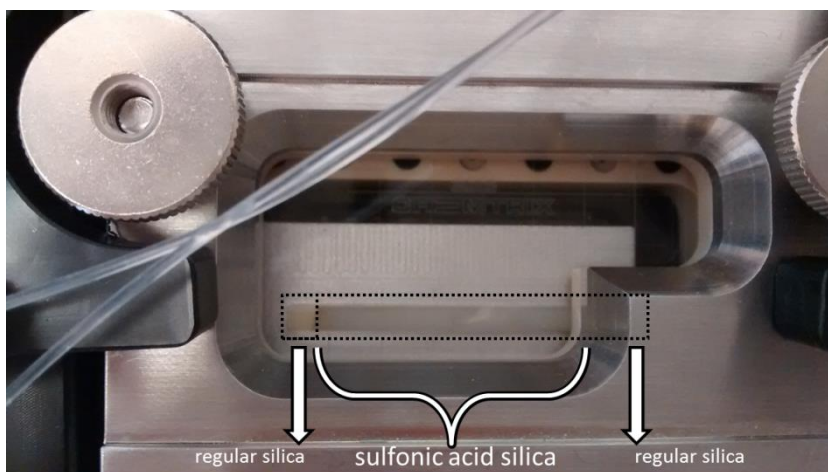
Figure S39: photograph of the filled glass microreactor (Chemtrix 3026). The packed bed is filled with a plug of regular silica, then silica-supported sulfonic acid and finally another plug of regular silica (obscured from view).

Appendix 5

Source code of kinetic parameter estimation script

This source code can also be found online at:

https://gist.github.com/barrebas/0aa2379cb1d42b895035

```python
#!/usr/bin/python

'''
global variables
'''
k1 = 1.0        # value for rate constant
goal = 0.88     # Goal is the experimentally observed ratio
                # between the peaks of undecenol DMPS ether and
                # menthol DMPS ether.
'''
Implementation of the Runge-Kutta 4th order algorithm.
'''
def rk4(fy, y, t, dt):
        y1 = dt * fy(y, t)
        y2 = dt * fy(y + 0.5 * y1, t + 0.5 * dt)
        y3 = dt * fy(y + 0.5 * y2, t + 0.5 * dt)
        y4 = dt * fy(y + y3, t + dt)

        # only return new y value, don't update t
        return (1.0/6.0 * (y1 + 2 * y2 + 2 * y3 + y4))


'''
Runs the simulation, given a value for k2, the rate constant
for the protection of menthol, the secondary alcohol.
'''
def run(k2):
        concU = 0.5     # Concentration of undecenol at t=0
        concM = 0.5     # Concentration of menthol at t=0
        concDS = 0.25   # Concentration of disilazane at t=0
        concS = 0.0     # Concentration of monosilazane at t=0
        concPU = 0.0    # Concentration of undecenol DMPS ether
        concPM = 0.0    # Concentration of menthol DMPS ether

        t = 0.0         # time
        dt = 0.005      # time step

        # Run the simulation for as long as there is disilazane present.
```

```python
while (concDS + concS) > 0.001:
        # Define functions used for the RK4 calculation.
        # These functions are derivatives of the concentration
        # equations.
        f_concU = lambda x, n: k1 * x * concDS
        f_concM = lambda x, n: k2 * x * concDS
        f_concU2 = lambda x, n: k1 * x * concS
        f_concM2 = lambda x, n: k2 * x * concS

        # Get delta values for updating the concentrations
        d_concU = rk4(f_concU, concU, t, dt)
        d_concM = rk4(f_concM, concM, t, dt)
        d_concU2 = rk4(f_concU2, concU, t, dt)
        d_concM2 = rk4(f_concM2, concM, t, dt)

        # Update concentrations.
        concU -= (d_concU + d_concU2)
        concM -= (d_concM + d_concM2)

        concDS -= d_concU
        concDS -= d_concM

        concS += (d_concU + d_concM)
        concS -= (d_concU2 + d_concM2)

        # If, for some reason, the concentration of concDS went
        # below zero, clamp it to zero.
        if concDS < 0:
                concDS = 0

        # Update concentrations of products.
        concPU += d_concU + d_concU2
        concPM += d_concM + d_concM2

        # Update t by adding dt.
        t += dt
# Return the values from the simulation.
```

183

```
        return (t, concDS, concPU, concPM)


if __name__=="__main__":
        # Attempt to find a value for k2 that satisfies
        # the goal condition.
        done = 0

        # Initial guess.
        k2 = 1.0

        done = 0
        while done != 1:
                (t,concDS,concPU,concPM ) = run(k2)
                # If the return value satisfies the goal value,
                # within a certain amount of error, terminate
                # the loop.
                if abs(goal-concPU/(concPM+concPU)) < 0.001:
                        done = 1
                # Adjust the k2 values and try again.
                else:
                        if concPU/(concPM+concPU) < goal:
                                k2 -= k2 * abs(goal - concPU/(concPM+concPU))
                        if concPM > goal:
                                k2 += k2 * abs(goal - concPU/(concPM+concPU))

        print "Simulation results\n"
        print "k2: %.3f" % k2
        print "k1/k2: %.3f" % (k1/k2)
        print "t: %3.f\n" % t
        print "Final concentrations:"
        print " DS | MENTHOL DMPS | UNDECENOL DMPS"
        print "-------+-------------+--------------"
        print " %.3f | %.3f  | %.3f" % (concDS, concPM, concPU)
        percent = 100 * concPM / (concPM + concPU)
        print "percent: %.2f\n" % percent
```

Appendix 6

Supporting Information for Chapter 5

Clickable Polylactic Acids by Fast Organocatalytic Ring-Opening Polymerization in Continuous Flow
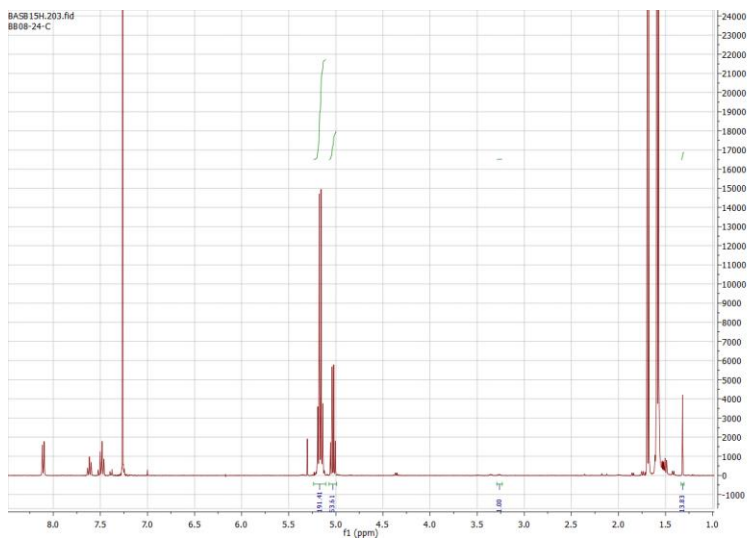
Figure S1. Example of ^{1}H NMR spectrum of the crude reaction mixture after solvent removal with a stream of nitrogen. The quartet at 5.16 ppm corresponds to the polymer backbone, the quartet at 5.03 ppm corresponds to the monomer, the triplet at 3.27 ppm corresponds to the catalyst and the singlet at 1.32 ppm corresponds to the *tert*-butyl group of initiator **1**. These NMR signals are used for determination of conversion, catalyst loading and degree of polymerization, respectively.
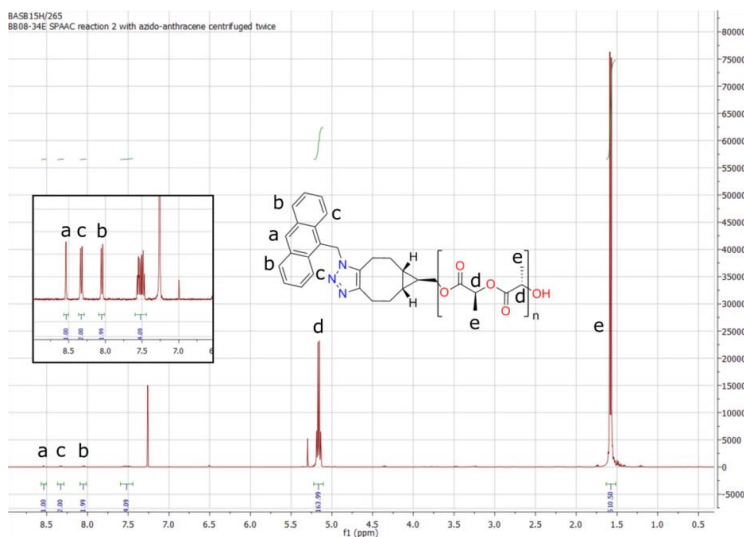
Figure S2. ^{1}H NMR of purified BCN-PLA reacted with azido-anthracene. The ratio of azido-anthracene proton **a** to the backbone protons **d** match well with full conversion of the DP=80 PLA molecule. Inset: zoom of aromatic region showing the anthracene protons.
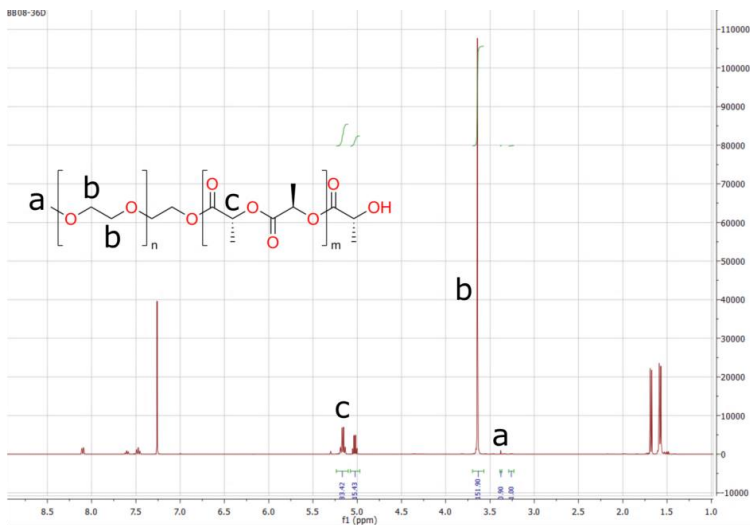
Figure S3. ^{1}H NMR spectrum of PEG-PLA block copolymer with a composition PEG$_{128}$-PLA$_{56}$, with 68% conversion of monomer. The signal at **a** was used to calculate the length of the PEG polymer. Signals at **b** and **c** were used to determine the composition of the block copolymer.
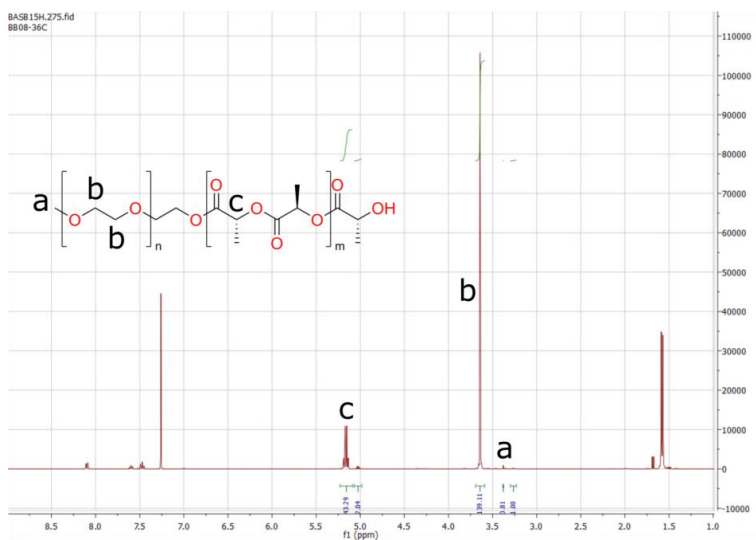
Figure S4. ^{1}H NMR spectrum of PEG-PLA block copolymer with a composition PEG$_{128}$-PLA$_{80}$, with 96% conversion of monomer. The signal at **a** was used to calculate the length of the PEG polymer. Signals at **b** and **c** were used to determine the composition of the block copolymer.
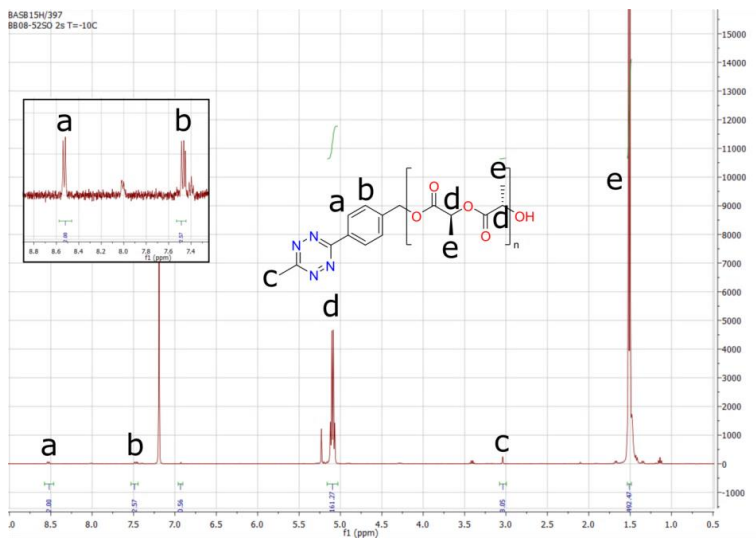
Figure S5. ^{1}H NMR of purified tetrazine-PLA. The ratio of protons **a** to the backbone protons **d** indicate a degree of polymerization of 80 monomers. Inset: zoom of aromatic region showing the tetrazine protons and a small amount of residual benzoic acid.
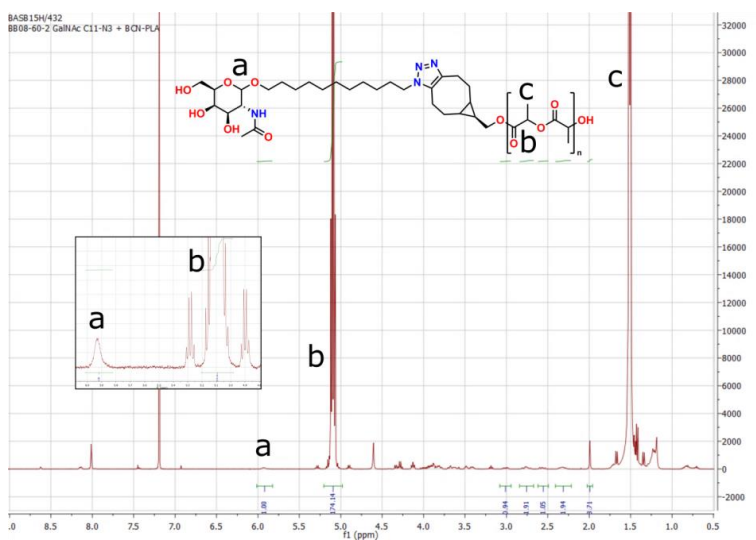
Figure S6. ^{1}H NMR of GalNAc-C$_{11}$-N$_3$ clicked to BCN-PLA. Inset shows region where anomeric proton of carbohydrate moiety is located.
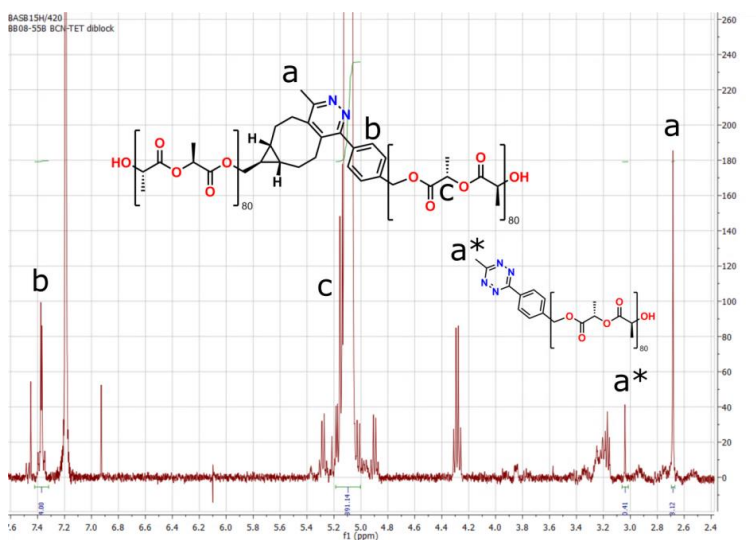
Figure S7. ^{1}H NMR of tetrazine-PLA clicked to BCN-PLA. A small amount of tetrazine-PLA is still present (peak of methyl marked **a***).

189
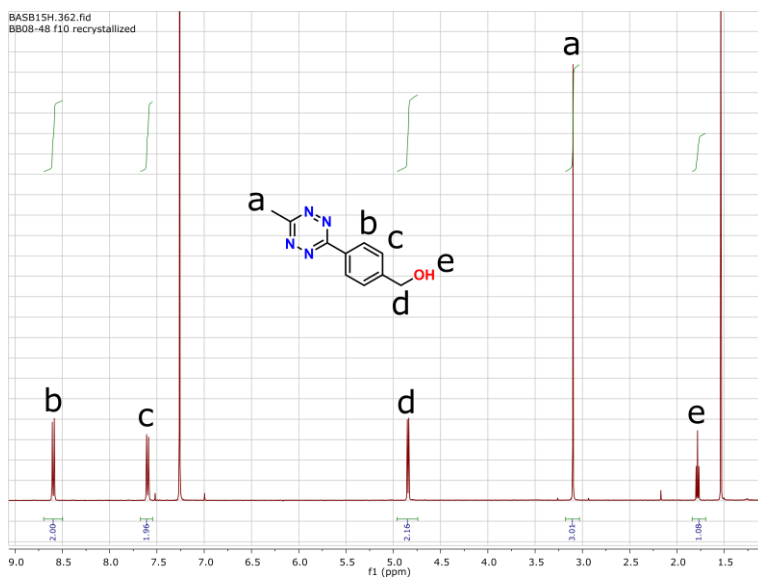
Figure S8. ^{1}H NMR of tetrazine-derivated initiator **4** obtained after recrystallization.
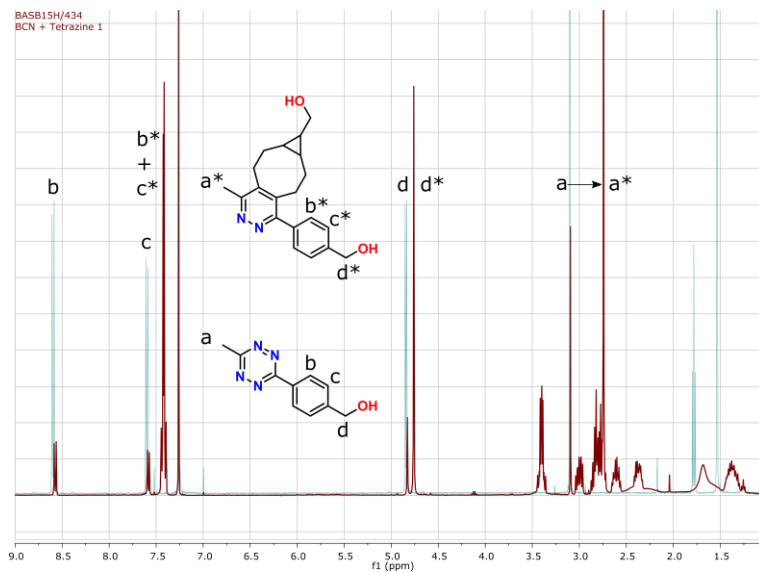
Figure S9. ^{1}H NMR of tetrazine-derived initiator **4** (light-blue trace) and the reaction mixture of *exo*-BCN **3** with tetrazine **4** (red trace). A clear difference in the chemical shift of the protons is observed.
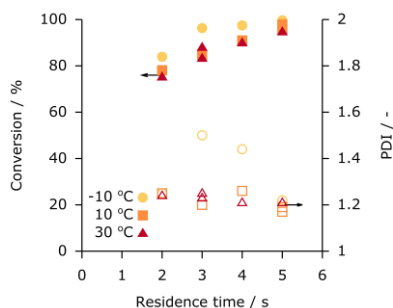
Figure S10. Conversion of monomer at targeted DP of 160, catalyst loading 0.6 mol%. The optimal residence time in this case is 5 s at a temperature of −10 °C.
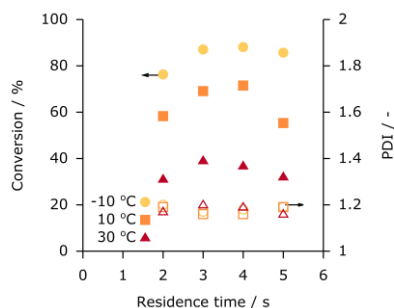
Figure S11. Conversion of monomer at targeted DP of 240, catalyst loading 0.75 mol%. The optimal residence time in this case is 4 s at a temperature of −10 °C.
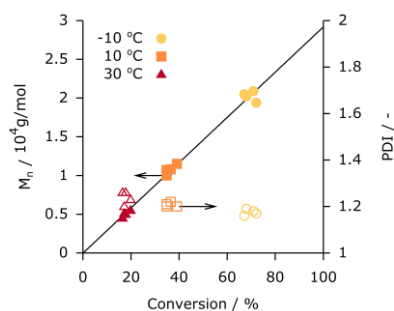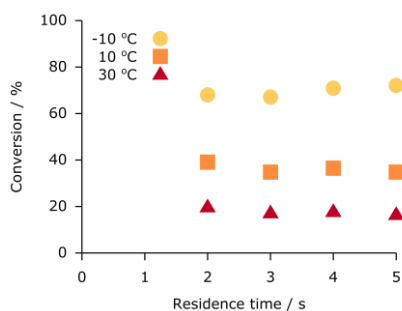

Figure S12. Left: Polymerization with a targeted DP of 160 and a catalyst loading of 0.35 mol%. The conversion reaches a plateau value. **Right:** M_n versus conversion follows a straight line, indicating a pseudo-living polymerization. Catalyst loading: 0.35 mol%. Closed symbols denote M_n, open symbols denote PDI.
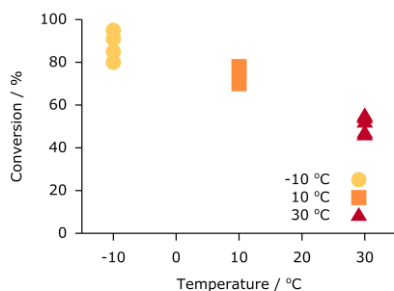
Figure S13. The conversion at a targeted DP of 80 and 0.25 mol% catalyst loading is less than quantitative and conversion is higher at lower temperature.
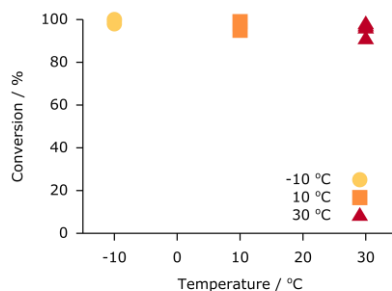

Figure S14. At higher catalyst loading (0.5 mol%) the effect of temperature on the conversion is observed (lower temperature, higher conversion), yet less pronounced. Targeted DP = 80.
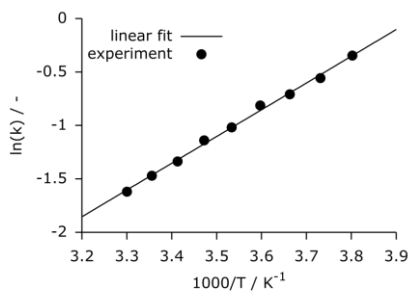

Figure S15. Van 't Hoff plot of the natural logarithm of conversion at nine different temperatures (every 5 °C from −10 to 30 °C; residence time 4 s, catalyst loading 0.25 mol%). The linear fit follows $\ln(K_{eq}) = \frac{-\Delta H^0}{RT} + \frac{\Delta S^0}{R}$; from the slope, ΔH^0 was determined to be −20.8 kJ/mol.
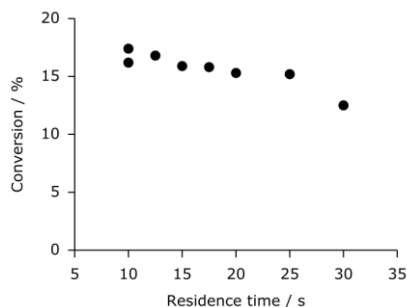

Figure S16. Conversion *vs* residence time for 0.1 mol% catalyst loading at a targeted DP of 80. The order of data point collection was randomized with respect to residence time.
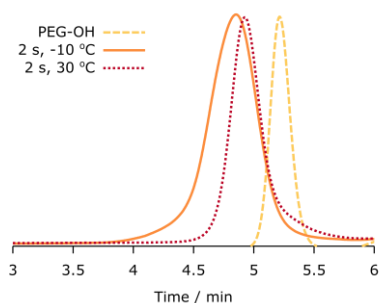
Figure S17. GPC traces of PEG-5000-OH macroinitiator (yellow) and block copolymers from PEG-5000-OH initiator (orange and red).
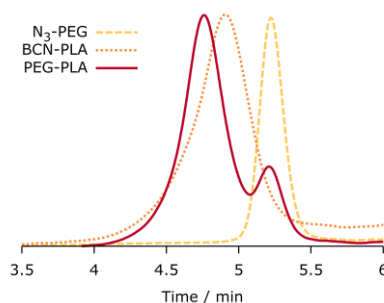

Figure S18. GPC traces of block copolymer synthesis using the SPAAC reaction. After reacting PEG-5000-N$_3$ (yellow trace) and BCN-PLA (red trace) for 24 h, the resulting block copolymer peak shifts left (orange trace) w.r.t. BCN-PLA, indicating that the click reaction works.
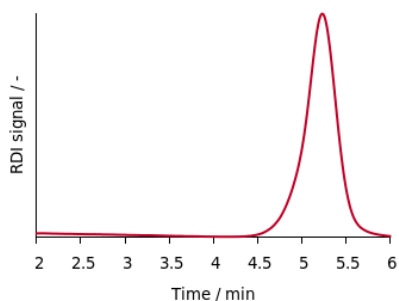

Figure S19. GPC trace of DP=80 PLA obtained at −10 °C and 5 s residence time, catalyst loading 0.25 mol%.
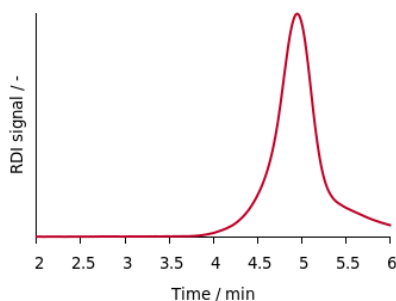

Figure S20. GPC trace of DP=160 PLA obtained at −10 °C and 5 s residence time, catalyst loading 0.6 mol%.

Figure S21. GPC trace of DP=240 PLA obtained at 30 °C and 5 s residence time, catalyst loading 1.2 mol%.

Figure S23. GPC trace of DP=80 tetrazine-initiated PLA obtained at -10 °C and 2 s residence time, catalyst loading 1 mol%.
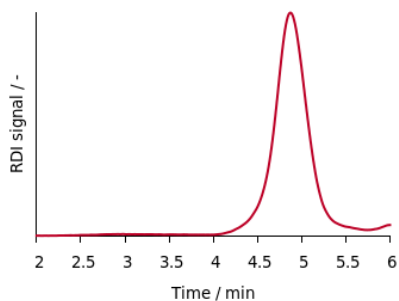
Figure S22. GPC trace of DP=80 BCN-initiated PLA obtained at -10 °C and 2 s residence time, catalyst loading 1 mol%.
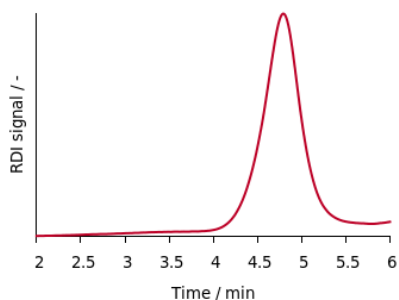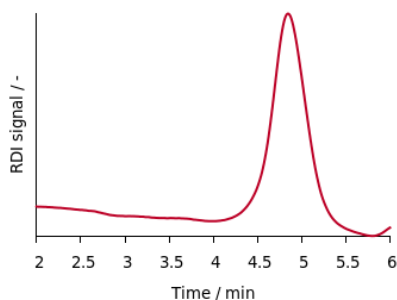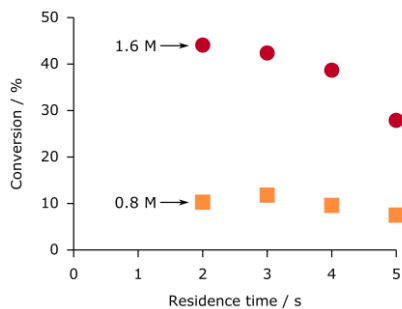

Figure S23. Polymerization conducted at two concentrations, T = 30 °C and targeted DP=80. Even though the catalyst loading w.r.t. monomer is equal, the conversion decreases four-fold.
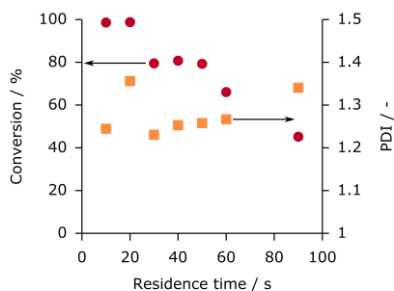
Figure S24. Polymerization conducted at T = 30 °C, 0.6 mol% catalyst and targeted DP=80. At long residence times, the conversion drops again due to the thermodynamic equilibrium being established.
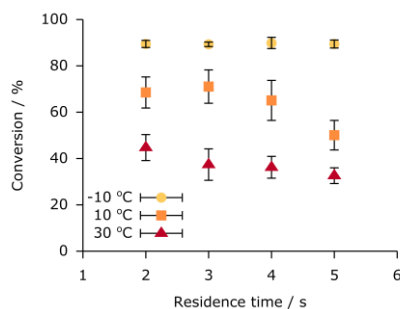
Figure S25. Polymerization conducted using 0.5 mol% catalyst and targeted DP=80. Data points were taken in triplicate to calculate the standard deviation. The lower conversion is attributed to the age of the TBD, which apparently still deactivates, even when kept in a glovebox.

195

Tabulated data for polymerizations

All M_n values are reported as M_n / 1,000. M_n and PDI were determined by GPC in THF *vs* PS standards.

Table S1. Data obtained from ROP of L-lactide using 0.25 mol% catalyst loading. Targeted DP = 80.

| Sample	Time / s	T / °C	Conversion	DP	M_n	PDI
A	5	−10	94.8%	77	12.5	1.21
B	5	30	46.5%	35	5.3	1.19
B'	5	30	46.3%	37	5.4	1.21
C	5	10	78.1%	62	10.6	1.19
D	2	10	71.7%	55	9.1	1.27
D'	2	10	70.3%	57	9.0	1.30
E	2	−10	79.5%	64	11.1	1.28
F	2	30	55.3%	42	6.6	1.24
G	4	10	77.4%	61	10.1	1.20
H	4	−10	90.8%	72	12.6	1.23
I	4	30	52.4%	40	6.3	1.18
J	3	30	54.2%	42	6.3	1.23
K	3	−10	84.7%	70	11.4	1.28
L	3	10	77.2%	62	10.4	1.24

Table S2. Data obtained from ROP of L-lactide using 0.5 mol% catalyst loading. Targeted DP = 80.

Sample	Time / s	T / °C	Conversion	DP	M_n	PDI
A	4	−10	99.7%	88	11.2	1.37
A'	4	−10	99.6%	76	12.1	1.43
B	4	10	99.1%	81	10.9	1.30
C	4	30	96.5%	78	10.1	1.26
D	5	30	97.8%	90	9.7	1.29
D'	5	30	96.6%	85	10.1	1.31
E	5	10	99.1%	85	11.5	1.34
F	5	−10	99.6%	92	12.4	1.52
G	3	30	96.1%	84	10.5	1.29
H	3	−10	99.4%	79	12.7	1.38
I	3	10	98.0%	90	11.9	1.28
J	2	−10	97.7%	91	12.9	1.24
K	2	30	91.5%	71	11.5	1.24
L	2	10	95.4%	82	10.2	1.27

Table S3. Data obtained from ROP of L-lactide using 1.2 mol% catalyst loading. Targeted DP = 80.

Sample	Time / s	T / °C	Conversion	DP	M_n	PDI
A	5	10	99.4%	79	14.0	1.61
A'	5	10	98.9%	88	13.2	1.46
B	5	−10	99.8%	89	15.6	1.78
C	5	30	99.0%	84	13.1	1.50
D	4	10	99.3%	83	15.1	1.52
D'	4	10	99.4%	84	16.7	1.36
E	4	−10	99.9%	87	16.1	1.46
F	4	30	98.8%	84	13.1	1.51
G	2	−10	99.6%	87	18.7	1.30
H	2	10	99.5%	90	15.0	1.36
I	2	30	98.5%	85	14.4	1.28
J	3	30	98.8%	83	14.2	1.36
K	3	−10	99.8%	85	15.6	1.44
L	3	10	99.3%	86	15.1	1.43

Table S4. Data obtained from ROP of L-lactide using 0.35 mol% catalyst loading. Targeted DP = 160.

Sample	Time / s	T / °C	Conversion	DP	M_n	PDI
D	5	30	16.5%	25	4.5	1.26
E	5	10	34.8%	52	10.0	1.21
F	5	−10	72.1%	112	19.4	1.17
G	4	−10	70.9%	111	20.9	1.18
H	4	10	36.5%	56	10.8	1.22
I	4	30	17.8%	27	5.0	1.26
J	2	30	19.8%	30	5.5	1.23
K	2	10	39.1%	59	11.5	1.20
L	2	−10	68.0%	105	20.2	1.19
M	3	−10	67.1%	106	20.5	1.16
N	3	10	34.8%	55	10.7	1.20
O	3	30	17.2%	26	5.1	1.20
D	5	30	16.5%	25	4.5	1.26
E	5	10	34.8%	52	10.0	1.21

Table S5. Data obtained from ROP of L-lactide using 0.6 mol% catalyst loading. Targeted DP = 160.

Sample	Time / s	T / °C	Conversion	DP	M_n	PDI
A	5	10	97.9%	154	25.3	1.17
A'	5	10	95.4%	154	25.0	1.19
B	5	−10	99.7%	169	27.4	1.22
C	5	30	94.7%	153	22.1	1.21
D	3	30	88.0%	139	21.3	1.23
D'	3	30	83.3%	135	20.8	1.25
E	3	10	84.8%	141	23.3	1.20
F	3	−10	96.3%	159	28.1	1.50
G	2	−10	83.9%	135	24.0	1.25
H	2	30	75.2%	127	19.3	1.24
I	2	10	78.1%	126	22.8	1.25
J	4	30	90.0%	147	22.2	1.21
K	4	−10	97.5%	150	25.4	1.44
L	4	10	91.0%	147	24.7	1.26

Table S6. Data obtained from ROP of L-lactide using 0.5 mol% catalyst loading. Targeted DP = 240.

Sample	Time / s	T / °C	Conversion	DP	M_n	PDI
A	3	10	29.0%	66	14.3	1.23
B	3	−10	52.2%	132	26.6	1.22
C	3	30	14.0%	34	7.9	1.22
D	5	30	13.5%	34	7.6	1.27
E	5	10	25.5%	64	14.9	1.23
F	5	−10	49.8%	141	27.0	1.21
G	2	−10	58.8%	131	24.8	1.22
H	2	30	12.1%	30	7.4	1.25
I	2	10	25.1%	62	12.7	1.27
J	4	10	23.6%	62	15.6	1.16
K	4	−10	55.2%	132	25.2	1.24
L	4	30	15.1%	34	7.5	1.25

Table S7. Data obtained from ROP of L-lactide using 0.75 mol% catalyst loading. Targeted DP = 240.

Sample	Time / s	T / °C	Conversion	DP	M_n	PDI
A	3	10	69.1%	164	28.3	1.16
B	3	−10	87.1%	207	41.9	1.17
C	3	30	39.1%	91	17.0	1.20
D	4	30	36.8%	87	16.3	1.19
E	4	10	71.5%	172	30.7	1.16
F	4	−10	88.1%	208	40.9	1.18
G	5	−10	85.7%	209	38.6	1.19
H	5	10	55.3%	136	24.9	1.19
I	5	30	32.1%	72	14.8	1.16
J	2	−10	76.3%	168	36.8	1.20
K	2	10	58.3%	135	25.6	1.19
L	2	30	31.1%	74	14.6	1.17

Table S8. Data obtained from ROP of L-lactide using 1.2 mol% catalyst loading. Targeted DP = 240.

Sample	Time / s	T / °C	Conversion	DP	M_n	PDI
A	3	10	99.2%	232	38.5	1.29
A'	3	10	97.9%	247	36.1	1.41
B	3	−10	99.3%	242	43.8	1.63
C	3	30	97.2%	230	34.0	1.28
C'	3	30	93.2%	236	31.8	1.35
D	5	30	98.8%	235	32.2	1.29
E	5	10	99.5%	238	36.8	1.37
F	5	−10	99.9%	247	44.0	1.53
G	2	10	95.4%	237	39.9	1.32
H	2	30	88.6%	217	33.5	1.32
I	2	−10	95.1%	237	43.4	1.62
J	4	−10	99.5%	240	44.4	1.60
K	4	30	97.7%	236	32.9	1.33
L	4	10	98.7%	252	37.3	1.43

Table S9. Data obtained from ROP of L-lactide using 1 mol% catalyst loading and tetrazine **4** as initiator. Targeted DP = 80.

Sample	Time / s	T / °C	Conversion	DP	M_n	PDI
A	3	10	99.7%	85	15.3	1.27
B	3	−10	99.8%	82	17.8	1.27
C	3	30	98.2%	81	14.2	1.24
D	5	30	98.9%	81	14.1	1.24
E	5	10	99.7%	81	15.5	1.33
F	5	−10	100.0%	81	17.0	1.38
G	2	−10	99.5%	79	17.6	1.20
H	2	30	95.1%	75	14.5	1.20
I	2	10	98.8%	80	16.5	1.19
J	4	10	99.6%	81	15.7	1.28
K	4	−10	99.7%	93	17.7	1.28
L	4	30	98.1%	76	14.4	1.21
SO	2	−10	100.0%	81	17.4	1.20

SO = scale out.

Table S10. Data obtained from ROP of L-lactide using 1 mol% catalyst loading and tetrazine **4** as initiator. Targeted DP = 80.

Sample	Time / s	T / °C	Conversion	DP	M_n	PDI
A	3	10	99.3%	97	15.2	1.29
B	3	−10	99.9%	109	17.7	1.28
C	3	30	96.6%	89	14.0	1.25
D	5	30	97.8%	102	13.9	1.25
E	5	10	99.1%	95	15.7	1.30
F	5	−10	99.8%	99	17.9	1.33
G	2	−10	99.6%	102	17.8	1.23
H	2	30	91.2%	88	14.1	1.23
I	2	10	97.9%	100	16.2	1.20
J	4	10	99.1%	98	15.3	1.28
K	4	30	94.6%	82	13.8	1.25
L	4	−10	99.5%	90	17.1	1.31
SO	2	−10	n.d.	n.d.	17.5	1.24

SO = scale out. n.d. = not determined.

Calculation of Gibbs free energy

Duda et al. reported the following values for the polymerization of L-lactide at 100 °C:[1]
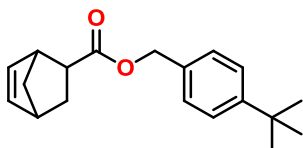
$\Delta H_p = -22.9$ kJ/mol

$\Delta S_p^{\,0} = -41$ J/mol K

Assuming these values are not dependent on temperature, we can calculate the Gibbs free energy **ΔG** via **ΔG = ΔH − TΔS**.

$\Delta G_{263K} = -22.9 - 263 * -41 = -12.1$ kJ/mol

$\Delta G_{303K} = -22.9 - 303 * -41 = -10.5$ kJ/mol

Synthesis of ester of 5-norbornene-2-carboxylic acid and 4-*tert*-butylbenzyl alcohol

To a solution of *N,N'*-dicyclohexylcarbodiimide (DCC, 2.6 g, 12 mmol) in 100 mL DCM stirred on ice was added 4-dimethylaminopyridine (DMAP, 0.2 g, 1 mmol) and 5-norbornene-2-carboxylic acid (1.4 g, 10 mmol, mixture of *endo* and *exo*) to give a white suspension. To this suspension was added 4-*tert*-butylbenzyl alcohol (1.6 g, 10 mmol). After 16 h, TLC (5% EtOAc:heptane) indicated complete conversion. The mixture was filtered over a silica plug and the solvent was removed *in vacuo* to yield the title compound as a colorless oil (1.8 g, 63%) consisting of a mixture of *endo* and *exo*.

Synthesis of GalNAc derivative 6
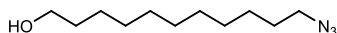
11-Azido-undecan-1-ol 9.[2] To a solution of 11-bromo-undecan-1-ol (10 g, 39 mmol, 1.0 eq) in DMF (50 mL) was added sodium azide (5.2 g, 80 mmol, 2.1 eq) and the reaction mixture was heated at 100 °C for 16 h. The reaction mixture was diluted with 50 mL of EtOAc, filtered, extracted with brine (3 × 50 mL). The organic phase was dried with Na_2SO_4, filtered and dried in vacuo. Purification by flash chromatography, eluent: isocratic cyclohexane/EtOAc 1:2, afforded compound **9** in 91% yield (7.6 g, 36 mmol) as a clear and colorless oil.

R_f (cyclohexane/EtOAc 1 : 2) = 0.60.

^{1}H NMR (CDCl$_3$, 400 MHz): δ (ppm) = 3.49 (t, 2H, J = 6.8 Hz, -CH_2OH), 3.16 (t, 2H, J = 7.0 Hz, -CH_2N$_3$), 2.95 (s, 1H), 1.52-1.44 (m, 4H), 1.20 (m, 14H).

^{13}C NMR (CDCl$_3$, 100 MHz): 63.1 (-CH_2OH), 51.5 (-CH_2N$_3$), 32.8, 29.6, 29.5, 29.4, 29.2, 28.9, 26.7, 25.8.

MS (ESI+) m/z = 214.20 [M+H]$^+$, calcd. ($C_{11}H_{24}N_3O^+$) = 214.19.
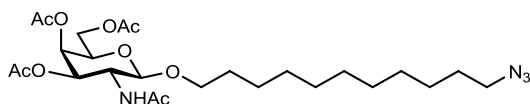
11-Azido-undecyl **2-acetamido-2-deoxy-3,4,6-tri-O-acetyl-β-d-galactopyranoside 10**.[3] A mixture of acetyl 2-acetamido-2-deoxy-3,4,6-tri-acetyl-d-galactopyranoside (0.50 g, 1.3 mmol, 1.0 eq), 11-azido undecan-1-ol **9** (0.33 g, 1.5 mmol, 1.2 eq), and 10 mg H_2SO_4-silica in 3 mL dicholoroethane were exposed to

MW irradiation (150 W) for 30 min at 110 °C. The white suspension turned into a clear brown solution during the reaction. The reaction mixture was filtered through celite, and concentrated *in vacuo*. Purification by column chromatography, eluent: heptane/EtOAc 4 : 1, afforded compound **10** in 84% yield (0.60 g, 1.1 mmol) as a pale yellow oil.

R$_f$ (heptane/EtOAc 4 : 1) = 0.35.

^{1}H-NMR (400 MHz, CDCl$_3$): δ = 6.43 (d, 1H, J = 8.8, -NH), 5.21 (m, 1H, H-4), 5.15 (m, 1H, H-3), 4.56 (d, 1H, J = 8.4 Hz, H-1), 4.00 (m, 2H, H-6a+b), 3.82 (m, 2H, H-2, H-5), 3.71 (m, 1H, -OCH_a-spacer), 3.34 (m, 1H, -OCH_b-spacer), 3.11 (t, 2H, J = 7.0 Hz, -CH_2N$_3$), 2.00 (s, 3H, -C(O)CH_3) 1.90 (s, 3H, -C(O)CH_3), 1.84 (s, 3H, -C(O)CH_3), 1.80 (s, 3H, -NHC(O)CH_3), 1.43 (m, 4H, -CH_2CH$_2$N$_3$, -CH_2CH$_2$O-), 1.13 (m, 14H, -CH$_2$-spacer).

^{13}C NMR (100 MHz, CDCl$_3$): δ = 170.2 (C=O), 170.1 (C=O), 170.0 (2 × C=O), 100.7 (C-1), 70.1 (C-5), 69.8 (C-3), 69.5 (-OCH_2-spacer), 61.3 (C-6), 51.0 (-CH_2N$_3$), 50.9 (C-2), 29.2, 29.1, 29.0, 28.7, 28.4, 26.3, 25.5, 22.9 (-NHC(O)CH_3) 20.3 (3 × -C(O)CH_3).

MS (ESI+) m/z = 543.30 [M+H]$^+$, calcd. (C$_{25}$H$_{43}$N$_4$O$_9^+$) = 543.30.
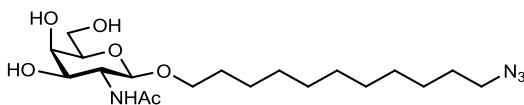
11-Azidoundecyl 2-acetamido-2-deoxy-β-d-galactopyranoside 6. Compound **10** (1.6 g, mmol, 1.0 eq) was exposed to standard Zemplén conditions (NaOMe in MeOH), until TLC indicated that all starting material was consumed. Subsequently, the reaction mixture was neutralized by addition of Dowex H$^+$ resin. The resin was

removed via filtration, rinsed with MeOH, and the combined filtrate was concentrated to quantitatively afford **6** (1.3 g, 3.0 mmol) as a white solid. **^{1}H-NMR** (400 MHz, MeOD): δ = 4.36 (d, 1H, J = 8.4 Hz, H-1), 3.90 (m, 2H, H-2, -OCH_a-spacer), 3.83 (m, 1H, H-4), 3.74 (m, 2H, H-6a+b), 3.59 (dd, 1H, J = 3.2, 10.7 Hz, H-3), 3.47 (m, 2H, -OCH_b-spacer, H-5), 3.28 (t, 2H, J = 6.8, -CH_2N$_3$), 1.98 (s, 3H, CH$_3$), 1.57 (m, 4H), 1.31 (m, 14H).

^{13}C NMR (100 MHz, MeOD): δ = 174.0 (C=O), 103.1 (C-1), 76.6 (C-5), 73.3 (C-3), 70.6 (-OCH_2-spacer), 69.7 (C-4), 62.5 (C-6), 54.4 (C-2), 52.5 (-CH_2N$_3$), 30.8, 30.73, 30.65, 30.5, 30.3, 29.9, 27.8, 27.2, 23.0;

MS (ESI+) m/z = 439.2580 [M+Na]$^+$, calcd. (C$_{19}$H$_{36}$N$_4$NaO$_6$$^+$) = 439.2527.

Figure S23. ^{1}H NMR spectrum 11-azidoundecyl 2-acetamido-2-deoxy-β-d-galactopyranoside **6**.

Figure S24. ^{13}C NMR spectrum 11-azidoundecyl 2-acetamido-2-deoxy-β-d-galactopyranoside **6**.

References

[**1**] A. Duda, A. Kowalski, J. Libiszowski, S. Penczek. Thermodynamic and Kinetic Polymerizability of Cyclic Esters. *Macromol. Symp.* **2005,** *224* (1), 71-84.

[**2**] S. M. Andersen, C.-C. Ling, P. Zhang, K. Townson, H. J. Willison, D. R. Bundle. Synthesis of ganglioside epitopes for oligosaccharide specific immunoadsorption therapy of Guillian-Barré syndrome. *Org. Biomol. Chem.* **2004,** *2*, 1199-1212.

[**3**] S. Mandal, N. Sharma, B. Mukhopadhyay. H2SO4-silica promoted direct formation of β-glycosides of N-acetyl glycosylamines under microwave conditions. *Synlett* **2009,** (19), 3111-3114.

Summary

Organocatalysis in Continuous Flow

A general introduction into the fields of microreactors, solid-supported catalysis, surface and click chemistry is given in **chapter 1**. Use of solid-supported catalysts within microfluidic systems was one of the goals of this project, with an emphasis on organocatalysis.

Chapter 2 describes the use of microwave assistance to speed up monolayer formation using 1-alkenes on silicon carbide (SiC) surfaces. The increase in speed is two to four orders of magnitude. Commercially available SiC microparticles can be modified using the same method, yet with a longer reaction time. The longer reaction time is probably caused by the porosity of the particles. By using $1,\omega$-dialkenes, this reaction permits easy access to "clickable" monolayers on SiC materials, amenable to thiol-ene click chemistry.

1-alkenes are also featured in **chapter 3** where they are used for the facile covalent functionalization of mesoporous silica, with high loadings that are comparable to or better than other methods. This allows the one-step modification of mesoporous silica with functionalized alkenes such as 1,7-octadiene. Monolayers derived from this dialkene are readily functionalized with surface-bound thiol-ene click reactions. Using a dithiol "glue" layer, complex alkenes such as quinine can be attached in a second follow-up thiol-ene click reaction. The quinine-functionalized mesoporous silica that was obtained was catalytically active for the thio-Michael addition reaction of 3-methoxythiophenol and cyclohex-2-en-1-one. This approach opens up a wide range of extremely mild and versatile functionalizations of mesoporous silica.

The lessons learned from the work in chapter 3 led to the application of sulfonic acid supported on mesoporous SBA-15 silica in the continuous flow system. In **chapter 4**, this silica-supported sulfonic acid is used for the protection of alcohols by tetrahydropyranyl or a range of silyl moieties under continuous flow conditions. The flow protocol outperforms both catalyzed batch reactions and previously reported catalyzed flow reactions in terms of reaction speed, versatility and output per hour. The laboratory-scale flow reactor can be used to generate synthetically relevant amounts of tetrahydropyranyl-, trimethylsilyl- and dimethylphenylsilyl-protected alcohols, demonstrated by producing more than 100 mg protected alcohol per run. The protection reactions can be used on a broad scope of alcohols. Selective protection reactions have been investigated, which show selectivity for primary alcohols over secondary alcohols, and for benzylic alcohols over phenolic alcohols. The same silica-supported sulfonic acid can be used for deprotection reactions of silyl ethers in methanol. Relatively mild reaction conditions (30 °C and 0.25 M concentration) gave > 98% conversion for the tested substrates. The effect of the bare silica support on the protection reaction was investigated, which shows that the silica itself is catalytically active yet the sulfonic acid is much more active. The silica-supported sulfonic acid catalyst could be re-used for at least five reactions over several days. Because the catalyst was trapped in the packed bed it need not be removed from the crude reaction mixture, which greatly simplified workup.

The ring-opening polymerization of L-lactide under continuous flow conditions is described in **chapter 5**. Using low catalyst loading and short residence times (0.25–1.2% TBD catalyst, residence times as short as 2 s) well-defined poly(lactic acid) (PLA) is obtained with high (95–100%) monomer conversions and PDIs of typically 1.2. Use of the microreactor allows for a rapid screening of optimal reaction conditions, consistently yielding the optimal values for high conversion and low polydispersity. This quickly revealed that longer residence times will give rise to higher conversions and a concomitantly broader molecular weight distribution due to transesterification of the polymer backbone by TBD. By adjusting the initiator-to-

monomer ratios, polymers up to a degree of polymerization of 240 (M_n 44,000 g/mol) have been synthesized in the same continuous flow reactor.

The organocatalytic, metal-free continuous flow method described is rapid and mild enough to allow the use of a PEG-5,000 macroinitiator (yielding block copolymers), *exo*-BCN alcohol and even a base-labile tetrazine-derived alcohol, the latter of which cannot be used under traditional batch conditions. The resulting BCN-PLA and tetrazine-PLA materials were then readily functionalized with small molecules and large polymers bearing azides and norbornenes via SPAAC and inverse electron demand Diels-Alder click chemistry.

Chapter 6 discusses and critically reflects on the results obtained in this thesis and gives directions for future research.

Acknowledgments

Organocatalysis in Continuous Flow

Trilling, Jelmer van der Rijst, Sebastiaan Roseboom, Florine Duval, Marijn Schrage, Geert Noordzij, Raoul Frijns, Pieter van der Scheer.

My two students, Raoul Frijns and Pieter van der Scheer: Thank you for choosing to spend significant parts of your education with me and contributing to this thesis! Pieter, supervising you wasn't always easy, yet you remained positive and creative and taught me a thing or two about myself. Raoul, your help laid the foundations for chapter 4 in a time where my enthusiasm was dwindling. Thank you both.

Thanks to the usual suspects and team Lutidine (Jorin, Tjerk, Sjoerd, Suzanne and many others): Many a (vrijdagmiddag)borrel was enjoyed and the pubquiz at the Orion will never be quiet again; Movie nights with (horror) movies picked by Jaime are simply the best (or worst, depending on your inclination); Large volumes of coffee were consumed while attempting to break Jaime's dart high-score; Lastly, thanks to my brofessor Fred for getting me (and others!) to frequent the gym and start lifting weights. All of you, keep on organizing things like this for the lab!

To my friends outside of the lab, Sander Thijssen and Richard Braamburg: thank you for being there for me whenever I need you, without judgement. Sometimes, just hanging out and having a beer is enough to put my feet back on the ground. You truly are great friends.

Thank you, Jorin and Tjerk, for allowing me to be your travel companion in Canada. You two pulled me through a rough period and I cannot express enough gratitude. It is an honor to have you as my paranymphs.

The same goes for my family: my mother Josette, father Jan and brother Rob. Your support and unconditional love keeps me going. I am forever grateful!

If there's one thing I've learned: the flow must go on.

Yours,

Bas

Publications

E. Spruijt, S. A. van den Berg, M. A. Cohen Stuart, J. van der Gucht, Direct Measurement of the Strength of Single Ionic Bonds between Hydrated Charges, *ACS Nano*, **2012**, *6* (6), pp 5297–5303. DOI: http://dx.doi.org/10.1021/nn301097y.

P. Lundberg, B. F. Lee, S. A. van den Berg, E. D. Pressly, A. Lee, C. J. Hawker, N. A. Lynd, Poly[(ethylene oxide)-co-(methylene ethylene oxide)]: A hydrolytically degradable poly(ethylene oxide) platform, *ACS Macro Letters*, **2012**, *1* (11), pp 1240–1243. DOI: http://dx.doi.org/10.1021/mz300477t.

S. A. van den Berg, J. Tu, K. M. Sliedregt, A. Kros, T. Wennekes, and H. Zuilhof, Clickable Mesoporous Silica via Functionalization with 1,ω-Alkenes, *Advanced Materials Interfaces*, **2014**, *1* (3), 1300061. DOI: http://dx.doi.org/10.1002/admi.201300061.

S.A. van den Berg, J. M. Alonso, K. Wadhwa, M. C. R. Franssen, T. Wennekes, and H. Zuilhof, Microwave-Assisted Formation of Organic Monolayers from 1-Alkenes on Silicon Carbide, *Langmuir*, **2014**, *30*, (35), pp 10562–10565. DOI: http://dx.doi.org/10.1021/la502197q.

S.A. van den Berg, R. A. M. Frijns, T. Wennekes, and H. Zuilhof, Continuous-Flow Alcohol Protection and Deprotection Reactions Catalyzed by Silica-Supported Sulfonic Acid, *Journal of Flow Chemistry*, **2015**, *5* (2), pp 95–100. DOI: http://dx.doi.org/10.1556/1846.2015.00006.

S.A. van den Berg, T. Wennekes, and H. Zuilhof, Clickable Polylactic Acids by Fast Organocatalytic Ring-Opening Polymerization in Continuous Flow. Submitted for publication.

Overview of completed training activities

Discipline-specific activities

Synthesis School "New vistas in organic chemistry"	HRSMC	2013
NWO CHAINS conference (presentation)	NWO	2012-14
Advanced Organic Chemistry	ORC	2011-15
NanoCity conference (presentation)	NWO	2014
MicroNanoConference (posters & presentation)	MinacNed	2011-14
NWO organic chemistry conference, Lunteren (posters)	NWO	2011-13
Final PoaC symposium, Eindhoven	NWO	2013
Wageningen Symposium on Organic Chemistry (posters & presentation)	KNCV	2012-2015

General courses

PhD Week	VLAG	2012
ACS on Campus event, Utrecht	ACS	2013
Analytic Storytelling	NanoNext	2014
IP & Valorisation Awareness	NanoNext	2015
Risk Analysis & Technology Assessment	NanoNext	2013
Project & Time Management	VLAG	2012
Techniques for Writing and Presenting a Scientific Paper	VLAG	2012
How to write a world-class paper	WUR	2013

Optionals

PhD study trips Germany/Switzerland and Canada	ORC	2013-15
Preparation of PhD proposal		2011
Colloquia	ORC	2011-15
Literature club	ORC	2012-14
Group meetings	ORC	2011-15

About the author

Bas was born on the 19th of June, 1988 in Uden, the Netherlands. At an early age, he developed a broad fascination for science and his choices in education reflected that. After completing high school, he studied Molecular Lifesciences at Wageningen University. He obtained his bachelor's degree with honors and decided to take the Molecular Lifesciences master at the WUR as well. This MSc program included a five month internship at the University of Santa Barbara, California where he worked under the supervision of Dr. Nate Lynd and Prof. Dr. Craig Hawker. He returned to the Netherlands to start his PhD in Organic Chemistry at Wageningen University in 2011. The results obtained in the period 2011-2015 are described in this thesis.

"Follow the white rabbit..."